Planning of Multi-Microgrids Considering Uncertainties and Spatial Characteristics

by

Enrique Gabriel Vera

A thesis
presented to the University of Waterloo
in fulfillment of the
thesis requirement for the degree of
Doctor of Philosophy
in
Electrical and Computer Engineering

Waterloo, Ontario, Canada, 2022

Examining Committee Membership

The following served on the Examining Committee for this thesis. The decision of the Examining Committee is by majority vote.

Supervisor:	Claudio Cañizares Professor, Electrical and Computer Engineering Department, University of Waterloo
Co-Supervisor:	Mehrdad Pirnia Professor, Department of Management Sciences, University of Waterloo
Internal Member:	Kankar Bhattacharya Professor, Electrical and Computer Engineering Department, University of Waterloo
Internal Member:	John Simpson-Porco Professor, Electrical and Computer Engineering Department, University of Waterloo
Internal-External Member:	Fatih Safa Erenay Professor, Department of Management Sciences, University of Waterloo
External Examiner:	Mohammad Shahidehpour Professor, Electrical and Computer Engineering Department, Illinois Institute of Technology

Author's Declaration

I hereby declare that I am the sole author of this thesis. This is a true copy of the thesis, including any required final revisions, as accepted by my examiners.

I understand that my thesis may be made electronically available to the public.

Abstract

Global warming is a serious issue that is being tackled from various fronts, one of them is the decarbonization of electrical energy systems, which may be addressed by introducing clean Distributed Energy Sources (DERs) such as Renewable Energy Resources (RESs) and Energy Storage Systems (ESSs). These types of technologies can be clustered to form Microgrids (MGs), which have proven to be technically and financially feasible solutions to supply electricity demand while reducing emissions and increasing resiliency. MGs can operate isolated or connected to the grid, both in rural and urban settings, which allows them to interact with the existing electricity grid to enhance its capabilities and functionalities, while improving power quality, reducing network congestion, increasing efficiency, reliability, and flexibility, and delaying investments in transmission and distribution systems. Hence, this thesis focuses on various relevant and timely aspects of MG planning, in particular for isolated Remote Communities (RCs) and for the interconnection of MGs and their integration with Active Distribution Networks (ADNs) to form Multi-Microgrid (MMG) systems.

The deployment of clean MGs to satisfy RC electricity needs, considering their inherent geographic characteristics, imposes a series of challenges that must be taken into account when planning them. Thus, delivering electricity to RCs is economically and environmentally expensive, as the main source of electricity is diesel generators, which present significant Greenhouse Gas (GHG) emissions, and Operations and Maintenance (O&M), transportation, and fuel costs. Therefore, an optimization model for the long-term planning of RC MGs to introduce RESs and ESSs is proposed in this thesis, with the objective of reducing costs and emissions. The presented model considers lithium-ion batteries and hydrogen systems as part of ESSs technologies. The model is used to investigate the feasibility of integrating these DERs in an MG in Sanikiluaq, an RC in the Nunavut territory in Northern Canada, where several planning scenarios with various combinations of resources are considered in order to assess the impact of different technologies. The results show that wind resources along with solar and storage technologies can play a key role in satisfying RC electricity demand, while significantly reducing costs and GHG emissions.

Independent MGs can be interconnected to form MMG systems in the context of ADNs, bringing valuable benefits such as energy use, power quality and stability improvements, as well as flexibility and thus economic enhancements for both costumers and utilities. Therefore, a Two Stage Stochastic Programming (TSSP) model is proposed for the planning of MMGs within ADNs at Medium Voltage (MV) levels to minimize the total costs, while benefiting from interconnections of MGs and considering uncertainties associated with electricity demand and RESs. Furthermore, the model includes long-term purchase

decisions and short-term operational constraints, using Geographical Information Systems (GIS) to realistically estimate rooftop solar limits. The planning model is used to study the feasibility of implementing an MMG system consisting of 4 individual MGs at an ADN in a municipality in the state of São Paulo, Brazil. The results show that the TSSP model tends to be less conservative than the deterministic model, which is based on simple and pessimistic reserve constraints, while being computationally more efficient than the usual, Stochastic Linear Programming (SLP) and Monte Carlo Simulations (MCS) approaches, with adequate accuracy.

Finally, the MMG planning model at MV is further extended to include the Low Voltage (LV) grid. Thus, a model is proposed for the realistic planning of MMGs in the context of ADNs, with the assistance of GIS. The model considers the distribution system grid with an adequate level of detail for multi-year planning as well as the geographic features of the studied region. Similar to the MV model, it also includes long-term purchase decisions and short-term operational constraints, and considers uncertainties associated with electricity demand and RESs using a TSSP approach. GIS along with Deep Learning (DL) are used to more accurately estimate the rooftop areas within the studied region for solar PV deployment, as well as for modelling the LV grid. The planning model is then used to study in more detail the feasibility of implementing the MMG system previously considered in São Paulo, Brazil. The results of the extended TSSP LV grid model are compared with the results obtained using MCS and the less detailed TSSP MV grid model, demonstrating that both TSSP solutions are close to those obtained with MCS at a lower computational cost, while providing accurate and practical planning results.

Acknowledgements

First, I want to thank God for enlightening my life and for providing me with the strength to succeed in this journey.

I would like to express my deepest gratitude to my thesis supervisors, Profs. Claudio Cañizares and Mehrdad Pirnia, for all the support they have provided to me during my graduate studies at the University of Waterloo. I would always be thankful for their mentoring and outstanding guidance.

My sincere appreciation for my Ph.D. Committee members: Profs. Kankar Bhattacharya and John Simpson-Porco from the Department of Electrical and Computer Engineering at the University of Waterloo, Prof. Fatih Safa Erenay from the Department of Management Sciences at the University of Waterloo, and Prof. Mohammad Shahidehpour from the Electrical and Computer Engineering Department at the Illinois Institute of Technology for their valuable comments and observations.

I thankfully acknowledge the funding and support provided by the SENESCYT in Ecuador and the Canadian Natural Sciences and Engineering Research Council (NSERC).

I am greatly indebted to Prof. Joel Melo, Prof. Ahda Grilo Pavani, Tatiana Guedes, and Byron Palate at the Federal University of ABC, in Santo André, Brazil for hosting me and providing relevant information and guidance that helped in the development of the research presented in this thesis.

I want to thank my friends and colleagues from the EMSOL lab: Anshul Goyal, Baheej Alghamdi, Behnam Tamimi, Bharat Solanki, Carlos Ceja, Dario Peralta, Emin Mammadov, Fabian Calero, Fabian Meyer, Hanwen Gu, Hisham Alharbi, Ivan Calero, Jean-Michell Clairand, Mauricio Restrepo, Mariano Arriaga, Matheus Zambroni de Souza, Muhammad Abuelhamd, Mostafa Farrokhabadi, Nitin Padmanabhan, Omar Alrumayh, Pablo Verdugo, Samuel Cordova, Talal Alharbi, Walter Violante, and William Mendieta. It was a pleasure sharing all this time with them. Very special thanks to Chioma Anierobi and Indrajit Das for their assistance during the first stages of my research.

Finally, I will be eternally grateful to my parents Mónica and Marcelo, my siblings Estefanía and Esteban, my Canadian family Alicia, Chaise, April, Alexia, Faith, Weston Walker, Lawson, Chester, and Hank, and especially my wife, Annette for their tireless and loving support during these past years.

Dedication

I dedicate this thesis to my biggest supporter, my perfect companion, my best friend, and the love of my life, my beautiful wife, Annette.

Table of Contents

List of Tables

List of Figures

List of Acronyms

RES Renewable Energy Resource

MG Microgrid

ESS Energy Storage System

DER Distributed Energy Resource

MMG Multi-Microgrid

GIS Geographical Information Systems

ADN Active Distribution Network

RoI Region of Interest

GHG Greenhouse Gas

MILP Mixed Integer Linear Programming

GA Genetic Algorithm

DS Distribution System

PCC Point of Common Coupling

RC Remote Community

SOC State of Charge

NPV Net Present Value

TSSP Two Stage Stochastic Programming

pdf probability distribution function

MM Moment Matching

GBM geometric Brownian motion

BM Brownian motion

NLP Nonlinear Programming

GI Geographic Information

DL Deep Learning

ML Machine Learning

NN Neural Network

CNN Convolutional Neural Network

FCNN Fully Convolutional Neural Network

Mask R-CNN Mask Region-Based Convolutional Neural Network

RPN Region Proposal Network

LV Low Voltage

MV Medium Voltage

MCS Monte Carlo Simulations

SSLP Single Stage Linear Programming

EV Electric Vehicle

MSP Multistage Stochastic Programming

LCOE Levelized Cost of Energy

MIP Mixed Integer Programming

EMS Energy Management System

Nomenclature

Parameters

$\overline{\mathcal{I}}$	Upper limit for installed capacity of RES [kW]
α	Remaining/useful life of existing/new diesel generators [h]
β	Demand reserves coefficient [pu]
δ	Depth-Of-Discharge (DoD) of a battery [pu]
η^{Ch}	Efficiency of battery charging [pu]
η^{Dch}	Efficiency of battery discharging [pu]
η_{ξ}	Efficiency of electrolizer [pu]
η_f	Efficiency of fuel cell [pu]
γ	Solar generation reserves coefficient [pu]
ι	Temperature coefficient of power for solar panels [pu/°C]
λ	Total number of representative days in a month
$\mathbb{E}$	Expected value
$\mathbb{V}ar$	Variance
$\mathcal{C}$	Total number of cycles of charge and discharge of a battery

$\mathcal{D}$	Cost of diesel [\$/l]
$\mathcal{H}$	Total amount of representative hours [h]
$\mathcal{M}$	A very large number
$\mathcal{R}$	Rated capacity of existing and new diesel generators [kW], RES [kW], or battery [kWh]
$\mathcal{T}$	Total number of hours available in an average year for diesel generators [h]
$\overline{\vartheta}, \underline{\vartheta}$	Upper/lower limits for hydrogen tank [pu]
$\overline{P}_{PCC}$	Upper limit for the power flow at the PCC [kW]
ψ	Minimum load operating level for existing and new diesel generators [pu]
ρ	Wind generation reserves coefficient [pu]
τ	Solar cell temperature [°C]
τ_{stc}	Solar cell temperature at standard test conditions [°C]
θ_j	Weight of the jth statistical property of interest for moment matching approach
φ	Derating factor of solar panels [pu]
ζ	Factor with normal distribution for geometric Brownian motion approach
c	Operation and Maintenance (O&M) cost [\$/kWh]
d	Discount rate [pu]
e_a	Cost of energy purchased from the ADN [\$/kWh]
e_l	Cost of energy purchased from MG "l" [\$/kWh]
e_m	Cost of energy sold by MG "m" [\$/kWh]

G	Solar irradiance [kW/m^2]
G_{stc}	Incident solar irradiance on solar panels at standard conditions [kW/m^2]
K	Unit cost of new diesel generators [\$/kW], RES [\$/kW] or battery [\$/kWh]
l_C	Hydrogen compressor load [pu]
P^d	Power demand [kW]
S_h	Wind speed
sk	Skewness
t^{ch}	Time duration a battery can charge continuously at a fixed power [h]
t^{dch}	Time duration a battery can discharge continuously at a fixed power [h]
V	Higher heating value of hydrogen [kWh/kg]

Variables

$\mathcal{A}$	Capacity addition of RES [kW] noRES [kW] or ESS [kWh]
$\mathcal{F}$	Fuel consumption [l]
$\mathcal{I}$	Total installed capacity of RESs [kW] or batteries [kWh]
$\mathcal{N}$	Number of types of RESs or batteries considered
$\mathfrak{D}$	Dummy variable for linearization
$C(\cdot)$	NPV of capital costs for the MMG system [\$]
$E^{buy}(\cdot)$	Total power purchased by the MMG system [kW]
$E^{sell}(\cdot)$	Total power sold by the MMG system [kW]
$O^B(\cdot)$	NPV of O&M costs of batteries for the MMG system [\$]

$O^S(\cdot)$	NPV of O&M costs of solar panels for the MMG system [$]
P	Power generated or consumed by $i \in \{E, F, N, S, W\}$ or $i \in \{\Xi\}$ [kW], respectively
P'^r	Power received by an MG from the ADN [kW]
P'^s	Power sent by a MG to the ADN [kW]
P^{ch}	Battery charging power [kW]
P^{dch}	Battery discharging power [kW]
P^r	Power received by an MG from other MGs [kW]
P^s	Power sent by a MG to other MGs [kW]
SOC	State-of-charge of battery [kWh] or hydrogen tank [kgh]
T	Low voltage transformer capacity [kW]
u	ON/OFF state of diesel generators
u'^s, u'^r	ON/OFF state for sending/receiving power to/from the ADN
u^{ch}, u^{dch}	ON/OFF state of battery charging or discharging
u^s, u^r	ON/OFF state for sending/receiving power to/from a MG
Z	Total Net Present Cost (NPC) [$]

Sub- and Super- scripts

I	Set of all generation and storage capacities $I = \{i\}$
E	Subset of existing diesel generators $E = \{e\} \in I$
N	Subset of new diesel generators $N = \{n\} \in I$

Π	Subset of RES and ESS $\Pi = \{p\} \in I$
S	Subset of solar panels $S = \{s\} \in \Pi$
W	Subset of wind turbines $W = \{\varrho\} \in \Pi$
B	Subset of batteries $B = \{b\} \in \Pi$
F	Subset of fuel cells $F = \{f\} \in \Pi$
Ξ	Subset of electrolizers $\Xi = \{\xi\} \in \Pi$
Q	Subset of hydrogen tanks $Q = \{q\} \in \Pi$
m, l	Indices for microgrids
t	transformers
h	hours
y	years
ω	Stochastic scenarios

Chapter 1

Introduction

1.1 Motivation

Recent catastrophic events related to global warming have raised concerns across the world and encouraged a paradigm shift in the generation and consumption of electricity [1, 2]. According to [3], 25% of the global emissions correspond to electricity and heat production, and therefore reducing emissions from energy generation is an important step in the fight against global warming. To address this concern, governments are promoting initiatives for decarbonization of the power sector, in which the use of Renewable Energy Resources (RESs) and Energy Storage Systems (ESSs) is advocated as their capital costs continue to decline [4]. These efforts have motivated the advent of small-scale clean energy generation initiatives across the world [5], reducing Greenhouse Gas (GHG) emissions at relatively lower costs, especially for those living in communities far from the grid.

Distributed Energy Resources (DERs) such as RES and ESS can be clustered to form Microgrids (MGs), which have proven to be technically and financially feasible solutions to supply electricity demand while reducing operational costs and emissions [5]. MGs can operate in both grid-connected and isolated forms, enabling the interaction with the existing electricity grid, enhancing its capabilities and functionalities, improving power quality, reducing network congestion, increasing energy efficiency, reliability and flexibility, and delaying investments in transmission and distribution systems [5–10]. These characteristics can service various types of locations, but are of most value for Remote Community (RC) or isolated MGs, where RES and ESSs can be introduced in order to reduce GHG emissions and costs associated with the use of fossil fuels for electricity generation, while improving

resilience [11]. Thus, the planning of an appropriate energy supply mix to satisfy electricity demand in RC MGs in the long-run needs to be properly addressed.

Coordinated and properly interconnected MGs, which are referred to as Multi-Microgrid (MMG) systems, can provide valuable benefits for consumers and system operators, as these systems can share resources and thus enhance reliability and reduce costs and GHG emissions [12]. Moreover, the coupling of one or more neighboring MGs can be used to overcome individual MG stability, control, and supply issues, as independent MGs can be clustered to better withstand disturbances and share DERs [10, 13]. Therefore, as individual MGs are known to be valuable to consumers and operators, it is important to consider the operation, control, and planning of MMGs.

MMG systems can be effectively integrated within Active Distribution Networks (ADNs). Hence, the development of a proper MMG long-term planning framework that takes into consideration real parameters and conditions associated with the location of RES is necessary. The planning of MMG systems is a decision-making issue, where technical and economic criteria must be considered to select the optimal location and mix of generation and storage resources that are necessary to satisfy the end-users energy requirements. Therefore, optimization models that include a wide variety of constraints are used, in which the complexity of the solution depends on the selected approach and degree of detail considered for modelling. In addition, planning models are prone to uncertainties associated with demand and availability of resources, and thus these need to be included in the mathematical formulation to obtain more accurate results.

Geographical Information Systems (GIS) are being applied to power systems, improving the management and development of conventional generation sources, addressing location-related problems, and helping in ADN real-time operation and maintenance when integrated with Supervisory Control and Data Acquisition (SCADA) systems [14]. Therefore, GIS allow the inclusion of georeferenced parameters within the optimization formulation, thus allowing the visualization of the results over the real network using maps. This can help enhance the decision-making process, while offering tools to better understand and interpret the results, which facilitates its implementation.

As per the aforementioned discussions, this thesis aims at providing an optimization model for the long-term planning of RC MGs, focusing on the inclusion of clean DERs. Then, based on the planning model developed for islanded MGs in RCs, which is a particularly challenging and somewhat unique planning problem, this research concentrates on the long-term planning of MMG systems in the context of ADNs, considering both the Medium Voltage (MV) and Low Voltage (LV) grids, utilizing a stochastic approach to solve such problems to consider uncertainties. GIS are used to estimate specific parameters within the

optimization models to account for the spatial features of the ADN. Thus, the next section provides an overview of the state of the art on RC MGs, MMG system planning under uncertainty and applications of GIS for RES estimation and MMG planning, identifying relevant gaps that form the basis for the main objectives of the research presented in this thesis.

1.2 Literature Review

In this section, a review of several papers relevant to the developed research is presented, followed by a discussion of the main gaps in the existing literature that this thesis addresses.

1.2.1 Remote Community Microgrids

RC MGs demand can be satisfied using a wide variety of DERs, including RES and ESS, to reduce GHG emissions and improve resiliency [15–18]. In this context, the feasibility of integrating hydrogen ESSs in RC MGs is a particularly relevant issue nowadays. Thus, this section focuses on discussing the state of the art on electrification of RC MGs using RESs and ESSs, including hydrogen systems.

Given the widespread use of fossil fuels for electricity generation in RCs, the integration of clean DERs has been extensively analyzed. For example, a deterministic model for planning the integration of RESs and ESSs in Canadian RC MGs is proposed in [19], aiming to reduce emissions and costs associated with the operation of diesel generators. In [20], a multiple-year planning model is presented to study the economic feasibility of integrating RESs in RC MGs, while maximizing social welfare. A model for the planning and operation of RC MGs is proposed in [21] using an integrated techno-economic optimization and power management approach, focusing on Levelized Cost of Energy (LCOE) and GHG emissions reduction; the proposed optimization model is solved applying meta-heuristics and is used to plan for the required solar panels, batteries, and wind turbines needed to satisfy the demand of an RC in India. The problem of ESS sizing is studied in [22] for isolated wind-diesel power systems, which is formulated using a Two Stage Stochastic Programming (TSSP) approach with the objective of minimizing the cost of supplied energy; it is observed that the use of ESSs can lead to costs reductions and flexibility enhancement of diesel-based RC MGs.

The integration of hydrogen systems as part of the ESSs considered for RCs is studied in the literature using different types of models. For instance, in [23], the feasibility of

replacing diesel generators with reformer and fuel cell systems in Canadian RCs is studied, it is observed that fuel cells can help improve the efficiency of the power-delivery system, while helping reduce emissions in the long-term. A heuristic algorithm is suggested in [24] for the long-term planning of isolated communities, where the size of wind and hydrogen ESSs is determined based on economic and reliability constraints. The MG planning for Canadian RCs using different mixtures of non-RESs and RESs, including hydrogen ESSs, is proposed in [25] using HOMER[1], it is observed that a significant reduction and even elimination of diesel generation is possible, with substantial savings. Similarly, in [26], the feasibility of implementing solar panels along with hydrogen ESSs in the isolated Brazilian Amazon region is studied using HOMER, concluding that one of the key points for the massive adoption of hydrogen ESSs is the reduction of its costs. RETScreen[2] is used in [27] to study the feasibility of implementing RESs and hydrogen ESSs in two RCs of Bhutan, a country in South Asia, demonstrating the technical feasibility of using DER mixes that include hydrogen ESSs.

1.2.2 Multi-Microgrid Planning

A set of interconnected or networked MGs is noted by different names such as community of MGs [28–30], MMG [31–36], nested MGs [37], or MG cluster [13,32,38]. Thus, given the focus of this thesis on MMG systems, relevant topics related to such systems are briefly presented next. For instance, references [39–46] explore different strategies for the control and interconnection of multiple ac and dc MGs for reliability enhancement, considering existing and new DERs. In [32,46–48] possible architectures for MMG systems connected to the grid are discussed, and [49] offers a concise guide for the design, operation, and integration of islanded MMG systems. The problems of day-ahead scheduling and energy management are examined in [50] and [51], and stability problems and solutions in MMG systems are studied in [52–58]. Finally, the need for MMG long-term planning studies that consider the interactions among MGs and ADNs is identified in [5,34,47,59]. Since, this research focuses on the long-term planning of interconnected MGs to develop relevant decision-making tools that properly consider the integration of MGs with RESs and ESSs in the context of ADNs, the rest of the section concentrates on discussing the state of the art on MMG planning.

The planning of MMGs includes the optimal sizing and sitting of DERs, which can significantly improve the resilience of the systems. This important aspect of the operation of

[1]Hybrid Optimization of Multiple Energy Resources software.
[2]RETScreen Clean Energy Management Software.

MGs has been analyzed through different planning-based resilience enhancement methods [60]. For example, in [61], a three-level Mixed Integer Linear Programming (MILP) problem to allocate DERs in MMGs is studied to reduce load shedding and increase resilience during extreme events. Similarly, [62] proposes an approach for the optimal reconfiguration of ADNs into MMGs, using stochastic models for representing uncertainties related to wind speed and solar irradiance, aiming at minimizing electricity costs and improving reliability and voltage profiles. In [29], the optimal interconnection of MMGs by using a probabilistic Minimal Cut-Set approach and a reliability cost/worth analysis to plan the optimal interconnection of MGs with RESs is proposed. Likewise, [63] proposes a method for planning MMG systems through generation and transmission system expansion simultaneously, while guaranteeing demand satisfaction with acceptable levels of reliability, minimizing investment and operational cost, with reduced load shedding. Similarly, [64] and [65] propose the planning of MMGs within ADNs for resilience, while improving the use of existing local DERs. The optimal partitioning of an ADN into interconnected MGs is proposed in [66], considering grid-connected and islanded modes of operation. However, even though the aforementioned approaches focus on some essential aspects of power system operations such as resilience, the majority assume DERs already exist in ADNs, and their goal thus is the planning of the optimal connection structure of MGs that would make the aggregated system more robust.

1.2.3 Microgrid Planning Under Uncertainty

Uncertain parameters related to RES generation and electricity demand affect short-term and long-term decisions, and therefore need to be included when planning MGs and MMG systems. Thus, a review of the main literature in which uncertainty is considered in the planning of those systems is presented next.

Uncertainties in RES generation and electricity demand are some of the parameters considered within the planning of MGs and MMGs [67,68]. For instance, in [62], probability distribution functions (pdfs) are used to address uncertainties related to solar and wind generation, while demand growth factors based on historical data are used for stochastic modelling. In [69], a two-stage chance-constrained stochastic model with enhanced bilinear Benders decomposition and stochastic scenarios is presented for the allocation of MMGs, where uncertainties related to RES generation, islanding, and load demand are considered as scenarios. A model is formulated in [70] for the operation and expansion planning of ADNs with MMGs, using robust optimization and a contingency-constrained approach to account for uncertainties related to generation capacity and electricity demand. In [71–73], game theory and Nash equilibrium principles are used to address the transactions

among all the participants; perfect forecast assumptions for electricity price and demand are used in [71], statistically-generated scenarios for RES generation are used in [72], and weather and demand forecast are used in [73]. A heuristic model is presented in [74] for the sizing and allocation of DERs in Distribution Systems (DSs) to form MGs, accounting for variability and uncertainties in load demand and power generation. Similarly, [75] considers uncertainties related to RES generation and demand, but proposes a stochastic multi-objective model along with a heuristic approach for risk assessment, which is used to plan MMG systems within real DSs. In [76], the planning of community MGs with a market-based approach is proposed, where a TSSP model with Benders decomposition is developed to consider uncertainties associated with electric load and substation, generation units, and transmission lines outages. Finally, [77] studies the planning of partially self-sufficient grid-connected MGs by proposing a data-driven model that limits the amount of energy transacted with the DS at the Point of Common Coupling (PCC), considering uncertainties related to electricity demand by selecting typical days from historical data.

1.2.4 Application of GIS for RES Evaluation and Power Systems Planning

The identification and estimation of RESs using GIS have been proposed by different authors. For instance, in [78], wind energy potential with consideration of environmental impacts is studied in different provinces of Turkey to identify proper sites for wind turbine installation. Similarly, in [79], an approach is proposed to establish suitable locations in the Canary Islands for the installation of wind turbines, considering technical, economic, and spatial constraints. GIS-based imagery analysis can also be used for determining solar energy potential, and is therefore used along with solar photovoltaic generation modelling in [80–83] to estimate the rooftop solar photovoltaic potential for various locations around the world. In this context, [84, 85] use GIS tools to determine suitable regions for solar energy development in India and Zambia, respectively. Some other applications more relevant to the proposed research framework in transmission lines, DS, and MG planning are discussed next in some detail.

GIS-based tools can be used for different aspects of power systems planning. For example, in [86, 87], GIS tools are used to identify optimal routes for transmission lines at minimum investment cost, while guaranteeing the security of the system. Similarly, a method for determining the optimal routing of medium voltage DSs in sparse rural areas using GIS, Genetic Algorithms (GAs), and Dijkstra's shortest path algorithm is proposed in [88]. Likewise, the problem of feeder routing in DSs is analyzed in [89], where

Geographic Information (GI) is used along with graph theory to decide on the optimal radial topology of the DS network, while considering uncertainty associated with rooftop solar generation and demand, and ensuring acceptable resilience levels at minimum cost. In [90], GIS tools are used over a raster map for the optimal planning of substations, considering geographic constraints and location-related costs, while ensuring proper service areas and overall economic minimization. The planning of substations is also studied in [91], where GIS tools are used to assist in specifying the location, capacity, and area coverage of substations, while guaranteeing minimum overall costs. As highlighted here, either the parameters obtained from GIS analysis can be introduced into an optimization formulation, or certain parameters can be optimized whiting a GIS-based software, but it is clear that the use of GIS enhances the sensibility and quality of planning results.

The use of GIS for the planning of MGs has also been studied in the literature. For instance, in [92], GIS tools are applied in the optimal sizing and allocation of DERs for MGs. In [93], nighttime satellite imagery and census data are used to estimate the size and structure of MGs in rural areas. A methodology is presented in [94] for the optimal formation of MMG systems, considering spatial characteristics. Similarly, in [95], a framework is proposed for forming and clustering LV DSs to form MMG systems, considering electrical, economic, and geographical constraints with minimum cost.

1.2.5 Discussion

Based on the overview of the existing state of the art on the types of DERs used for RC MGs, different technologies have been proven to be feasible, including solar panels, battery ESSs, and wind turbines. However, hydrogen ESSs have not been widely considered, which should be addressed, as these systems have started to gain more attention, given their current state of development and the considerable reduction in their capital costs.

As discussed in the preceding sections, the focus of existing research has been mainly on the planning of independent MGs and of interconnected MGs forming MMG systems. In this context, the majority of the available papers consider ADNs as the natural choice for the formation of MMGs, due to the availability of existing DERs as well as the required infrastructure. However, in most of the existing literature, the main focus of the MMG planning models has been the creation of MGs within the ADNs, without considering the required investments along the planning horizon. Furthermore, with respect to the level of detail of the planning models, there is a trade-off between the level of granularity of the ADN and DS and the level of complexity of the models used for the solution of the planning problem. Hence, most papers make simplifying assumptions to manage the

model complexities, which leads to impractical results. In addition, most papers do not properly consider the fact that MGs in MMG systems only have one PCC through which transactions among MGs should take place, assuming that the MGs forming the system are all interconnected with each other, which is unrealistic.

It has been observed that the proposed approaches in the literature are based on topological considerations, not giving much attention to the geographical characteristics of the MGs locations, leading to inaccuracies or unpractical planning results. On the other hand, it can be observed that GIS can assist in finding not only feasible, but realistic areas for the installation of transmission lines, substations, transformers, and protection equipment. The use of GI and GIS tools has been also extended to the planning of RESs, with the practical application of the results obtained from planning models, especially in locations with limited space, where buildings are in close proximity to each other, which is the case of many DSs and ADNs. In addition, when the location of many elements of the network is unknown or overlooked, the results may be feasible (from an optimization viewpoint) but not possible to implement. Likewise, it is important to highlight the possibility of extracting or validating information over imagery, throughout the use of GIS, while applying GI-based parameters to improve the economic impact of the solution of the optimization problems. Thus, planners can integrate RESs and ESSs with more confidence in order to support clean energy policies to motivate carbon footprint reduction pathways.

It is the intention of the research conducted in this thesis to fulfill the aforementioned gaps identified in the existing literature. Therefore, a model for the planning of RC MGs that considers hydrogen systems as part of its ESSs is first proposed. This model is then used as the basis of an MMG stochastic planning model, which includes the most relevant features of MGs, ADNs, and DERs, with an adequate level of detail for practical decision-making; nevertheless, given the nature of MMG systems, hydrogen and diesel systems are not considered in the MMG planning problem. Finally, GIS are used to model elements of the ADN, better estimate parameters required for the planning models, and improve the interpretation and visualization of the planning results on the ADN, aiming at producing more useful results.

1.3 Research Objective

Based on the aforementioned discussion, the primary contributions and objectives of the present thesis are as follows:

- Propose a long-term multi-year planning model for the integration of RESs and ESSs,

including batteries and hydrogen storage systems, in RC MGs for GHG emission and cost reduction.

- Propose a novel long-term multi-year planning model for creating MMG systems considering an ADN at MV level, where the actual grid is represented by considering the maximum power transfer capacity at the PCC. The model includes long-term purchase decisions and short-term operational constraints, and the formulation of the energy transactions among all participants, i.e., between the independent MGs and between each MG and the ADN.

- Apply TSSP to develop a new cost minimization model to consider uncertainties related to RES and demand, relying on an optimization-based scenario tree generation approach based on geometric Brownian motion (GBM) and statistical measures to represent scenarios.

- Extend the MMG long-term multi-year planning model to include the LV grid, without considering the electrical characteristics of the feeders. This model includes long-term purchase decisions for RESs and ESSs, long-term transformers capacity selection, short-term operational constraints, and the formulation of the energy transactions among all participants.

- Propose a methodology to estimate the location of the MV and LV ADN and define the number of users connected to each MV/LV transformer inside the MMG system using GIS tools. Furthermore, use Deep Learning (DL) techniques on high-resolution imagery to identify the rooftops of the buildings in the studied region, to determine the real available solar capacity.

- Test and validate the MV and LV planning models in a real system, based on an ADN at a municipality in the state of São Paulo Brazil, and compare the performance of the proposed TSSP planning models against deterministic, Single Stage Linear Programming (SSLP), and Monte Carlo Simulations (MCS).

1.4 Thesis Outline

The rest of the thesis is organized as follows:

- Chapter 2 presents a review of background topics relevant to the novel research reported in this thesis. Thus, an overview is provided of RC MGs, MG and MMG

planning, stochastic optimization, and the use and applications of GI-based parameters and GIS tools for MMG planning.

- Chapter 3 presents a deterministic optimization model for the long-term planning of RC MGs utilizing RESs and ESSs, including hydrogen systems. The model is used to investigate the feasibility of integrating these types of DERs in an MG in an RC in Northern Canada. Various results and comparisons of the proposed planning model in terms of DER capacities, costs, and GHG emissions are provided.

- Chapter 4 presents a model for the planning of MMGs in the context of ADNs at MV level. The model aims to minimize the total costs and considers uncertainties associated with electricity demand and RES using a TSSP approach. The planning model is used to study the feasibility of implementing a 4-MG system at an ADN in Brazil. Planning results and comparisons are presented for deterministic, SSLP, MCS, and TSSP models.

- Chapter 5 presents an extension of the model presented in Chapter 4 for the planning of MMGs in the context of ADNs at LV levels. The planning model is used to study the feasibility of implementing the previously studied 4-MG system in Brazil, using GIS for modelling the MV and LV grids and for estimating the maximum solar PV potential of the MMG system. Various results and comparisons in terms of DER capacities and costs obtained with TSSP and MCS models are presented.

- Chapter 6 summarizes the thesis content and presents the main conclusions and contributions of the research, as well as a possible scope for future work.

Chapter 2

Background Review

In this chapter, an overview of the relevant background on the main topics for this research is provided. Thus, pertinent fundamentals on RC MGs, MG and MMG planning, stochastic optimization, and GIS are presented next.

2.1 Canadian Remote Community Microgrids

Canadian northern territories, Nunavut, Northwest Territories, and Yukon, which are nearly 40 percent of Canada's land mass are massive and sparsely populated. Of the 114,000 people who live in northern territories, many reside in the territorial capitals of Iqaluit, Yellowknife, and Whitehorse. The largest of the 13 provinces and territories in Canada is Nunavut, illustrated in Figure 2.1 [96], with a total landmass of 1,936,113 km^2, distributed along 25 fully differentiated communities.

RCs' unique features such as distant location, extreme weather conditions, energy consumption patterns, limited availability of energy sources, and absence of connection to the bulk power system have made supplying their electricity needs a challenging problem. Moreover, since these communities are spread across Canada they cannot benefit from the economy of scale or low-cost generation, and in some cases, it can be unpractical and relatively expensive to interconnect them. Furthermore, with the exception of a few local hydro grid-tied communities in Yukon, Northwest Territories, and Quebec, the main source of electricity in the majority of these RCs is diesel generators. Thus, electricity delivery is economically and environmentally expensive due to the significant Operation and Maintenance (O&M), transportation, and fuel costs, since the fuel is purchased and shipped in

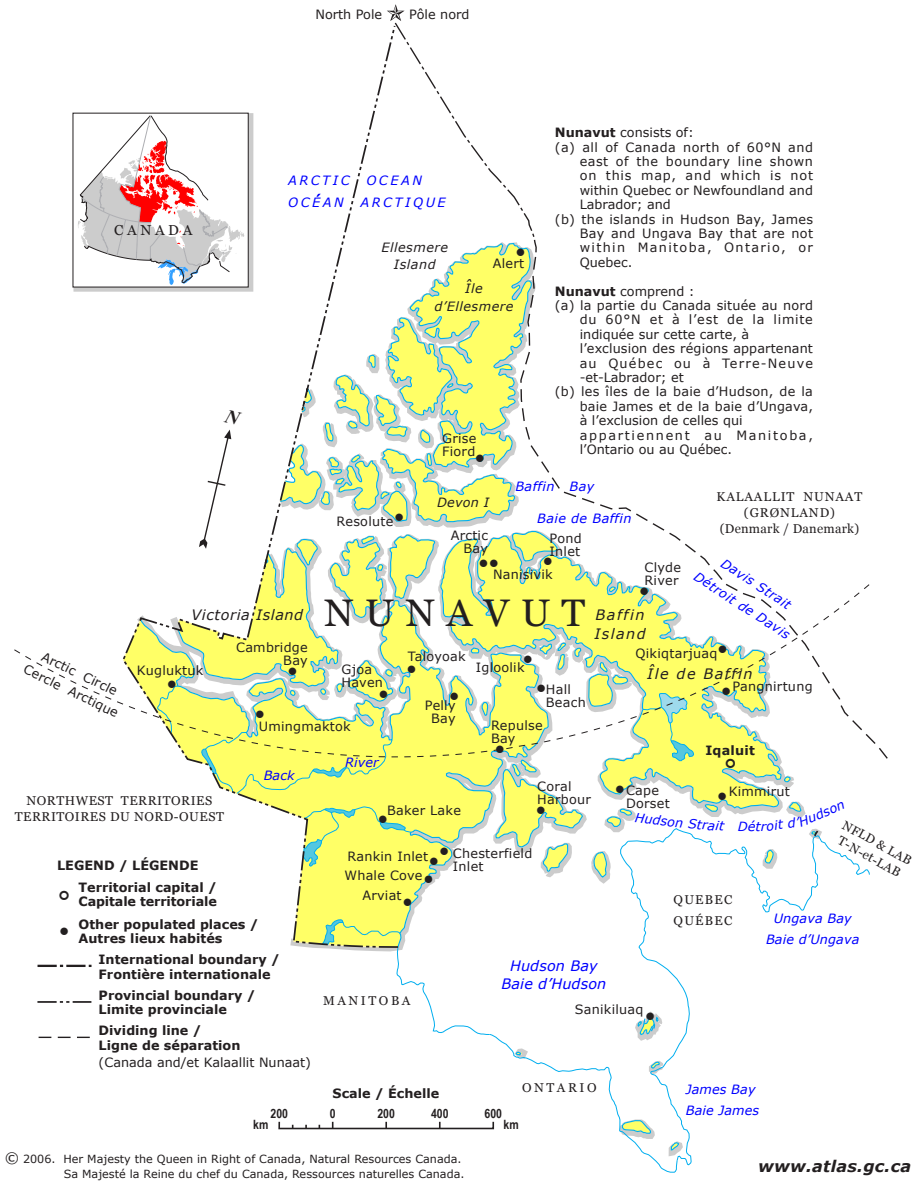

Figure 2.1: Nunavut.

bulk during the short summer seasons and stored in tank facilities in each community for

the longer cold seasons [15–17, 19, 20, 97, 98].

Due to the aforementioned challenges and particular needs of RCs, the reduction in the use of fossil fuels is required for environmental and economic reasons. Thus, RC MGs should be planned to guarantee the supply of their demand with enhanced flexibility and reliability, while reducing the consumption of fossil fuels, thus reducing GHG emissions in the long term. Consequently, the development of planning models that consider the cost challenges in RCs, intermittency of RESs, effective strategies for operating ESSs, and the integration of these technologies with the existing generation is required, as explained next.

2.2 Microgrid Planning

Current power systems face new challenges in supplying electricity demand, as global warming worsens and thus the need for clean DERs increases to help address climate change. These technologies have remarkably matured in the last decade, which has facilitated their incorporation through different mechanisms, among which the implementation of MGs stands out [99]. In addition, the declining costs of ESSs and RESs, technological advances in monitoring and control, and recent movement towards smart, decentralized, and resilient networks are facilitating the development and operation of MGs in both rural and urban settings, in isolated and/or grid modes. Thus, the development of a proper long-term planning framework is fundamental to analyzing integration barriers and future real-time operation challenges within MGs. In this thesis, two different, but related, planning frameworks are studied, one for isolated MGs, which is applied for RCs, and another one for MMG systems in the context in ADNs.

2.2.1 Isolated Microgrid Planning

Due to the unique features and needs of RCs, the deployment of clean MGs to supply their electricity demand is proposed in this thesis, as MGs have the potential to reduce GHG emissions, and increase flexibility and reliability using RESs and ESSs [7, 16, 17]. The planning of MGs can be defined as a strategic process that justifies the installation/upgrade of new/existing equipment, particularly DERs that include RESs and ESSs [100]. As explained in [34], the planning of MGs must determine the investment decisions on DERs to satisfy demand, with comprehensive consideration of their costs, operating conditions, and system status. In addition, contrary to the traditional grid planning models, the planning of MGs should consider their capability to operate connected or isolated from the ADN, and also the inherent RES variability in addition to other uncertainties.

The planning of MGs can be formulated as an optimization problem, where an objective function is minimized or maximized and a set of parameters and decision variables are included, while considering operational, geographical, and environmental constraints. The MG planning framework applied in this thesis is shown in Figure 2.2, where the objective function seeks to minimize the costs associated with the investments and operations of the MG. The formulation of the problem includes the MG electricity demand, which should be modeled for the planning horizon using growth factors or statistical properties due to its uncertain nature. Moreover, operating reserve constraints are essential in stand-alone MG planning to guarantee system adequacy at all times, given the absence of a connection with the bulk power system. As per DERs modelling, the power outputs are a function of environmental parameters such as solar irradiance and wind speed and are subject to operating constraints and uncertainty.

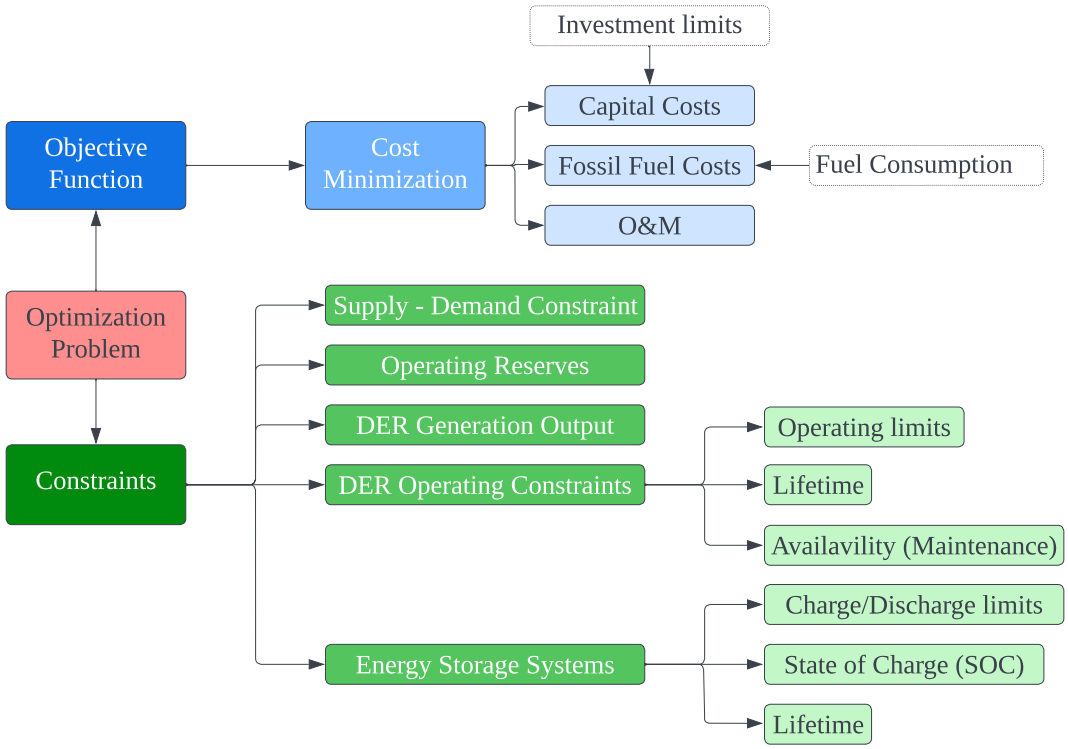

Figure 2.2: General framework for the planning of MGs.

2.2.2 Multi-Microgrid System Planning

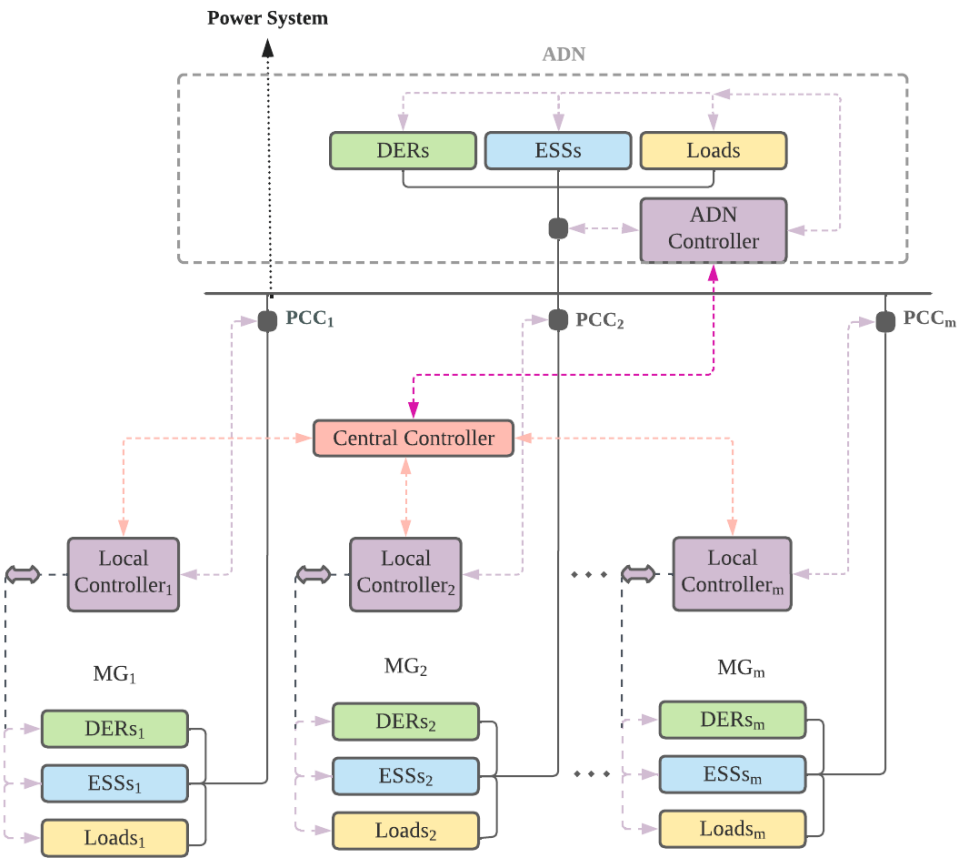

Figure 2.3: General overview of an MMG system.

An MMG system can be defined as a cluster of independent MGs, where each MG is connected to the ADN through a single PCC, as depicted in Figure 2.3 [12]. In this context, each MG is managed by its own controller, while the central controller coordinates the connection among MGs and the ADN; thus, from the Energy Management System (EMS) perspective, the central controller optimizes the transactions among individual MGs and the ADN, whereas the local controllers optimally dispatch DERs. An MMG planning model can be also posed as an optimization problem, where an objective function is minimized or maximized, and different types of constraints are considered to decide on the installation/upgrades of new/existing equipment, in particular DERs such as RESs and ESSs, which are an essential part of MGs but shared with the MMG system.

Thus, binary variables representing ESS operational states or DER purchase decisions in multiple interconnected MGs appear in this type of problem, which results in a large computational burden. Other factors that contribute to the latter are the level of granularity of the ADN grid, the consideration of uncertainty in one or more parameters of the model, and the consideration of the interactions among the participant MGs and the ADN, since the electricity demand can be satisfied by DERs inside each MG and by the shared ADN.

The MMG planning framework applied in this thesis is shown in Figure 2.4, where the objective function seeks to minimize the costs associated with the investments, operations, and energy transactions of the MMG system. The formulation of the problem includes the consideration of each MG's demand, which should account for growth factors and uncertainties. In this case, the operating reserves constraint is used to guarantee overall system adequacy by ensuring each MG can operate disconnected from the ADN. Since in MMG systems energy is transacted at the MG PCCs, constraints reflecting these interactions need to be considered. Finally, as in isolated MGs, DER modelling requires environmental parameters such as solar irradiance and wind speed, and are also subject to operating constraints and uncertainty.

Different types of decision variables, i.e., continuous, integer, or binary, are used in the mathematical formulation of MG and MMG planning models. In addition, the constraints, which restrict or define the values of the decision variables, can be linear and nonlinear; thus, the optimization planning model is usually described using Mixed Integer Programming (MIP) linear or nonlinear approaches [101]. Furthermore, the set of parameters that constitute the inputs of the optimization problem is illustrated in Figure 2.5:

- Technical and operational: These include parameters related to the functionality of DERs such as lifetime and power generation curves (wind turbines, thermal energy generators); requirements for the normal operation of DERs such as their upper or/and lower generation limits, O&M schedule for certain DERs; and normal operation requirements such as limits of the PCC, distribution transformers, and feeders. Additional operational restrictions may be the charge and discharge of ESSs, trading restrictions between individual MGs and the ADN, and specific boundaries for the installation of DERs.

- Economic: These are fuel costs and consumption curves for certain DERs, electricity prices, DER investment costs, and DER O&M costs.

- Environmental: These parameters are related to the location of the MGs and thus include but are not limited to: GHG emission limits, RES generation limits, ge-

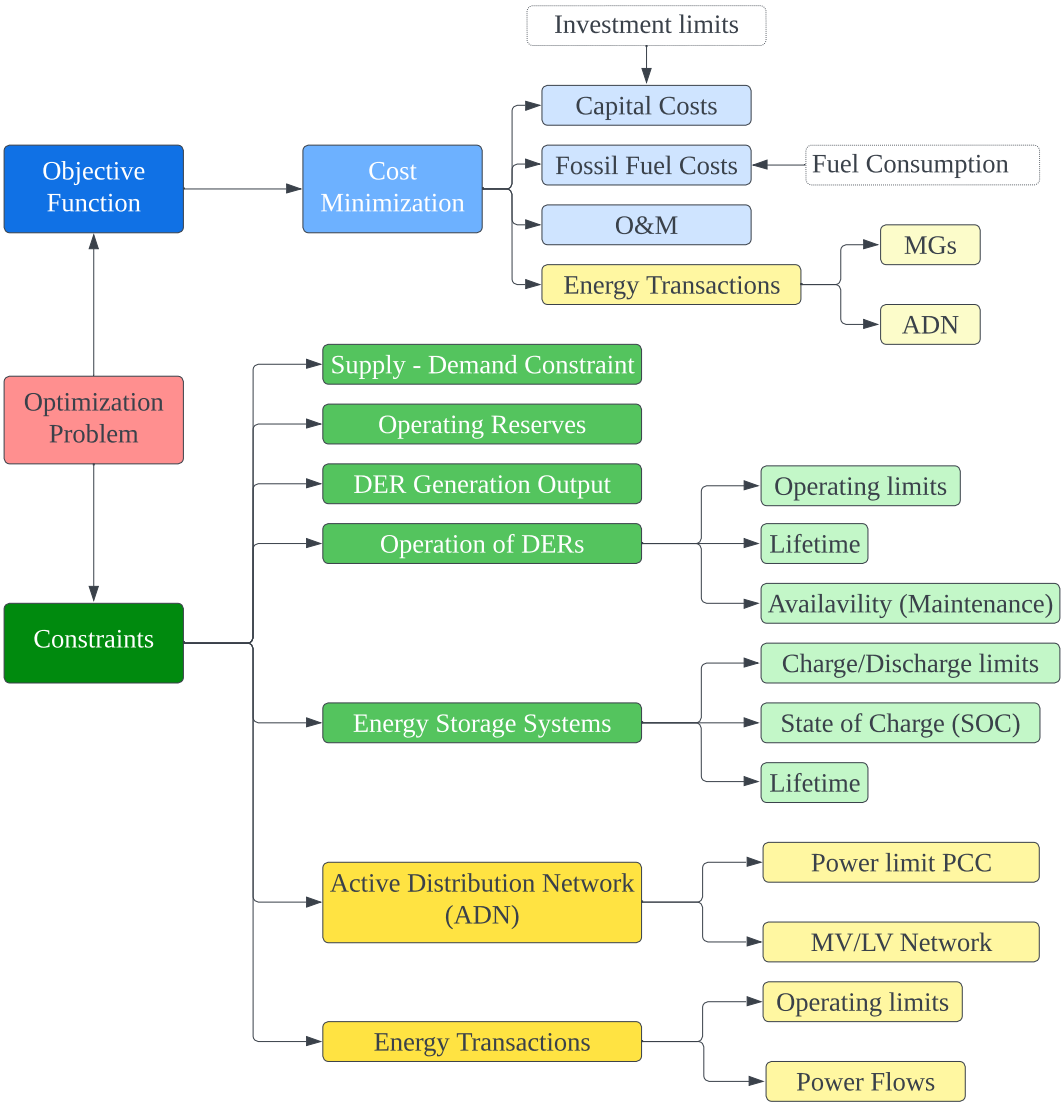

Figure 2.4: General framework for the planning of MMG systems.

ographical location of MGs and ADN's elements such as distribution transformers and feeders, and cadastral information.

On the other hand, the following are the possible outputs of the planning problem and are illustrated in Figure 2.5 as well:

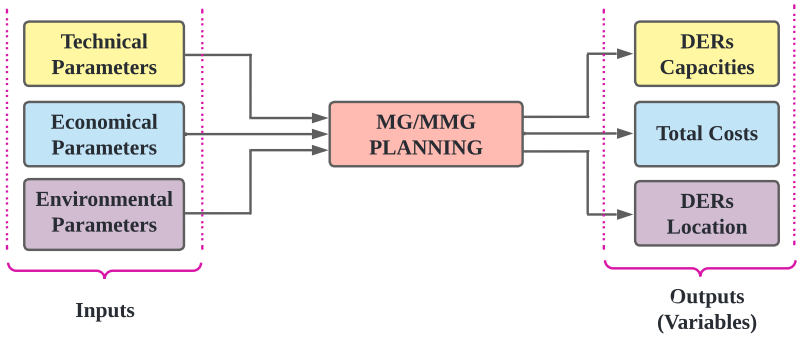

Figure 2.5: General overview of the inputs and outputs of the MG and MMG problem.

- DER capacities and mix of technologies to invest in, plus the optimal annual capacity additions until the end of the planning horizon.
- The total cost and breakdown of individual costs, which includes fuel cost, DER investment cost, energy transaction costs, and DER O&M cost.
- The exact location of DERs, which can be linked to the PCC or MV/LV transformers, depending on the details of the model.

2.3 Optimization under Uncertainty

Optimization under uncertainty refers to most practical engineering applications where randomness, which is prevalent and inevitable, is present, and thus should be considered in the inputs and outcomes of mathematical formulations. Some sources of uncertainty can be associated with the lack of information or knowledge, or lack of ability to measure and model the physical world, which may be reduced or eliminated by collecting more data. Other sources of uncertainty are random variations, and even though these can not be suppressed or reduced by collecting more knowledge or information, they can be controlled [102, 103].

In the context of uncertainty in mathematical models, consider the following optimiza-

tion problem:

$$\begin{aligned} \min_{x,y} \quad & c^T x + q^T y \\ \text{s.t.} \quad & Ax = b \\ & Tx + Wy = \omega \\ & x \geq 0, \;\; y \geq 0 \end{aligned} \tag{2.1}$$

where x and y are decision variables, c and q are parameters of the objective function and A, b, T, and W are constraint parameters. For the deterministic case, ω can be assumed to be a constant parameter, whereas, for stochastic problems, ω may be considered a random variable. The modelling of these uncertainties, in the long run, is a challenging task in the planning problem, for which a variety of techniques such as Stochastic and Robust Optimization are available to consider the impact of uncertainties in these types of studies. Stochastic programming is a well-recognized approach for decision-making under uncertainty, where some parameters are assumed to be described by random variables with a known pdf. The three stochastic programming methods used in this thesis are MCS, SSLP, and TSSP, which are described next.

2.3.1 Monte Carlo Simulations (MCS)

For the cases when ω is uncertain in (2.1), MCS can be applied to generate samples of the outputs, using random samples of the inputs, based on a known pdf. This method is based on the Central Limit Theorem, which states that the sample means follow a normal distribution for a large number of samples, and the Strong Law of Large Numbers, which guarantees that the sample mean converges to a constant value. Thus, consider the expected value of the random variable x, i.e, $\mu = \mathbb{E}(x)$, where a set of random and independent values $x_1, x_2, ..., x_n$ is defined using x's pdf. The average of these sampled values can be determined as follows:

$$\hat{u}_n = \frac{1}{n} \sum_{i=1}^{n} x_i \tag{2.2}$$

which is considered an estimate of the expected value μ. This principle can be used to solve (2.1) for a large set of samples $\Omega = \{\omega_1, \omega_2, \omega_3, ...\omega_{N_c}\}$ defined using ω's pdf, for which the optimization problem (2.1) is solved N_c times, where the average value of the objective function converges to a constant value. Thus, the following problem is solved for

$k = 1, .., N_c$:

$$\begin{aligned} \min_{x_k, y_k} \quad & c^T x_k + q^T y_k \\ \text{s.t.} \quad & Ax_k = b \\ & Tx_k + Wy_k = \omega_k \\ & x_k \geq 0, \;\; y_k \geq 0 \end{aligned} \tag{2.3}$$

2.3.2 Single Stage Stochastic Linear Programming (SSLP)

For stochastic approaches, the uncertainties can be considered as continuous time random variables, for a finite number of possible values or realizations $\Omega = \{\omega_1, \omega_2, \omega_3, ...\omega_N\}$ with corresponding probabilities $p_1, p_2, p_3, ..., p_N$. In this case, (2.1) can be written for each realization of the uncertain value ω_k as the following equivalent stochastic model:

$$\begin{aligned} \min_{x_k, y_k} \quad & \sum_{k=1}^{N} (c^T x_k + q^T y_k) p_k \\ \text{s.t.} \quad & Ax_k = b \qquad\qquad \forall k = 1, ..., N \\ & Tx_k + Wy_k = \omega_k \\ & x_k \geq 0, \;\; y_k \geq 0 \end{aligned} \tag{2.4}$$

thus minimizing the expected value $\mathbb{E}$ of the objective function, which yields in one stage the optimal values of all possible realizations considered.

2.3.3 Two-Stage Stochastic Programming (TSSP)

The decisions on the capacities needed to satisfy the MMG system's demand are non-anticipative in nature, i.e., these decisions are made "here and now" without any knowledge of the associated uncertainties. On the other hand, the operating decisions are anticipative, i.e., they are considered as a "wait and see" response to the observed uncertainty outcomes. This type of sequential decision-making process, which is based on the continuous realization of some stochastic processes, can be handled by a TSSP approach, which efficiently combines the aforementioned characteristics of the problem by dividing the decisions into two stages. Thus, the objective function includes the first stage function (non-anticipative), which corresponds to the purchase decisions, and the expected value

of the second stage function (anticipative), which corresponds to the operating decisions [104]. Replacing the random parameters with their expected values addresses the limitations associated with the increasing dimension of the problem, which is a common issue in Multistage Stochastic Programming (MSP) approaches [105]. Thus, in this method, two optimization problems need to be solved, with the following second stage problem being introduced first for clarity:

$$\begin{aligned} \min_{y_k} \quad & \mathcal{Q}_k = q^T y_k \\ \text{s.t.} \quad & Tx_k + Wy_k = \omega_k \qquad \forall k = 1, ..., N \\ & y_k \geq 0 \end{aligned} \tag{2.5}$$

where y_k are the second stage decision vectors and x_k are the first stage decision vectors. The optimal values of this stage can be defined as $\mathcal{Q}_k^*(x, \Omega)$. On the other hand, the first stage problem can be formulated as follows:

$$\begin{aligned} \min_{x} \quad & c^T x + \mathbb{E}[\mathcal{Q}_k^*(x, \Omega)] \\ \text{s.t.} \quad & Ax = b \\ & x \geq 0 \end{aligned} \tag{2.6}$$

Hence, the two stages can be integrated into one as follows:

$$\begin{aligned} \min_{x, y_k} \quad & c^T x + \sum_{k=1}^{N} p_k q^T y_k \\ \text{s.t.} \quad & Ax = b \\ & Tx + Wy_k = \omega_k \qquad \forall k = 1, ..., N \\ & x_k \geq 0, \;\; y_k \geq 0 \end{aligned} \tag{2.7}$$

which can be solved using any suitable linear solver such as CPLEX, Xpress, or Gurobi.

2.3.4 Scenario Tree Generation

Within certain stochastic optimization approaches (TSSP and SSLP), uncertain parameters Ω are assumed to follow a probability p^{Ω}. Thus, these can be treated as continuous time random variables and can be approximated by discrete pdfs using scenario trees. For the MMG planning model presented in this thesis, the scenario tree is generated using a Moment Matching (MM) approach where, on one hand, uncertainties associated with RES

are handled using their inherent statistical properties [106,107]. On the other hand, uncertainties related to electricity demand are handled using GBM, since demand evolves with time and there is an underlying annual growth rate relative to previous years [107, 108]. This approach assumes a normal and log-normal fit of the data; however, other scenario generation and reduction techniques based on other pdfs could be used to build the scenario tree to fit the statistical properties of the data [109].

Geometric Brownian Motion

Any continuous stochastic process $X(t)$ is a Brownian motion (BM) with drift coefficient μ and variance σ^2 if $X(0) = 0$, $X(t)$ has stationary and independent increments, and $X(t)$ is normally distributed with mean μ_t and variance σ_t^2. The stochastic process $S(t) = e^{X(t)}$ is called GBM, where the measure $\zeta(t) = \log\left(\frac{S(t+1)}{S(t)}\right)$ is normally distributed with mean u_S and standard deviation σ_S, and therefore has the expected value $\mathbb{E}$, variance $\mathbb{V}ar$, and skewness sk of a Log-normal pdf, as follows [108]:

$$\mathbb{E}\big(S(t+1)\big) = S(t)e^{\mu_S + \frac{\sigma_S^2}{2}} \tag{2.8}$$

$$\mathbb{V}ar\big(S(t+1)\big) = S(t)^2(e^{\sigma_S^2} - 1)e^{2\mu_S + \sigma_S^2} \tag{2.9}$$

$$sk\big(S(t+1)\big) = (e^{\sigma_S^2} + 2)\sqrt{e^{\sigma_S^2} - 1} \tag{2.10}$$

Moment Matching Approach

In order to generate scenarios with relevant states for RES and electricity demand and represent all the required time periods, an MM technique is used, which is a data-driven approach to systematically generate scenarios considering relevant statistical properties. Therefore, the uncertain parameters of the TSSP problem and its probabilities become variables of a Nonlinear Programming (NLP) problem. The purpose of the NLP problem is to define the optimal values for a pre-specified structure for the scenario tree, which minimizes the squared difference between the statistical properties calculated from the

tree and the ones calculated directly from the existing data, as follows [110]:

$$\begin{aligned} \min_{x,p} \quad & \sum_j \theta_j \left(f_j(X,P) - S_{VAL_j} \right)^2 \\ \text{s.t.} \quad & \sum_{j \in S} p_s = 1, \\ & p_s \geq 0 \end{aligned} \tag{2.11}$$

where S is the set of all specified statistical properties j, and S_{VAL_j} is the specified value for the jth statistical property in terms of the original random variables. X represents a single pair of representative values of the uncertainties, i.e., demand and RES, and P represents the associated probabilities; $f_j(X,P)$ is the mathematical discrete expression of the jth statistical property of interest, computed for X and P; and θ_j denotes the weight for the jth statistical property [107, 108].

2.4 Geographic Information Systems

GI is defined as a set of facts, data and/or evidence related to events, activities, and objects located on or near the surface of the earth, including spacial or geospatial data [111]. GI usually associates location information with attribute information describing the object and temporal information [111]. In addition, GI is organized and displayed using maps, which are instruments to communicate, calculate, display, and understand the interrelation of objects, using locations and attributes [112]. Therefore, georeferenced data have two main components: A spatial description of the location or spatial distribution of a geographical phenomenon, and a set of attributes describing the properties of the geometrical data (see Figure 2.6-a) [113]. GI can be represented using one or a combination of the following approaches [113]:

- *Raster Data Model*: Uses an array of cells or pixels to represent real-world objects. This model stores data using a matrix of grid values, which can represent a continuous field (elevation, temperate), an image (satellite image, scanned map), or category numbers, as shown in Figure 2.6-b. They are extensively used for analytical applications such as disease dispersion models, surface-water flow analysis, and electricity demand growth [14, 113].
- *Vector Data Model*: It is used to represent lines, points, areas, and geographic features according to their coordinates, as depicted in Figure 2.6-c. This model is

associated with the discrete view of the objects, and is widely used to represent built-environment entities such as road borders and buildings [14, 113].

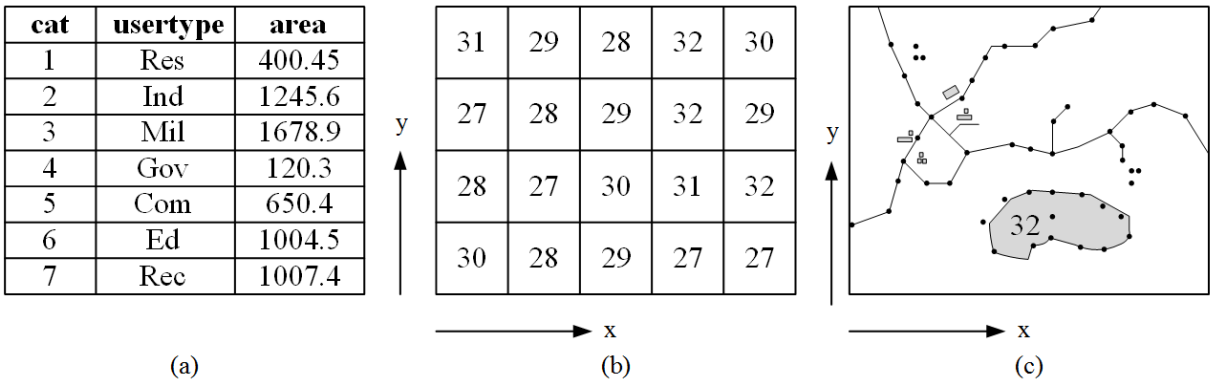

cat	usertype	area
1	Res	400.45
2	Ind	1245.6
3	Mil	1678.9
4	Gov	120.3
5	Com	650.4
6	Ed	1004.5
7	Rec	1007.4

Figure 2.6: Data models in GIS: (a) Attribute Data Model, (b) Raster Data Model, and (c) Vector Data Model.

GIS are computer-based information systems that provide a way to create, manage, visualize, analyze, and interpret GI [114]. By uncovering rich information such as relationships and patterns from the data, GIS can assist in making smarter decisions [114]. A modern GIS has at least three main capabilities: (1) georeferenced data management by means of layers that contain the features of the system (see Figure 2.7 [14]): (2) spatial analysis tools allowing spatial regressions, distance optimization analysis, population, and land use identification, among others; and (3) decision-making awareness for planning and O&M [113].

In the context of power systems, utilities can use GIS to build a consolidated view of the grid, which provides enough resources to solve location-related problems, improves the understanding of the real-time operation, and provides insights for network planning [14]. In addition, GIS tools are useful for the management and development of generation sources, and can make an important difference when planning and developing RESs due to their close relationship with the environment. GIS tools can also be used for solving and modelling a variety of problems such as water reservoirs for hydroelectric plants considering environmental parameters (i.e., infiltration, rainfall, soil types, and evaporation), load forecasting, risk management, fossil fuel-based plants emissions, wind speed prediction for wind farms considering topographic and environmental parameters (i.e., noise level profiles, bird migration patterns, and strobe light effects), and O&M scheduling for solar and wind generation.

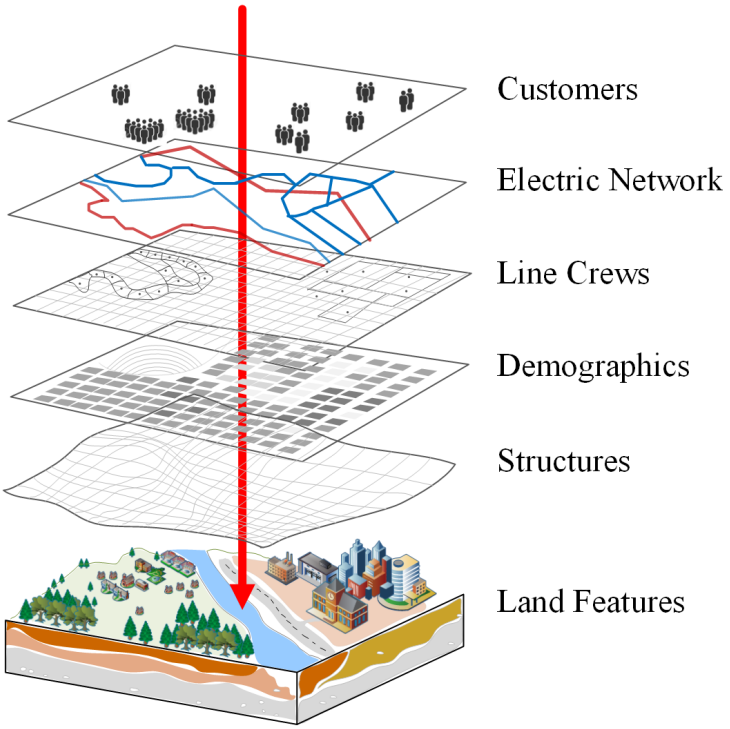

Figure 2.7: Example of information layers of GIS for electrical utilities.

2.4.1 Deep Learning

Deep Neural Networks (NNs) or DL is a Machine Learning (ML) tool widely used for image recognition, which allows automatic image feature extraction for image classification [115]. DL refers to a wide class of supervised and unsupervised ML techniques and architectures, where knowledge is extracted using many layers of non-linear information processing that are hierarchical in nature [116]. The majority of DL techniques use NN architectures, and contrary to traditional NNs containing 2-3 hidden layers, DL can use as many as 150 layers [117]. Thus, large sets of labeled data and NN architectures, that learn features directly from the data without the need for manual feature extraction, are needed for training DL models [118]. In this research, as an application of DL, Mask Region-Based Convolutional Neural Networks (Mask R-CNNs) are utilized to process high-resolution imagery to extract higher-dimensional and more abstract information for detecting feasible areas for installing solar PV. This approach uses Convolutional Neural Networks (CNNs) as its backbone, and a description is thus presented next.

Convolutional Neural Networks (CNN)

CNNs are one of the most popular types of DL, which are specialized NNs for processing data with known grid-like topology and have superior performance with images, speech, or audio signal inputs [119]. The structure of image data is of particular interest to this research, as it can be seen as a two-dimensional grid of pixel values that denote brightness and color, as depicted in Figure 2.8 [120]. Therefore, taking advantage of matrix multiplication and convolution operation, CNNs can identify patterns within an image using three main types of layers, as follows [116]:

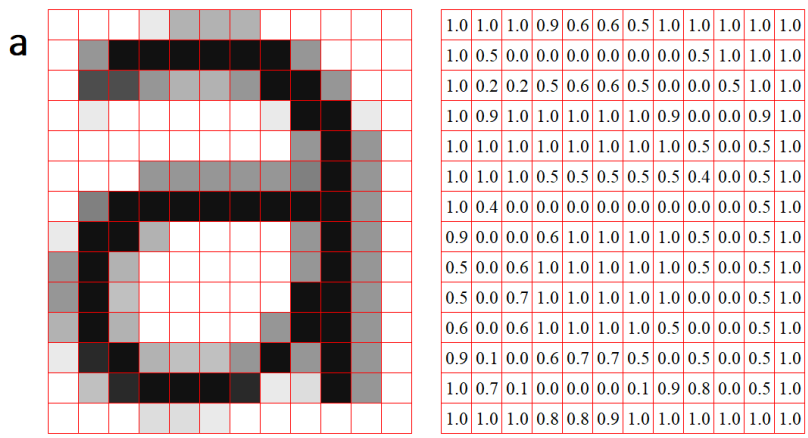

Figure 2.8: Image represented as a grid of pixels.

- Convolutional Layer: This is the fundamental building block of a CNN. Using this layer, dot product between two matrices, one containing the set of parameters to learn (kernel) and another parameter describing the interaction between each input and each output unit, is performed. When the forward pass is made, the kernel slides across the height and width of the image, creating an image representation of the receptive region. A kernel response is generated by computing an activation map in two dimensions, which results in a representation of the image for each spatial position. Convolution combines three important ideas: *sparse interaction* by making the kernel smaller than the input, *parameter sharing* by using the same parameter for more than one function in a model, and *equivariance* by affecting the inputs and outputs in the same way.

- Pooling Layer: Any CNN layer has three stages, one where several convolutions are performed in parallel to produce a set of linear activations[1], a second one where the linear activations are run through a nonlinear activation, and a third one (the pooling layer) where the output of the layer is modified. Pooling is a downsampling operation, which is in charge of replacing the net's output at a certain location with a summary statistic of nearby outputs, ensuring invariance to translation. The most common pooling operations are max pooling, where the pixel with maximum value within the current view is selected, and average pooling, where the average values of the current view are extracted.

- Fully-connected Layer: In this layer, the pixel values of the input are connected to all neurons and are used at the end of a CNN for classification.

Mask Region-Based Convolutional Neural Networks (Mask R-CNNs)

Image segmentation, which is the precise delineation of objects in an image, uses traditional object vision to localize and classify objects using bounding boxes, and semantic segmentation to classify each pixel into a predefined set of categories [121]. Thus, this is used here to detect building footprints, which is very useful for defining potential areas for solar PV installation. There are different methods for image segmentation, and their applicability depends on the purpose of the study, characteristics of each Region of Interest (RoI)[2], and information availability; in this research, since the buildings in the studied region are very close to each other, a Mask R-CNN method is used [122].

Mask R-CNN, depicted in Figure 2.9, is a specialized kind of NN that can be employed to process image data, which predicts objects class and bounding boxes by using two stages, as follows [121, 123]:

- Stage 1: This stage consists of two NNs (backbone and Region Proposal), which proposes candidate object bounding boxes, and is based on a Fully Convolutional Neural Network (FCNN)[3] that is trained end-to-end. It uses a method called Region Proposal Network (RPN) to recommend multiple objects that can be identified within an image, and the output is a set of rectangular proposals (RoIs), which are used for further processing.

[1] An activation function is a small mathematical expression which decides whether a neuron fires up or not.

[2] RoI is defined as a proposed region from the original image.

[3] In a FCNN, the fully-connected layers of a CNN are replaced by convolutional layers, which is useful for pixel classification.

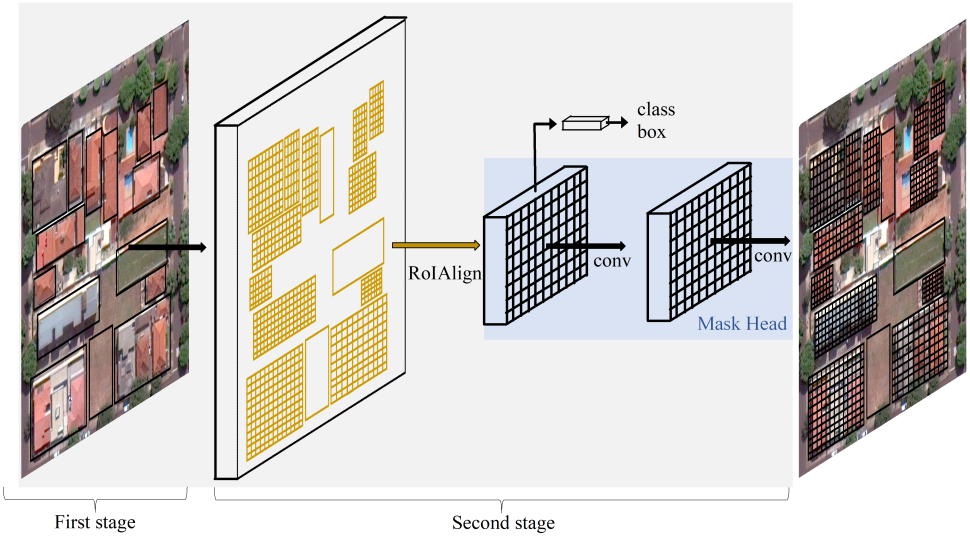

Figure 2.9: The Mask R-CNN framework for instance segmentation.

- Stage 2: In this stage, using a method called RoiPool, features are extracted from each candidate box and classification and bounding-box regression[4] are performed. At the same time, segmentation masks (desired features) are predicted on each RoI using a method called RoIAlign. The output from RoIAlign layer is then fed into the mask head, which consists of two convolution layers, predicting a segmentation mask for each RoI with a pixel-to-pixel correspondence.

2.5 Summary

In this chapter, an overview of Canadian RC MGs was presented, discussing their unique characteristics relevant to planning. Then, the planning frameworks for stand-alone MGs and MMG systems were discussed, highlighting the main features of the associated optimization models as well as their relevant inputs and outputs. Finally, important concepts related to the use GIS for MMG planning and modelling of their associated grids were discussed, including the use of DL for rooftop detection.

[4]Bounding-box regression is a technique that regresses from either region proposals or fixed anchor boxes to nearby bounding boxes of a pre-defined target object classes [124].

Chapter 3

Renewable Energy Integration in Canadian Remote Communities

In this chapter, an optimization model for the long-term planning of RC MGs utilizing RESs and ESSs, including hydrogen ESSs, with the objective of reducing costs and emission is proposed. The model presented in this chapter intends to help RCs recognize and quantify the potential benefits of implementing MGs through the use of RESs and ESSs, promoting their adoption for RC MGs decarbonization. The particular gap this model addresses is the inclusion of hydrogen systems as part of the ESS technologies considered in the planning process.

3.1 Planning Model Description

The proposed planning model is formulated using the optimization framework presented in Section 2.2.1 to plan the energy resources in RCs using solar panels, diesel, and wind generators, in combination with battery and hydrogen ESSs. In addition to the planning constraints, restricting the type and amount of generation in different years, the model contains operational constraints with binary variables associated with the hourly on/off status of diesel generators, and the charging and discharging status of batteries and hydrogen ESSs. Integer variables are used to prescribe the quantities of different technologies for economic evaluation, while the variables representing the generation, State of Charge (SOC) of batteries, and hydrogen ESSs are continuous. The model can therefore be characterized as a MILP problem as described in detail next.

In the equations that follow, all generators and storage capacities are part of the set $I = \{i\}$, while existing diesel generators, new diesel generators, and RESs and ESSs form the sub-sets $E = \{e\}$, $N = \{n\}$, and $\Pi = \{p\}$, respectively. The subset Π includes subsets of solar panels $S = \{s\}$, wind turbines $W = \{\varrho\}$, batteries $B = \{b\}$, fuel cells $F = \{f\}$, electrolyzers $\Xi = \{\xi\}$, and hydrogen tanks $Q = \{q\}$. Finally, y is the index used for years, and the index h is used for representative hours.

3.1.1 Objective Function

The following objective function represents the summation of the Net Present Value (NPV) of the capital, fuel, and O&M costs of the generators in the MG:

$$Z = \sum_{i,y\ \forall i \in \{N,\Pi\}} K_{i,y}\mathcal{A}_{i,y} + \sum_{i,y,h\ \forall i \in \{E,N\}} \lambda \mathcal{D}\mathcal{F}_{h,y,i} + \sum_{i,y,h\ \forall i \in \{E,F,N\}} \lambda c_i P_{i,y,h} + \sum_{i,y\ \forall i \in \Pi - F} \lambda \mathcal{H} c_i \mathcal{I}_{i,y} \tag{3.1}$$

where $K_{i,y}$ is the NPV of the capital cost of a generation unit i, installed in year y; $\mathcal{A}_{i,y}$ is the amount of installed capacity of i in year y; $\mathcal{D}$ is the unit cost of diesel fuel; $\mathcal{F}_{i,y,h}$ is the hourly diesel fuel consumption[1]; c_i is the hourly O&M cost; $P_{i,y,h}$ is the generated power from generator i, in year y and hour h; and $\mathcal{I}_{i,y}$ is the total installed capacity of generator i in year y. Note that the total capital cost in the first term of (3.1) is defined over generators Π and N, and the fuel cost is considered only for N and E. Since the representative hours h are considering one day in each month, to reduce the size of the problem for computational feasibility while maintaining adequate accuracy, there is 24 (average hours/month) $\times$ 12 (months), which equals 288 hours for each variable or parameter indexed by h. Factor λ represents the days of the month, i.e., $\lambda = 30$. The units of each parameter and variable are shown in the Nomenclature section.

[1] $\mathcal{F}_{i,y,h}$ is computed using the fuel curves available in [19], which are nonlinear and thus piece-wise linearization is used for their representation.

3.1.2 Constraints

Installed DER Capacity

The total installed capacity $\mathcal{I}_{i,y}$ for $i \in \{N, \Pi\}$ each year is calculated by updating the total installed capacity of the previous year $\mathcal{I}_{i,y-1}$, as follows:

$$\mathcal{I}_{i,y} = \mathcal{A}_{i,y} + I_{i,y-1} \qquad \forall i \in \{N, \Pi\}, y \tag{3.2}$$

where the capacity additions $\mathcal{A}_{i,y}$ for $i \in \{N, \Pi - S\}$ at each year is defined by the product of the number of generators added each year $\mathcal{N}_{i,y}$, and their respective individual rated capacity $\mathcal{R}_i$, as follows:

$$\mathcal{A}_{i,y} = \mathcal{N}_{i,y}\mathcal{R}_i \qquad \forall i \in \{N, \Pi - S\}, y \tag{3.3}$$

Note that $\mathcal{N}_{i,y}$ is an integer variable for $i \in \Pi - S$, and is a binary variable for $i \in N$, since only one diesel generator of a predefined capacity is allowed to be added to the generation portfolio each year, to constraint emissions. Finally, the capacity additions of solar $\mathcal{A}_{s,y}$ is a continuous variable, as the installation of solar panels is more versatile since power fractions can be accommodated in practice.

Supply-Demand Balance

The summation of the power generated by existing and new diesel generators $P_{e,y,h}$ and $P_{n,y,h}$, solar panels $P_{s,y,h}$, wind turbines $P_{\varrho,y,h}$, fuel cells $P_{f,y,h}$, and battery storage discharge $P^{dch}_{b,y,h}$ should satisfy the total consumers' demand $P^{d}_{y,h}$, the battery storage charge $P^{ch}_{b,y,h}$, and the power consumed by the hydrogen ESS's electrolyzer $P_{\xi,y,h}$, at each hour h and year y, as follows:

$$\sum_{i \in \{E,F,N,S,W\}} P_{i,y,h} + \sum_{B} P^{dch}_{b,y,h} = P^{d}_{y,h} + \sum_{B} P^{ch}_{b,y,h} + \sum_{\Xi} P_{\xi,y,h} \qquad \forall h, y \tag{3.4}$$

Operating Reserves

To accommodate the uncertainties associated with demand, solar, and wind generation, the rated capacity of existing diesel generators $\mathcal{R}_e$ and the total installed capacity of new diesel generators $\mathcal{I}_{n,y}$ and fuel cells $\mathcal{I}_{f,y}$, plus the batteries SOC per hour $SOC_{b,y,h}$, have to be greater than the hourly consumers demand $P^{d}_{y,h}$ by a given factor β, and solar and

wind generation by given factors γ and ρ, respectively, for every hour during the planning horizon, as follows:

$$(1+\beta)P^{d}_{y,h} + \gamma \sum_{S} P_{s,y,h} + \rho \sum_{W} P_{\varrho,y,h} \leq \sum_{E} R_e + \sum_{i \in \{F,N\}} \mathcal{I}_{i,y} + \sum_{B} SOC_{b,y,h} \qquad \forall h, y \tag{3.5}$$

Diesel Generator Limits

At every hour during the planning horizon, the power generated by diesel generators $P_{i,y,h}$ for $i \in \{E, N\}$ has to be less than or equal to the rated capacity of existing generators $\mathcal{R}_e$ and the total installed capacity of new diesel generators $\mathcal{I}_{n,y}$, and should also be greater than the minimum loading level defined by ψ_i for $i \in \{E, N\}$, which is a factor of the rated capacity, as follows:

$$P_{n,y,h} \leq \mathcal{I}_{n,y} u_{n,y,h} \qquad \forall n, h, y \tag{3.6}$$

$$P_{e,y,h} \leq \mathcal{R}_e u_{e,y,h} \qquad \forall e, h, y \tag{3.7}$$

$$P_{n,y,h} \geq \psi_n \mathcal{I}_{n,y} u_{n,y,h} \qquad \forall n, h, y \tag{3.8}$$

$$P_{e,y,h} \geq \psi_e \mathcal{R}_e u_{e,y,h} \qquad \forall e, h, y \tag{3.9}$$

where $u_{i,y,h}$ for $i \in \{E, N\}$ is a binary variable indicating the operating on/off state of new and existing diesel generators. Equations (3.6) and (3.8) are nonlinear, and therefore are linearized by introducing the continuous variable $\mathfrak{D}_{n,y,h}$, for which $0 \leq \mathfrak{D}_{n,y,h} \leq \Upsilon$, to replace the product $\mathfrak{D}_{n,y,h} = \mathcal{R}_e u_{e,y,h}$, as follows [125]:

$$P_{n,y,h} \leq \mathfrak{D}_{n,y,h} \qquad \forall n, y, h \tag{3.10}$$

$$P_{n,y,h} \geq \psi_n \mathfrak{D}_{n,y,h} \qquad \forall n, y, h \tag{3.11}$$

where the following constraints must be added to force $\mathfrak{D}_{n,y,h}$ to take the value of $\mathcal{R}_e u_{e,y,h}$:

$$\mathfrak{D}_{n,y,h} \leq \Upsilon \cdot u_{n,y,h} \qquad \forall n, y, h \tag{3.12}$$

$$\mathfrak{D}_{n,y,h} \leq \mathcal{I}_{n,y} \qquad \forall n, y, h \tag{3.13}$$

$$\mathfrak{D}_{n,y,h} \geq \mathcal{I}_{n,y} - \Upsilon(1 - u_{n,y,h}) \qquad \forall n, y, h \tag{3.14}$$

$$\mathfrak{D}_{n,y,h} \geq 0 \qquad \forall n, y, h \tag{3.15}$$

Diesel Generator Service Life

The useful life of new diesel generators and the remaining life of existing diesel generators α_i for $i \in \{E, N\}$, in hours, is taken into account by computing their total amount of operating states $u_{i,y,h}$ for $i \in \{E, N\}$ during the planning horizon as follows:

$$\sum_{h,y} \lambda u_{i,y,h} \leq \alpha_i \qquad \forall i \in \{E, N\} \tag{3.16}$$

Note that the factor $\lambda = 30$ is used to represent the life of the generators over a year.

Diesel Generator Availability

This constraint is used to reflect the maintenance of existing and new generators during the planning horizon. Thus, a percentage of the total number of available hours $\mathcal{T}$ in an average year is assigned for this purpose, as follows:

$$\sum_{h} u_{i,y,h} \leq \mathcal{H}(1 - \mathcal{T}) \qquad \forall i \in \{E, N\}, y \tag{3.17}$$

Solar Power Generation

The solar power generation output is computed as a direct function of the hourly incident irradiance G_h, hourly cell temperature τ_h, and derating factor φ, which is a scaling factor to account for effects of dust, wire loses, and other deviations of the solar output from its ideal value, as follows:

$$P_{s,y,h} = \varphi \mathcal{I}_{s,y} \left(\frac{G_h}{G_{stc}} \right) [1 + \iota(\tau_h - \tau_{stc})] \quad \forall s, y, h \tag{3.18}$$

where *stc* stands for standard test conditions.

Wind Power Generation

The wind power is computed as a function of the hourly wind speed S_h as follows:

$$P_{\varrho,y,h} = W(\mathcal{I}_{\varrho,y}, S_h) \qquad \forall \varrho, y, h \tag{3.19}$$

where the power generated by every wind turbine is computed using its turbine power curve $W(\cdot)$ and the wind speed S_h at every time-step [126].

Battery SOC and Limits

The following constraint computes the SOC of the batteries as a function of the batteries' charge $P^{ch}_{b,y,h}$ and discharge $P^{dch}_{b,y,h}$ for every hour of operation h, considering the charging η^{ch} and discharging η^{dch} efficiency rates:

$$SOC_{b,y,h+1} - SOC_{b,y,h} = \eta^{ch} P^{ch}_{b,y,h} - \frac{P^{dch}_{b,y,h}}{\eta^{dch}} \qquad \forall b, y, h \tag{3.20}$$

In order to track the continuity of the battery's SOC through the years, the SOC at the first hour of the next year considers the SOC of the last hour of the previous year as follows:

$$SOC_{b,y+1,1} - SOC_{b,y,\mathcal{H}} = \eta^{ch} P^{ch}_{b,y,\mathcal{H}} - \frac{P^{dch}_{b,y,\mathcal{H}}}{\eta^{dch}} \qquad \forall b, y, h \tag{3.21}$$

In addition, this SOC is subject to the following constraints reflecting the minimum and maximum capacity of the batteries:

$$SOC_{b,y,h} \leq \mathcal{I}_{b,y} \qquad \forall b, y, h \tag{3.22}$$

$$SOC_{b,y,h} \geq \delta \mathcal{I}_{b,y} \qquad \forall b, y, h \tag{3.23}$$

where δ is a factor to indicate the depth of discharge of the batteries.

The following constraints reflect the maximum charging and discharging limits respectively, and are functions of the depth of discharge δ, the total installed battery capacity $\mathcal{I}_{b,y}$, and the continuous time duration of charging t^{ch} and discharging t^{dch}, which are battery parameters chosen to keep reasonable equipment costs, while having adequate energy resources in a day:

$$P^{dch}_{b,y,h} \leq \left(\frac{1-\delta}{t^{dch}}\right) \mathcal{I}_{b,y} \quad \forall b, y, h \tag{3.24}$$

$$P^{ch}_{b,y,h} \leq \left(\frac{1-\delta}{t^{ch}}\right) \mathcal{I}_{b,y} \quad \forall b, y, h \tag{3.25}$$

Furthermore, the following constraints guarantee minimum charging/discharging power at a given hour:

$$P^{dch}_{b,y,h} \geq u^{dch}_{b,y,h} \qquad \forall b, y, h \tag{3.26}$$

$$P^{ch}_{b,y,h} \geq u^{ch}_{b,y,h} \qquad \forall b, y, h \tag{3.27}$$

where $u^{dch}_{b,y,h}$ and $u^{ch}_{b,y,h}$ are binary variables indicating the battery operating states. Finally, in order to prevent charging and discharging from occurring at the same time, the following equation is used:

$$P^{dch}_{b,y,h} P^{ch}_{b,y,h} = 0 \qquad \forall b, y, h \tag{3.28}$$

which is not linear and is therefore substituted by the following set of equations:

$$P^{dch}_{b,y,h} \leq u^{dch}_{b,y,h} \mathcal{M} \qquad \forall b, y, h \tag{3.29}$$

$$P^{ch}_{b,y,h} \leq u^{ch}_{b,y,h} \mathcal{M} \qquad \forall b, y, h \tag{3.30}$$

$$u^{dch}_{b,y,h} + u^{ch}_{b,y,h} \leq 1 \qquad \forall b, y, h \tag{3.31}$$

where $\mathcal{M}$ is a large number used to ensure (3.29) and (3.30) are redundant if their associated binary variable becomes 1. Finally, the following constraint defines the life span of each battery for $\mathcal{C}$ cycles of charge and discharge, assuming that each cycle is defined as one sequence of charge and discharge:

$$\sum_{h,y} (P^{ch}_{b,y,h} + P^{dch}_{b,y,h}) \leq \mathcal{C} \sum_{y} \mathcal{A}_{b,y} \qquad \forall b \tag{3.32}$$

Hydrogen System

The hydrogen system is composed of an electrolyzer, consuming electricity $P_{\xi,y,h}$ for generating the hydrogen that is stored at high pressure in tanks, which is used later by the fuel cells to generate electricity $P_{f,y,h}$, as illustrated in Figure 3.1. For this system, the SOC of the hydrogen tank for every hour of operation $SOC_{q,y,h}$ is a function of the power generated by the fuel cells $P_{f,y,h}$ and the power consumed by the electrolyzer $P_{\xi,y,h}$, which can be transformed into hydrogen consumption as follows [127]:

$$SOC_{q,y,h+1} - SOC_{q,y,h} = \frac{1}{1 + l_C} \frac{P_{\xi,y,h} \eta_\xi}{V} - \frac{P_{f,y,h}}{V \eta_f} \qquad \forall q, y, h \tag{3.33}$$

In order to track the continuity of the hydrogen tank SOC through the years, the SOC at the first hour of the next year considers the SOC of the last hour of the previous year as follows:

$$SOC_{q,y+1,1} - SOC_{q,y,\mathcal{H}} = \frac{1}{1 + l_C} \frac{P_{\xi,y,\mathcal{H}} \eta_\xi}{V} - \frac{P_{f,y,\mathcal{H}}}{V \eta_f} \qquad \forall q, y, h \tag{3.34}$$

where, for every year y, the hourly SOC limits of the hydrogen tank are constrained as follows:

$$SOC_{q,y,h} \leq \overline{\vartheta}\mathcal{I}_{q,y} \qquad \forall q, y, h \tag{3.35}$$

$$SOC_{q,y,h} \geq \underline{\vartheta}\mathcal{I}_{q,y} \qquad \forall q, y, h \tag{3.36}$$

V is the Higher Heating Value of Hydrogen; l_C is the hydrogen compressor load; $\mathcal{I}_{i,y}$ is the net capacity of the hydrogen tank; η_f and η_e are the efficiency of fuel cells and electrolyzers, respectively; and $\overline{\vartheta}$ and $\underline{\vartheta}$ are per unit constants defining the maximum and minimum hydrogen tank limits.

In addition, the power generated by the fuel cells $P_{f,y,h}$ and the power consumed by the electrolyzers $P_{\xi,y,h}$ are constrained by their total installed capacity $\mathcal{I}_{i,y}$ for $i \in \{F, \Xi\}$ as follows:

$$P_{i,y,h} \leq \mathcal{I}_{i,y} \qquad \forall i \in \{F, \Xi\}, y, h \tag{3.37}$$

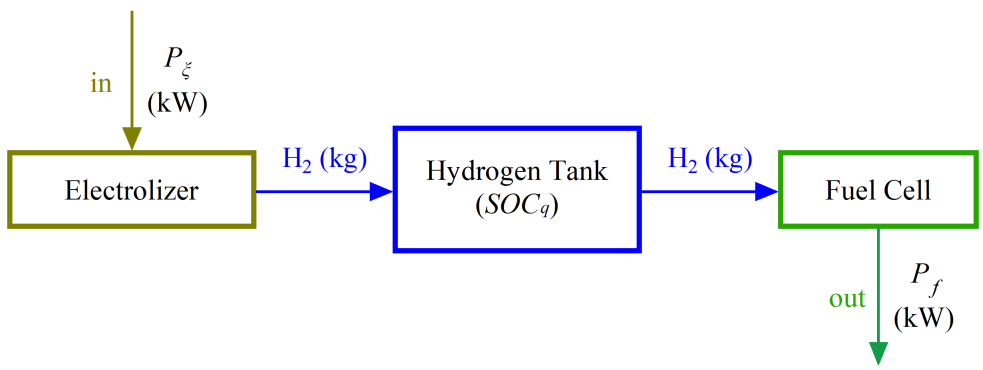

Figure 3.1: Schematic representation of a hydrogen storage system.

3.2 Case Study

The model proposed in Section 3.1 is used to investigate the feasibility of integrating RESs and ESSs in the planning of the MG of Sanikiluaq. This is an Inuit RC of 850 residents that is located in the southernmost part of Nunavut, about 150 kilometers off the west coast of Nunavik, Quebec, on the Belcher Islands (see Figure 3.2 [96]). Sanikiluaq is the only permanent settlement of the archipelago and the center of administration, trade, and communal life, as other parts of the islands serve as temporary residences. This community generates and distributes its own electricity in an independent/islanded fashion, and diesel

is used for electricity generation, in addition to its use for heating and transportation [128]. The various parameters needed to apply the planning model presented in Section 3.1 to this RC are provided next.

Figure 3.2: Sanikiluaq community.

Electricity Demand

The hourly load for the Sanikiluaq community was extracted from [19] and [126] and is depicted in Figure 3.3. This data can be used to calculate the hourly averages for a year with 288 representative hours, as explained in Section 3.1.

Existing Diesel Generators

The main characteristics of the existing diesel generators are presented in Table 3.1. It is assumed that the minimum load of these generators is a typical 40% of their nominal

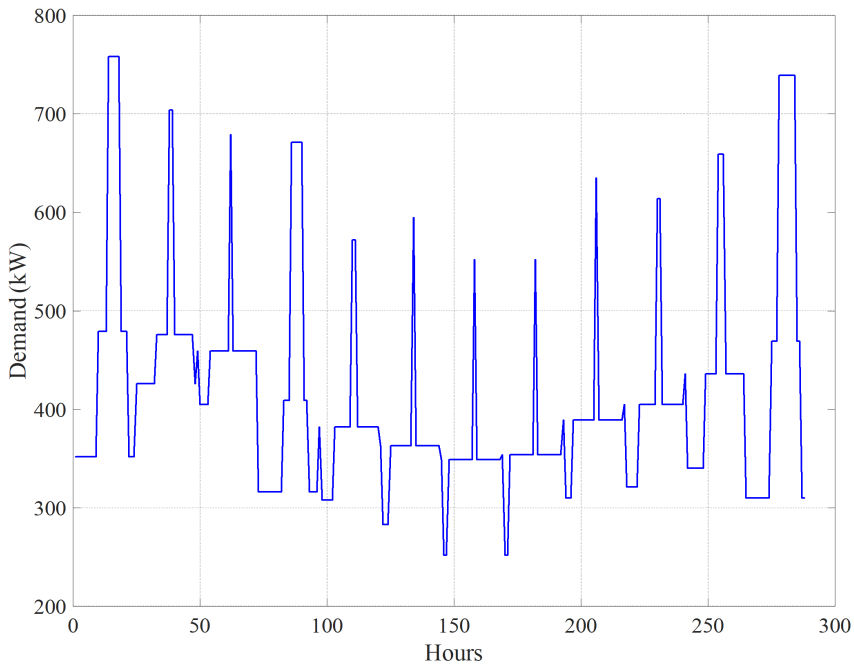

Figure 3.3: Sanikiluaq's yearly average load profile.

power, i.e., $\psi_e = 0.4$. In addition, Generators 1, 2, and 7 are in standby mode during even years, whereas Generators 3, 4, 5, and 6 are in standby mode during odd years, throughout the planning horizon. All generators, including those in standby mode, are assumed to act as reserves for the MG, as per [19] and [126].

New Diesel Generators

It is assumed that diesel generators may be aggregated to the generation portfolio for load supply and as reserves. Therefore, two types of diesel generators were considered, with their main characteristics being presented in Table 3.2. It was assumed that the minimum load of these generators is also a typical 40% of their nominal power, i.e., $\psi_n = 0.4$, as per [19] and [126].

Table 3.1: Main Generators' characteristics at Sanikiluaq

Gen.	Capacity [kW]	Lifetime [h]	Fuel consumption curve parameters		
			a $[l/h/kW^2]$	b $[l/h/kW]$	c $[l/h]$
1	330	35,339	-0.0006	0.5212	-15
2	330	21,600	-0.0006	0.5212	-15
3	330	14,400	-0.0006	0.5212	-15
4	330	7,200	-0.0006	0.5212	-15
5	500	64,696	0.00003	0.2105	10.3
6	540	68,820	0.00003	0.2144	10.3
7	550	100,000	0.00003	0.2105	10.3
O&M	0.0218 $/kWh - For all generators				

Table 3.2: New diesel generator parameters

Gen.	Capacity [kW]	Lifetime [h]	a $[l/h/kW^2]$	b $[l/h/kW]$	c $[l/h]$
1	320	100,000	-0.0002	0.3287	3
2	520	100,000	-0.00003	0.2227	10.3
Cost	727 $/kW - For all generators				
O&M	0.0191 $/kWh - For all generators				

Solar Panels and Irradiance

Solar panels are assumed to be connected through an inverter to the MG. The solar cell temperature τ and monthly solar irradiance G, with their averages, are illustrated in Figure 3.4, as per [19, 129]. The operational parameters and costs associated with the panels are shown in Table 3.3.

Table 3.3: Solar panels parameters at Sanikiluaq

Cost [$/kW]	O&M [$/kWh]	ι [pu/°C]	φ [%]	Lifetime [years]	τ_{stc} [°C]	G_{stc} [kW/m^2]
5,082	0.0145	-0.041	98	20	25	1

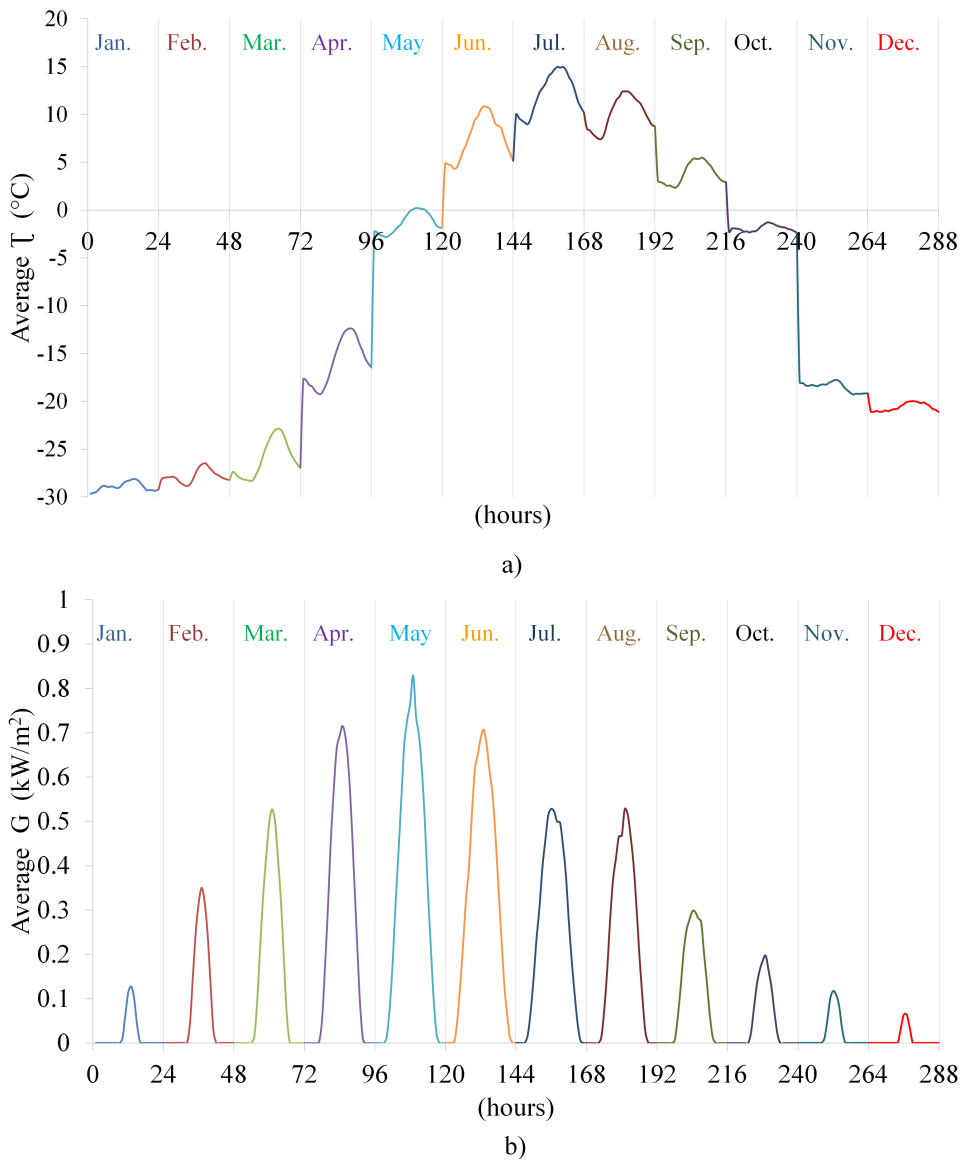

Figure 3.4: Sanikiluaq's monthly average (a) temperatures τ and (b) solar irradiance G.

Wind Turbines and Speed

Wind generators with 250 kW of nominal capacity were considered with the monthly average wind speeds shown in Figure 3.5. The economic and technical input parameters

for the model are presented in Table 3.4, as per [129]. The turbine curve $W(\cdot)$ was assumed linear between the cut-in and nominal speed, based on the actual power curves provided in [126], as shown in Table 3.4:

Table 3.4: Parameters of wind generators

Cut-in Speed [m/s]	Nominal Speed [m/s]	Cut-out speed [m/s]	Lifetime [years]
2.5	7.5	25	20
Power Curve	$W(S) = 30S - 75$ kW for $2.5 \leq S < 5$ $W(S) = 35S - 100$ kW for $5 \leq S < 7.5$ $W(S) = 250$ kW for $S \leq 7.5 < 25$ $W(S) = 0$ kW Otherwise		
Cost	7,943 \$/kW		
O&M	0.0363 \$/kWh		

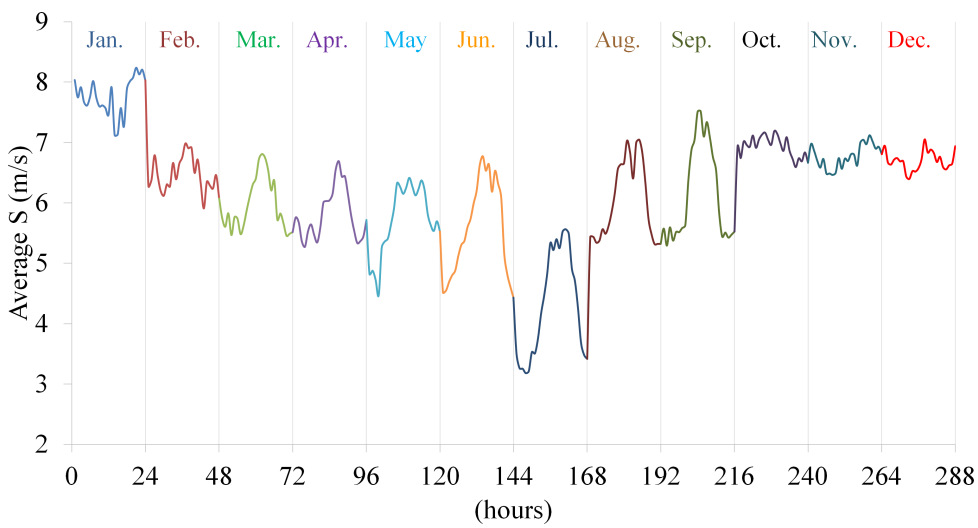

Figure 3.5: Average wind speed S at 21m hub height.

Batteries

The battery modules in the MG planning model are assumed to be lithium-ion batteries with 100 kWh and 20 kW peak power of charge/discharge, i.e., $t^{ch} = t^{dch} = 4h$ for $\delta = 0.2$, as per [19] and [126]. The economic and technical parameters for the implemented battery model are presented in Table 3.5.

Table 3.5: Battery parameters

Cost [$/kWh]	O&M [$/kWh]	SOC_0 [%]	η_{Ch} [%]	η_{DCh} [%]
1,504	0.0069	50	95	95

Hydrogen System

To model a hydrogen system, the fuel cells, an electrolyzer, and a hydrogen tank need to be considered. The costs and main characteristics of these elements are presented in Table 3.6, as per [129, 130].

Table 3.6: Hydrogen system parameters

Parameter	Fuel Cells	Electrolyzer	Hydrogen Tank
Capacity	250 kW	330 kW	200 kg
Cost	168,581 $/u	1,279,000 $/u	249,745 $/u
O&M	2 $/h	194 $/y	12,400 $/y
Efficiency	$\eta_{FC} = 60\%$	$\eta_E = 70\%$	-
Lifetime	50,000 h	15 y	25 y
System Constants	$V = 39.4$ kWh, $l_C = 0.02$ pu $\overline{\vartheta} = 0.95$ pu, $\underline{\vartheta} = 0.15$ pu		

3.2.1 Scenarios

Five scenarios are defined to apply the long-term planning model presented in Section 3.1. Note that in order to highlight the contributions of solar generators, each scenario includes one case with solar and one case without solar generators. The cases with solar generation are labeled with A, and the ones without solar are labeled with B. Thus, the main characteristics of these scenarios, considering all possible combinations of DERs, are as follows:

- Business-As-Usual (BAU) or Base Case: In this scenario, the only source of generation considered is diesel generation. Other DERs are not included here, as a base of comparison for other scenarios considered in terms of costs, use of diesel, and GHG emission reductions.

- 1A (I) and 1B ($I - S$): These scenarios include all DERs, i.e., diesel (E, N), solar (S), wind (W), batteries (B), and hydrogen (F, Q, Ξ).

- 2A ($I - B$) and 2B ($I - \{B, S\}$): All DERs except batteries are considered in these scenarios.

- 3A ($I - \{F, Q, \Xi\}$) and 3B ($I - \{F, S, Q, \Xi\}$): All DERs except hydrogen ESSs are considered in these scenarios.

- 4A (Π) and 4B ($\Pi - S$): In these scenarios, only RESs and ESSs are considered. Diesel generation is considered but exclusively for reserves, to represent an MG supplied primarily by renewable generation.

3.2.2 Assumptions and Criteria

The MILP model, described in Section 3.1, was solved using GAMS [131], with the CPLEX solver. The following are the assumed values for the remaining model parameters [19, 126, 129]:

- A typical discount rate of 8% for private investments is used.

- A reasonable planning horizon of 20 years is considered.

- Standard operating reserves for system adequacy of 50% for wind ($\rho = 0.5$), 25% for solar ($\gamma = 0.25$), and 10% for load ($\beta = 0.1$) are considered [126, 132].

- An average load growth of 1.0%/year is considered for this RC MG considering the undergoing plans for energy efficiency and district thermal generation [133].

- It is assumed that the cost of the technology will not be changing throughout the planning horizon, as the balance of the increasing equipment transportation costs and decreasing capital costs may cancel each other for RCs.

- Ramping up/down constraints are not considered, since all diesel generators are able to turn on and off in fractions of an hour.

- The cost of diesel is fixed at 2.391 \$/l, which is a high unsubsidized cost, as per [126].
- The maintenance time for all diesel generators is $\mathcal{T} = 0.1$ [126].
- The cycles of charge and discharge for the batteries is $\mathcal{C} = 3000$ [126].
- To control the inclusion of certain RESs and ESSs, for the considered scenarios, at least one battery module, 1% of the annual energy supplied by solar, and/or one hydrogen system module are assumed, otherwise, the model does not include these DERs due to the cost minimization approach.
- The investment in RESs is allowed only in the first 5 years, assuming that this will be a pilot project for RES integration in RCs, and new diesel generators are assumed to be added from the 3rd to 10th year as per [126].
- For the cases where hydrogen is included in the MG, one full system is included in the first year as part of a pilot implementation, leaving the algorithm to decide for additional capacities assumed to be in future years. Thus, at least one electrolyzer needs to be replaced at year 16, according to its useful lifetime, assuming a zero salvage value.

3.2.3 Results and Discussion

The results of the simulations are shown and discussed in this section. Thus, the energy mix resulting from running each scenario can be observed in Figure 3.6, which illustrates the following:

- Scenarios 1B and 3B, in which solar generation is not considered, recommend investment in diesel generation. Note that larger diesel generation capacities are recommended in Scenario 3B, in which the only source of storage is batteries. Wind generators do not replace solar generation as they have a larger capacity, which is not needed to satisfy demand.
- Note that Scenario 3A shows the least capacity additions needed for the long-term operation of the RC MG, where neither diesel generators nor fuel cells are considered, and also highlights the versatility of solar PV, as explained in Section 3.1.2. In addition, the total capacity in Scenario 3B is higher than the one in Scenario 3A since more than one diesel generator is required to supply the demand.

- In all scenarios, storage capacities of either fuel cells or batteries are used. For example, in the scenarios with only fuel cells (2A and 2B), the energy that has not been served by RESs or diesel generators is served by hydrogen ESSs. Also, in Scenarios 3A and 3B, batteries are used, as these are the only available storage capacity.

- In Scenarios 1A and 1B, in which the model can choose between investment in hydrogen or batteries, it recommends a portion of both ESSs.

- Observe that, for the scenarios where hydrogen ESSs are considered, the electrolyzer capacity additions have been included in Figure 3.6. These elements will increase the demand during the operation of the RC MG, as explained in Section 3.1.2.

- In Scenarios 4A and 4B, in which diesel generators are not allowed, more investment in storage capacities is recommended due to the required system operating reserves that account for variability for wind, solar, and load.

In Figures 3.7 and 3.8 the comparisons among costs and GHG emission reductions for different scenarios are illustrated. Thus, Figure 3.7 depicts different types of costs associated with each scenario, and Figure 3.8 illustrates the reductions of the total cost, O&M costs, and GHG reductions in relation to BAU. As observed in Figure 3.8, the total O&M costs decrease from 41% (3B) to 82% (4A), and the total costs decrease from 16% (3B) to 34% (1B), with respect to BAU. Similarly, the cost of fuel is reduced from 52% (3B) to 100% (4A and 4B), with respect to BAU. The most expensive scenario is 4B, in which all RESs except solar are recommended, surpassing the total cost of BAU by only 0.16%, while reducing GHG emissions by 100%. In addition, even though Scenarios 3A and 3B recommend the lowest capacity additions among other scenarios, their O&M and fuel costs are higher, resulting in a considerably higher total cost. Observe also that the cases with only hydrogen storage systems (2A and 2B) are less expensive than the cases with only batteries as the storage capacity (3A and 3B).

Figures. 3.9 and 3.10 present the hourly operation of the MG generators and storage systems versus demand, according to (3.4), during the 10th year of its operation for Scenarios 1A and 4A, which are chosen as they differ on their type of generation. Note that Scenario 1A allows all DERs including diesel, while Scenario 4A allows only ESSs and RESs. As shown, both batteries and hydrogen ESSs in combination with other DERs are incorporated in the generation mix of the MG to satisfy the hourly demand. Observe also that the hydrogen systems can considerably increase the total demand of the MG because of the presence of electrolyzers, but the cost is still reasonable with very low or zero GHG emissions.

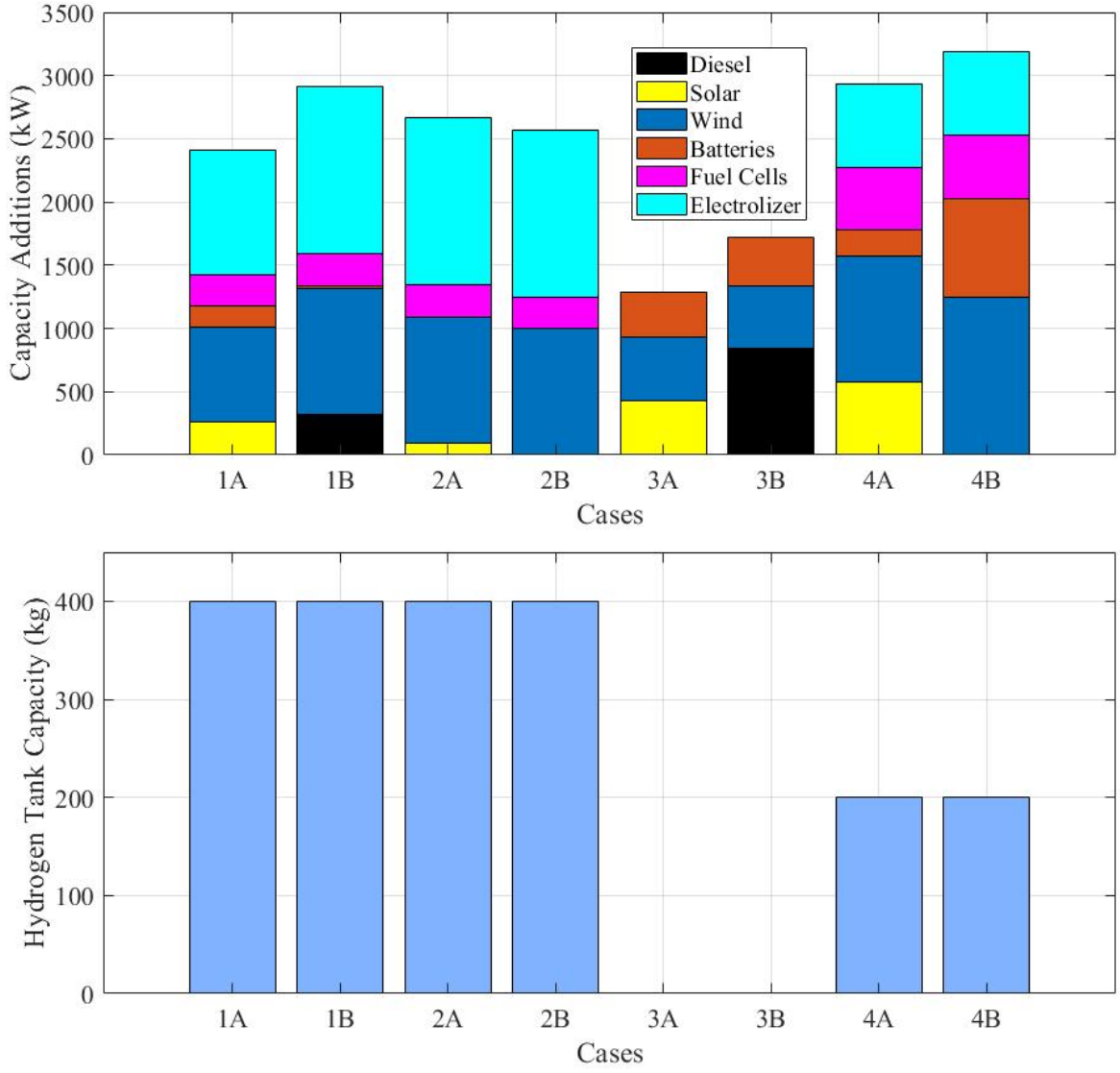

Figure 3.6: Total capacity additions during the planning horizon.

3.3 Summary

In this chapter, an optimization model for the long-term planning of RC MGs including RESs and ESSs was proposed with the objective of reducing costs and GHG emissions.

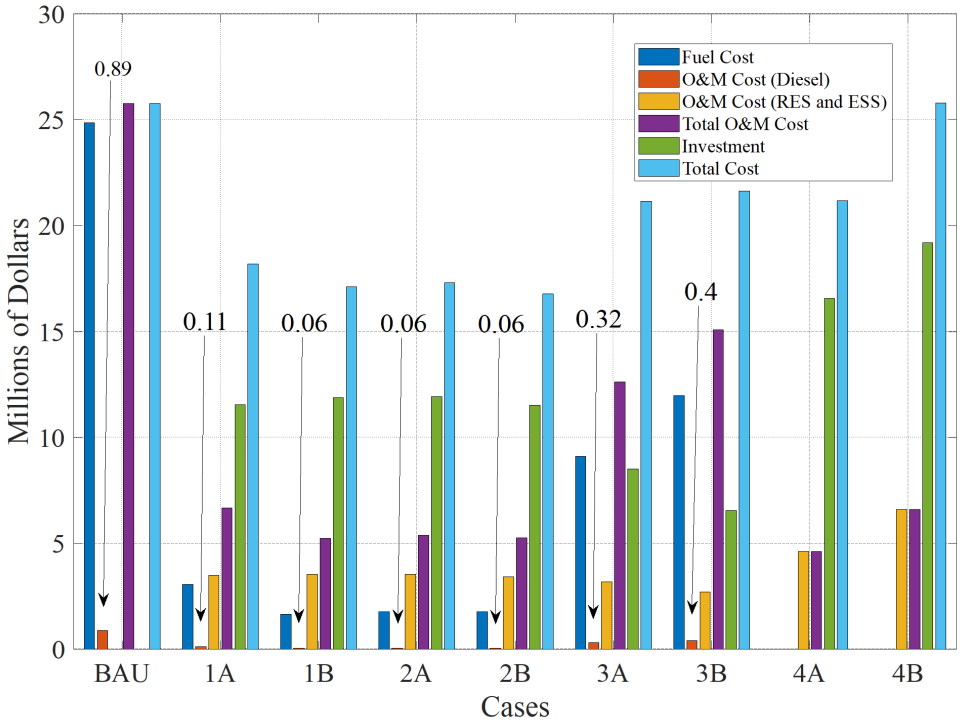

Figure 3.7: Associated costs of the MG planning for 20 years.

The proposed model considers lithium-ion batteries and hydrogen systems as part of ESSs technologies. The model was used to investigate the feasibility of integrating RESs and ESSs in an MG in Sanikiluaq, an RC in the Nunavut territory in Northern Canada. The results showed that wind resources along with solar and storage technologies can play a key role in satisfying RC electricity demand, while significantly reducing costs and GHG emissions.

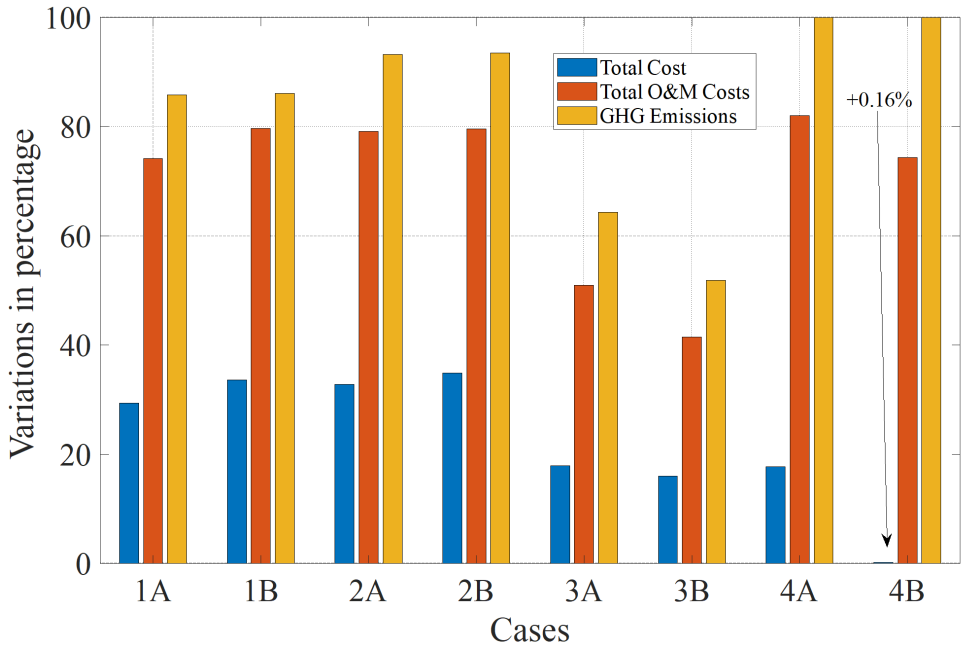

Figure 3.8: Reduction of cost and emission compared to the Base Case (BAU).

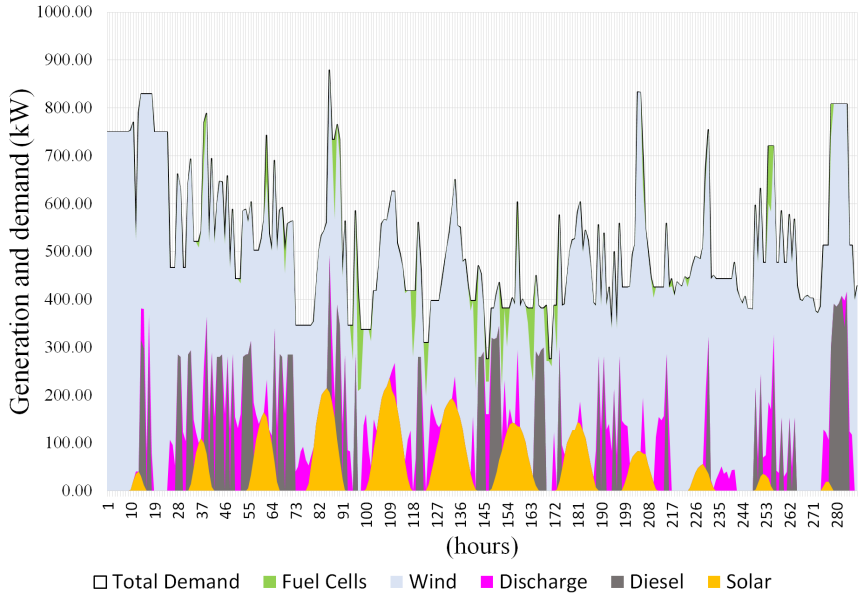

Figure 3.9: Case 1A operation of the MG for the 10th year.

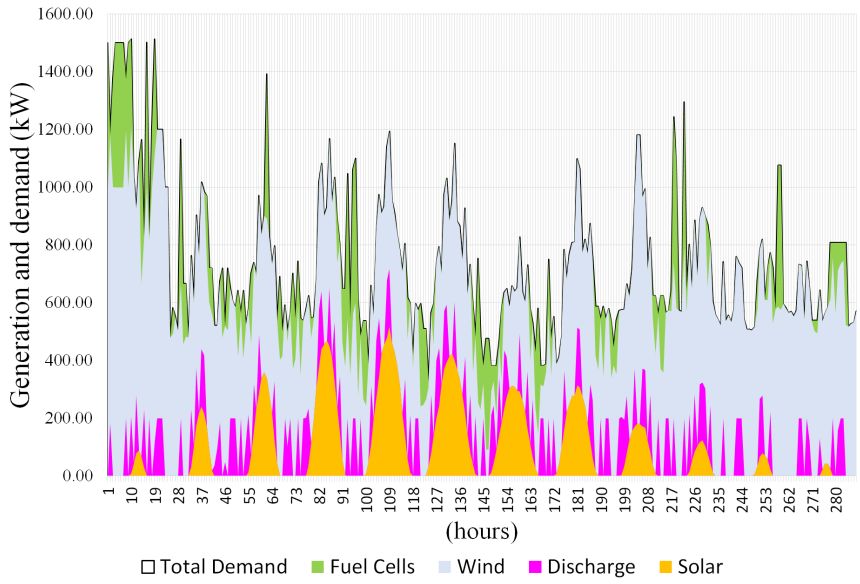

Figure 3.10: Case 4A operation of the MG for the 10th year.

Chapter 4

Two-Stage Stochastic Optimization Model for Multi-Microgrid Planning

In this chapter, the model presented in Chapter 3 is expanded by incorporating uncertainties associated with demand and RES using a TSSP approach for the planning of interconnected MGs in the context of ADNs. The model presented in this chapter is from the point of view of the system operator to support their long-term planning decision-making, while considering the MV network. This model is further expanded in Chapter 5 to include the LV network with the help of GIS and ML tools for more realistic MMG planning.

4.1 Planning Model for Medium Voltage Grid

The proposed planning model is based on the one presented in Chapter 3, where the index m is added to variables and parameters related to demand, RESs, and ESSs to indicate their operations and investment within each MG, and the index l is added to indicate the transactions between two independent MGs as part of the supply-balance constraints. In addition, for the operational constraints, index ω is introduced to account for the stochastic scenarios since this model is formulated using the TSSP optimization framework introduced in Section 2.3.3.

The planning model in this chapter is used to plan the energy resources in an MMG system, using RESs and ESSs, without considering neither diesel generation nor hydrogen ESSs, i.e., $i \in \{S, B\}$, as these DERs are atypical in urban ADNs, where MMG systems

are expected to evolve, due to space and environmental considerations. The MV grid is modeled by considering the maximum power transfer capacity at the PCC, without including the electrical characteristics of the feeders. Furthermore, in addition to planning constraints defining the type and amount of RESs and ESSs in each year, the model contains operational constraints with binary variables associated with the hourly charging and discharging status of batteries, and the power transactions between the participant MGs and the ADN. Integer variables are used to specify the size of RESs and ESSs for planning decisions, while the variables representing the power generation, batteries charge, discharge and hourly SOC, and the power transactions are considered continuous. The model can thus be characterized as an MILP problem, as described in detail next.

4.1.1 Objective Function

In this model, the objective function is formulated as the summation of the discounted capital costs or NPV (first stage objective function) and the expected discounted O&M and energy transaction costs (second stage objective function) of different stochastic scenarios ω with corresponding probabilities p_ω. Thus, (3.1) is modified to include these transaction costs as follows:

$$\begin{aligned} Z = C(\mathcal{A}_{i,y,m}) + \sum_{\omega} \Big(& O^B_\omega(P^{ch}_{b,y,h,m,\omega}, P^{dch}_{b,y,h,m,\omega}) + O^S_\omega(P_{s,y,h,m,\omega}) \\ & + E^{buy}_\omega(P^r_{y,h,m,l,\omega}, P'^r_{y,h,m,\omega}) - E^{sell}_\omega(P^s_{y,h,m,l,\omega}, P'^s_{y,h,m,\omega}) \Big) p_\omega \end{aligned} \tag{4.1}$$

where the discounted capital cost, discounted O&M cost for RESs and batteries, and the discounted cost of the energy purchased and sold are given by the following functions $C(\cdot)$, $O^S_\omega(\cdot)$, $O^B_\omega(\cdot)$, $E^{buy}_\omega(\cdot)$, and $E^{sell}_\omega(\cdot)$ respectively:

$$C(\mathcal{A}_{i,y,m}) = \sum_{i,y,m} K_{i,y,m} \mathcal{A}_{i,y,m} \tag{4.2}$$

$$O^S_\omega(P_{s,y,h,m,\omega}) = \lambda \sum_{s,y,h,m} c_{s,y,m} P_{s,y,h,m,\omega} \quad \forall \omega \tag{4.3}$$

$$O^B_\omega(P^{ch}_{b,y,h,m,\omega}, P^{dch}_{b,y,h,m,\omega}) = \lambda \sum_{b,y,h,m} c_{b,y,m} \big(P^{ch}_{b,y,h,m,\omega} + P^{dch}_{b,y,h,m,\omega}\big) \quad \forall \omega \tag{4.4}$$

$$E_{\omega}^{buy}(P_{y,h,m,l,\omega}^{r}, P_{y,h,m,\omega}^{'r}) = \lambda \sum_{y,h,m} \left(\sum_{l} P_{y,h,m,l,\omega}^{r} e_l + P_{y,h,m,\omega}^{'r} e_a \right) \quad \forall \omega \tag{4.5}$$

$$E_{\omega}^{sell}(P_{y,h,m,l,\omega}^{s}, P_{y,h,m,\omega}^{'s}) = \lambda \sum_{y,h,m} e_m \left(\sum_{l} P_{y,h,m,l,\omega}^{s} + P_{y,h,m,\omega}^{'s} + P_{y,h,m,\omega}^{d} \right) \quad \forall \omega \tag{4.6}$$

where factors $\lambda = 30$ and $\mathcal{H} = 288$ are used to carry out the calculations over the whole year, where $\mathcal{H}$ is the total number of representative hours in a year, i.e., $24 \times 12 = 288$ hours, based on a 24-hours average day for each of the 12 months. This approach is used to reduce the problem size in view of the long-term horizon typical of planning models, as described in Section 3.1. The units of each parameter and variable, for this and the following definitions and equations, are presented in the Nomenclature section.

4.1.2 Constraints

Installed DER Capacity

For each MG m, (3.2) can be used to calculate the total yearly installed capacity, while (3.3) can be used to update the amount of installed capacity at each year, as follows:

$$\mathcal{I}_{i,y,m} = \mathcal{A}_{i,y,m} + \mathcal{I}_{i,y-1,m} \quad \forall i, y, m \tag{4.7}$$

$$\mathcal{A}_{i,y,m} = \mathcal{N}_{i,y,m} \mathcal{R}_i \qquad \forall i, y, m \tag{4.8}$$

Note that in practice, the RESs of urban MGs, which is where MMG systems would be likely developed, are mainly solar generators. In addition, RES generation is limited by renewable resources; for example, the capacity of solar panels is limited by the real rooftop area of the houses inside each MG (e.g., see Figure 4.1). Thus:

$$\sum_{y} \mathcal{A}_{s,y,m} \leq \overline{\mathcal{I}}_m \qquad \forall s, m \tag{4.9}$$

Constraints (4.2), and (4.7) to (4.9) belong to the first stage optimization problem, where the decision on the required capacities of DERs for each MG is made without any realization of the uncertainties, i.e., there is no consideration of stochastic scenarios for these variables. Constraints (4.3) to (4.6) and all the equations discussed next belong to the second stage optimization problem, where the realization of the uncertainties influences the operation of the MMG system.

Figure 4.1: Sample of the roof areas considered in the case study determined using GIS tools.

Supply-Demand Balance

For the planning of MMG systems, in addition to the RESs and ESSs satisfying the demand within each MG and neighboring MGs, the ADN can also interact to sell and buy power. Thus, the summation of the power generated by RESs, batteries storage discharging power, the power received from other MGs, and the power received from the ADN should satisfy the MG consumer's demand plus the batteries storage charging power, the power sold to other MGs, and the power sold to the ADN, as follows:

$$\begin{aligned}\sum_{S} P_{s,y,h,m,\omega} + \sum_{B} P^{dch}_{b,y,h,m,\omega} + P^{r}_{y,h,m,\omega} + P'^{r}_{y,h,m,\omega} = P^{d}_{y,h,m,\omega} + \sum_{B} P^{ch}_{b,y,h,m,\omega} \\ + P^{s}_{y,h,m,\omega} + P'^{s}_{y,h,m,\omega} \quad \forall y, h, m, \omega\end{aligned} \tag{4.10}$$

Note that the variables and parameters in (4.10) are indexed by ω to show the realization within each scenario. Also, the power received/sold from/to other MGs are defined as follows:

$$P^{r}_{y,h,m,\omega} = \sum_{l} P^{r}_{y,h,m,l,\omega} \qquad \forall y, h, m, \omega \tag{4.11}$$

$$P^{s}_{y,h,m,\omega} = \sum_{l} P^{s}_{y,h,m,l,\omega} \qquad \forall y, h, m, \omega \tag{4.12}$$

with $P^{r}_{y,h,m,l,\omega} = P^{s}_{y,h,m,l,\omega}$ for any specific hour of the planning horizon. Furthermore, in order to prevent two MGs from selling and receiving power at the same time, the following

constraint is used:

$$P^{r}_{y,h,m,\omega} P^{s}_{y,h,m,\omega} = 0 \qquad \forall y, h, m, \omega \tag{4.13}$$

Similarly, any independent MG is not allowed to sell/receive power to/from the ADN at the same time, which can be modeled by:

$$P'^{r}_{y,h,m,\omega} P'^{s}_{y,h,m,\omega} = 0 \qquad \forall y, h, m, \omega \tag{4.14}$$

Operating Reserves

To accommodate uncertainties related to the interruption of electricity delivery from other MGs and the ADN, the batteries storage power capacity per hour $SOC_{b,y,h,\omega}$ has to be greater than the hourly demand and RES generation. Thus, (3.5) is modified as follows:

$$\sum_{B} SOC_{b,y,h,m,\omega} \geq P^{d}_{y,h,m,\omega} - \sum_{S} P_{s,y,h,m,\omega} \quad \forall h, y, m, \omega \tag{4.15}$$

This guarantees that each MG can withstand a failure that may disconnect it from the ADN at the PCC.

Operating Limits

The maximum power that any individual MG can sell to other MGs and the ADN at any hour and year during the planning horizon is given by the available RES power and battery storage discharge, as follows:

$$P^{s}_{y,h,m,\omega} + P'^{s}_{y,h,m,\omega} \leq P_{s,y,h,m,\omega} + P^{dch}_{b,y,h,m,\omega} \qquad \forall b, s, y, h, m, \omega \tag{4.16}$$

In addition, the power flow at the PCC is limited by the upper limit of the MV link, as follows:

$$|(P^{s}_{y,h,m,\omega} + P'^{s}_{y,h,m,\omega}) - (P^{r}_{y,h,m,\omega} + P'^{r}_{y,h,m,\omega})| \leq \overline{P}_{PCC} \quad \forall y, h, m, \omega \tag{4.17}$$

RES Generation

For every MG m, and stochastic scenario ω, the solar power generation output is computed using (3.18), as follows:

$$P_{s,y,h,m,\omega} = \varphi \mathcal{I}_{s,y,m} \left(\frac{G_{y,h,\omega}}{G_{stc}} \right) [1 + \iota(\tau_h - \tau_{stc})] \qquad \forall s, y, h, m, \omega \tag{4.18}$$

For wind power generation, (3.19) can be used, which considers wind speed and the turbine characteristics; however, as previously discussed, this type of generation is not expected in general in urban MGs, which are at the core of MMGs systems. Therefore, the models, simulations, and results presented in this chapter focus on solar generation.

Battery SOC and Limits

For every MG m and stochastic scenario ω (3.20) to (3.28) and (3.32) can be used to define the battery SOC, its boundaries, and the associated charging and discharging power limits. Thus, the following constraints are used to compute the SOC of the batteries:

$$SOC_{b,y,h+1,m,\omega} - SOC_{b,y,h,m,\omega} = \eta^{ch} P^{ch}_{b,y,h,m,\omega} - \frac{P^{dch}_{b,y,h,m,\omega}}{\eta^{dch}} \qquad \forall b, y, h, m, \omega \tag{4.19}$$

$$SOC_{b,y+1,1,m,\omega} - SOC_{b,y,\mathcal{H},m,\omega} = \eta^{ch} P^{ch}_{b,y,\mathcal{H},m,\omega} - \frac{P^{dch}_{b,y,\mathcal{H},m,\omega}}{\eta^{dch}} \qquad \forall b, y, h, m, \omega \tag{4.20}$$

where its upper and lower limits are imposed by:

$$SOC_{b,y,h,m,\omega} \leq \mathcal{I}_{b,y,m} \qquad \forall b, y, h, m, \omega \tag{4.21}$$

$$SOC_{b,y,h,m,\omega} \geq \delta \mathcal{I}_{b,y,m} \qquad \forall b, y, h, m, \omega \tag{4.22}$$

The maximum charging and discharging power limits are defined using the following constraints:

$$P^{dch}_{b,y,h,m,\omega} \leq \left(\frac{1-\delta}{t^{dch}} \right) \mathcal{I}_{b,y,m} \qquad \forall b, y, h, m, \omega \tag{4.23}$$

$$P^{ch}_{b,y,h,m,\omega} \leq \left(\frac{1-\delta}{t^{ch}} \right) \mathcal{I}_{b,y,m} \qquad \forall b, y, h, m, \omega \tag{4.24}$$

and the minimum discharging and charging power at a given hour are imposed by:

$$P^{dch}_{b,y,h,m,\omega} \geq u^{dch}_{b,y,h,m,\omega} \qquad \forall b, y, h, m, \omega \tag{4.25}$$

$$P^{ch}_{b,y,h,m,\omega} \geq u^{ch}_{b,y,h,m,\omega} \qquad \forall b, y, h, m, \omega \tag{4.26}$$

In order to prevent charging and discharging from occurring at the same time, the following equation is used:

$$P^{dch}_{b,y,h,m,\omega} P^{ch}_{b,y,h,m,\omega} = 0 \qquad \forall b, y, h, m, \omega \tag{4.27}$$

Finally, the life span of each battery for $\mathcal{C}$ cycles of charge and discharge is defined by the following constraint:

$$\sum_{h,y} (P^{ch}_{b,y,h,m,\omega} + P^{dch}_{b,y,h,m,\omega}) \leq \mathcal{C} \sum_{y} \mathcal{A}_{b,y,m} \quad \forall b, m, \omega \tag{4.28}$$

Equations (4.13), (4.14), and (4.27) are nonlinear and are linearized using the big $\mathcal{M}$ technique, as in (3.28) [125]. Equation (4.17) is also nonlinear thus absolute value properties are applied for its linearization as follows:

$$(P^{s}_{y,h,m,\omega} + P'^{s}_{y,h,m,\omega}) - (P^{r}_{y,h,m,\omega} + P'^{r}_{y,h,m,\omega}) \leq \overline{P}_{PCC} \quad \forall y, h, m, \omega \tag{4.29}$$

$$-(P^{s}_{y,h,m,\omega} + P'^{s}_{y,h,m,\omega}) + (P^{r}_{y,h,m,\omega} + P'^{r}_{y,h,m,\omega}) \leq \overline{P}_{PCC} \quad \forall y, h, m, \omega \tag{4.30}$$

4.1.3 TSSP Model

Using the set of equations described previously, the TSSP problem can be formulated as an MILP problem as follows:

$$\begin{aligned}
\min_{\mathcal{A}_i, P^r, P'r, P^s, P'^s} \quad & \text{Eq. (4.1)} \rightarrow \text{Total capital and operating costs} \\
\text{s.t.} \quad & \text{Eqs. (4.2) to (4.6)} \rightarrow \text{Costs functions} \\
& \text{Eqs. (4.7), to (4.9)} \rightarrow \text{Installed capacity} \\
& \text{Eqs. (4.10) to (4.14)} \rightarrow \text{Supply-demand} \\
& \text{Eq. (4.15)} \rightarrow \text{Reserves} \\
& \text{Eqs. (4.16) , (4.29) , (4.30)} \rightarrow \text{Operating limits} \\
& \text{Eq. (4.18)} \rightarrow \text{Solar power generation} \\
& \text{Eqs. (4.19) to (4.28)} \rightarrow \text{Batteries}
\end{aligned}$$

where capital and operating costs are minimized, considering cost functions that reflect the transactions among individual MGs and the ADN and the investment in DERs. This model considers the hourly operation of batteries and solar generation.

4.1.4 SSLP and Deterministic Models

The planning model presented in Sections 4.1.1 and 4.1.2 can also be formulated as a SSLP problem, where the first stage objective function and constraints are modified, as follows:

$$\begin{aligned} Z = \sum_{\omega} \Big(& C_{\omega}(\mathcal{A}_{i,y,m,\omega}) + O^{B}_{\omega}(P^{ch}_{b,y,h,m,\omega}, P^{dch}_{b,y,h,m,\omega}) + O^{S}_{\omega}(P_{s,y,h,m,\omega}) \\ & + E^{buy}_{\omega}(P^{r}_{y,h,m,l,\omega}, P'^{r}_{y,h,m,\omega}) - E^{sell}_{\omega}(P^{s}_{y,h,m,l,\omega}, P'^{s}_{y,h,m,\omega}) \Big) p_{\omega} \end{aligned} \tag{4.31}$$

$$C_{\omega}(\mathcal{A}_{i,y,m,\omega}) = \sum_{i,y,m} (K_{i,y,m}\mathcal{A}_{i,y,m,\omega}) \quad \forall \omega \tag{4.32}$$

$$\mathcal{I}_{i,y,m,\omega} = \mathcal{A}_{i,y,m,\omega} + \mathcal{I}_{i,y-1,m,\omega} \quad \forall i, y, m, \omega \tag{4.33}$$

$$\mathcal{A}_{i,y,m,\omega} = \mathcal{N}_{i,y,m,\omega}\mathcal{R}_{i} \qquad \forall i, y, m, \omega \tag{4.34}$$

$$\sum_{y} \mathcal{A}_{s,y,m,\omega} \leq \overline{\mathcal{I}_{m}} \qquad \forall m, \omega \tag{4.35}$$

The equation defining the solar power generation output is adjusted to consider (4.33) as follows:

$$P_{s,y,h,m,\omega} = \varphi \mathcal{I}_{s,y,m,\omega} \left(\frac{G_{y,h,\omega}}{G_{stc}} \right) [1 + \iota(\tau_{h} - \tau_{stc})] \qquad \forall s, y, h, m, \omega \tag{4.36}$$

Likewise, the constraints defining the SOC upper and lower limits, minimum charging and discharging power, and life span of the batteries need to be adjusted, respectively, so that the decisions on the yearly capacity additions are also included in the stochastic scenarios as follows:

$$SOC_{b,y,h,m,\omega} \leq \mathcal{I}_{b,y,m,\omega} \qquad \forall b, y, h, m, \omega \tag{4.37}$$

$$SOC_{b,y,h,m,\omega} \geq \delta \mathcal{I}_{b,y,m,\omega} \qquad \forall b, y, h, m, \omega \tag{4.38}$$

$$P^{dch}_{b,y,h,m,\omega} \leq \left(\frac{1-\delta}{t^{dch}} \right) \mathcal{I}_{b,y,m,\omega} \quad \forall b, y, h, m, \omega \tag{4.39}$$

$$P^{ch}_{b,y,h,m,\omega} \leq \left(\frac{1-\delta}{t^{ch}}\right) \mathcal{I}_{b,y,m,\omega} \quad \forall b, y, h, m, \omega \tag{4.40}$$

$$\sum_{h,y} (P^{ch}_{b,y,h,m,\omega} + P^{dch}_{b,y,h,m,\omega}) \leq \mathcal{C} \sum_{y} \mathcal{A}_{b,y,m,\omega} \qquad \forall b, m, \omega \tag{4.41}$$

Therefore, the planning model formulated as a SSLP problem is as follows:

$$\begin{aligned}
\min_{\mathcal{A}_i, P^r, P'^r, P^s, P'^s} \quad & \text{Eq. (4.31)} \rightarrow \text{Total capital and operating costs} \\
\text{s.t.} \quad & \text{Eqs. (4.32), (4.3) to (4.6)} \rightarrow \text{Costs functions} \\
& \text{Eqs. (4.33) to (4.35)} \rightarrow \text{Installed capacity} \\
& \text{Eqs. (4.10) to (4.14)} \rightarrow \text{Supply-demand} \\
& \text{Eq. (4.15)} \rightarrow \text{Reserves} \\
& \text{Eqs. (4.16), (4.29), (4.30)} \rightarrow \text{Operating limits} \\
& \text{Eqs. (4.36)} \rightarrow \text{Solar power generation} \\
& \text{Eqs. (4.19), (4.20), (4.37) to (4.40), (4.25) to (4.27), (4.41)} \rightarrow \text{Batteries}
\end{aligned}$$

The deterministic model can be obtained from the aforementioned SSLP model with only one scenario with probability one, where the uncertainties are approximated by their average values. In addition, (4.15) needs to be modified as follows:

$$\sum_{B} SOC_{b,y,h,m,\omega} \geq (1+\beta) P^{d}_{y,h,m,\omega} + \gamma \sum_{S} P_{s,y,h,m,\omega} \qquad \forall h, y, m, \omega \tag{4.42}$$

where β and γ represent arbitrary reserve values for demand and solar power. This conservative adequacy constraint is typically used to guarantee enough reserves to manage demand and solar RES uncertainties, as described in Section 3.1.2.

4.2 Simulations and Results

4.2.1 Case Study

The planning model presented in Section 4.1.3 is used to study the feasibility of implementing an MMG system consisting of 4 individual MGs, as illustrated in Figure 4.2, based

in Figure 2.3, embedded in an ADN at a municipality in the state of São Paulo, Brazil. The results of this model are compared with those obtained with the SSLP and deterministic models presented in Section 4.1.4 and MCS. All the input data, including technical, economic, and environmental parameters used for this case study are introduced next.

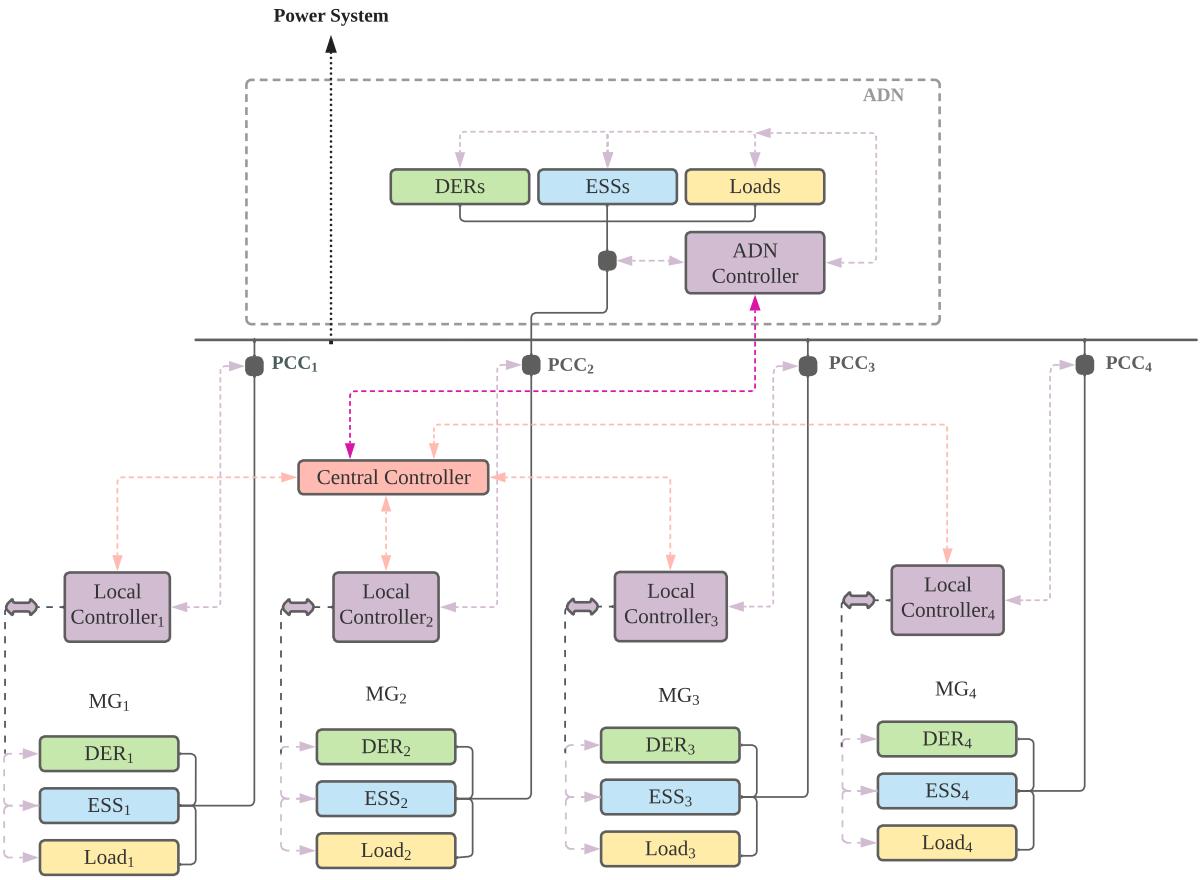

Figure 4.2: MMG system considered for the case study.

MMG System

For this case study, the MV grid of an ADN at a municipality in the state of São Paulo, Brazil is clustered to form MGs, taking into account the presence of rooftop solar panels and Electric Vehicle (EV) charging stations. Dijkstra's algorithm is used to find the shortest

paths between them, providing the location of a set of independent MGs, which are then ranked according to their performance in terms of voltage profiles and power losses using OpenDSS. For the case study, 7 clusters were identified as potential MGs. Furthermore, the deterministic long-term planning model presented in Section 4.1.4 is applied to each MG, considering null transactions with other MGs and the ADN, i.e., in isolated mode. With these considerations, only 4 MGs achieved an optimal solution and are therefore part of the MMG that is used for this case study. This process is summarized in Figure 4.3, and was led by colleagues at the University of ABC, in Santo André, São Paulo, Brazil.

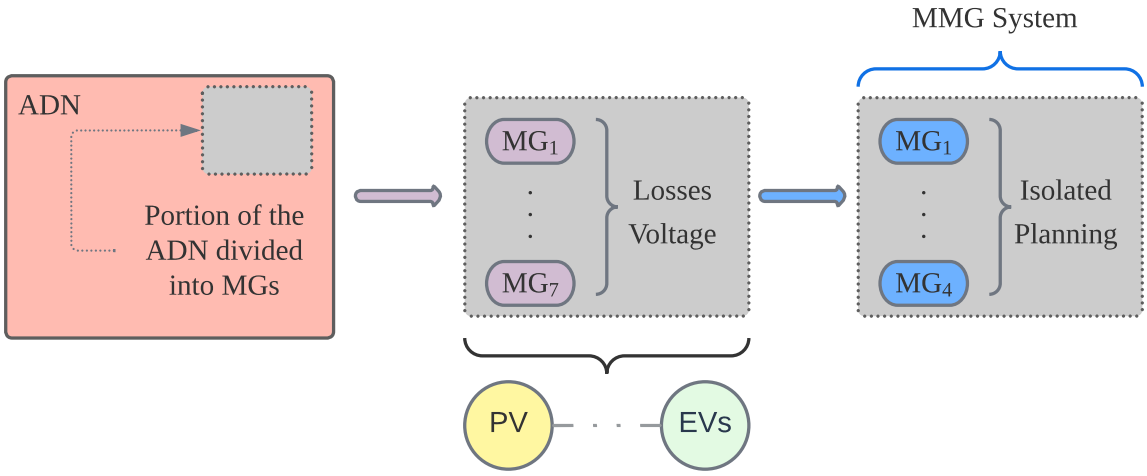

Figure 4.3: Selection of MGs for MMG system.

Electricity Demand

The hourly load for the 4 MGs is used to calculate the hourly averages for a year with 288 representative hours, as explained in Section 4.1.1. The load has been divided into variable and fixed parts, with the fixed demand representing EV demand not changing thorough the planning horizon, as depicted in Figure 4.4, since the adoption of EVs within the studied region is expected to be conservatively low for the considered planning horizon. The variable demand has been modeled using electricity demand obtained from [134] and growth rates obtained from [135], while the fixed demand has been modeled considering users' routine and traffic patterns in the state of São Paulo, Brazil, without considering smart chargers, as per [136].

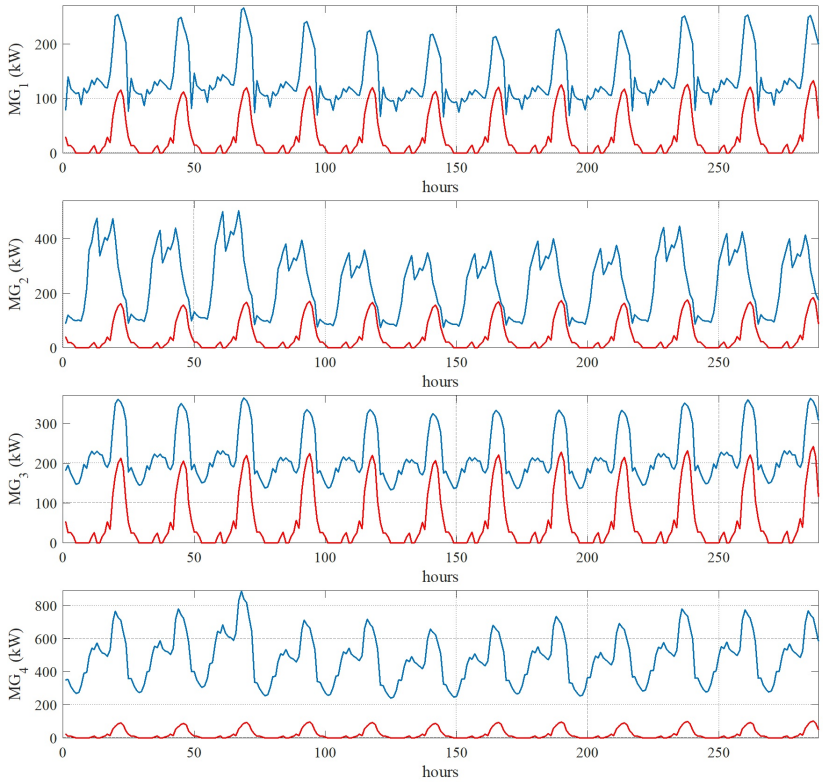

Figure 4.4: MG demand: variable in blue, and fixed (EVs) in red.

Solar Panels

Solar panels are assumed to be connected through an inverter to the MGs. Hourly data for solar irradiance and ambient temperature are synthetically generated using PVsyst software considering statistical and meteorological constraints [137, 138]. The cell temperature, which is the temperature of the surface of the PV array, is computed considering the ambient temperature and other manufacture parameters, according to [139]. Thus, the average solar irradiance, cell temperature, and resulting power obtained using (3.18) are presented in Figure 4.5, which are computed using the monthly hourly average for cell temperature and solar irradiance. The operational parameters and costs associated with the panels are shown in Table 4.1, as per [129,140]. In addition, the limits for solar capacity for all MGs, obtained using GIS tools, are 3271 kW for MG_1, 2665 kW for MG_2, 3834 kW for MG_3, and 1562 kW for MG_4.

Table 4.1: Solar panels parameters

$K_{s,1,m}$ $\forall m$ [\$/kW]	$c_{s,1,m}$ $\forall m$ [\$/kWh]	ι [pu/°C]	φ [%]	τ_{stc} [°C]	G_{stc} [kW/m^2]	Lifetime [years]
871	0.002487	-0.041	98	25	1	20

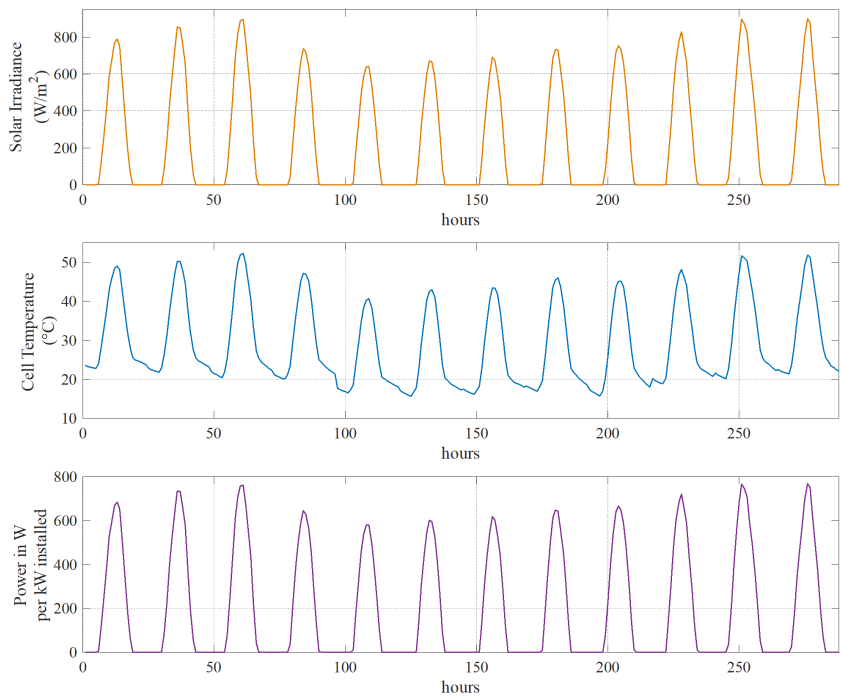

Figure 4.5: Average solar irradiance, cell temperature, and resulting power availability in W per kW installed for a municipality in the state of São Paulo, Brazil.

Batteries

The battery packs in the MMG planning model are assumed to be lithium iron phosphate batteries with 20 kWh and 8 kW peak power of charge/discharge, i.e., $t^{ch} = t^{dch} = 2h$ with

$\delta = 0.2$. The economic and technical parameters for the implemented battery model are presented in Table 4.2, as per [129,141], which yields a battery capital cost of 1,380 \$/kW.

Table 4.2: Battery parameters

$K_{b,1,m}$ $\forall m$ [\$/kWh]	$c_{b,1,m}$ $\forall m$ [\$/kWh]	η_{Ch} [%]	η_{DCh} [%]	Lifetime [Cycles]
654	0.00187	81.6 %	81.6%	10,000

Scenario Tree

The first step in building the scenario tree is the definition of the statistical properties of the uncertain parameters. Daily average solar irradiance between 1983 and 2007 and total electricity consumption for Brazil between 1985 and 2020 are used to estimate the load and irradiance pdfs from the given data. For the demand, a goodness-of-fit test indicates that the parameter ζ and the increments in demand can be approximated by a Normal distribution (Figure 4.6-a and Figure 4.6-b), and its statistical properties are presented in Table 4.4. A goodness-of-fit test is used for solar irradiance, as depicted in Figure 4.6-c, showing that this parameter can also be approximated with a Normal distribution, and its statistical properties are presented in Table 4.3. This information is used to build the GBM statistical properties according to Section 2.3.4, which are presented in Table 4.5.

The scenario tree presented in Figure 4.7 has been created considering three statistical measures for both demand and solar irradiance: expected value $\mathbb{E}$, variance $\mathbb{V}ar$, and skewness sk. In addition, the scenario tree has been built so that the probability of each scenario is greater than 2% or confidence levels greater than 98%; this assures that scenarios with extremely low probabilities of occurrence are not included in the planning process. The model follows the approach presented in Section 2.3.4, and aims to minimize the square distance between the specified discrete statistical measures and the observed statistical measures presented in Tables 4.3 and 4.5, respectively [138, 142]. Given the nonlinear nature of the MM approach, and assuming that the probabilities of the scenarios are problem variables, a high number of statistical properties could be obtained, which can lead to costly computation and infeasible solutions of the NLP problem. Therefore, in order to maintain a proper balance between the statistical characteristics of the scenarios and the size of the tree, the total number of scenarios should be at least equal to the total number of statistical measures plus one degree of freedom. Therefore, for the present case

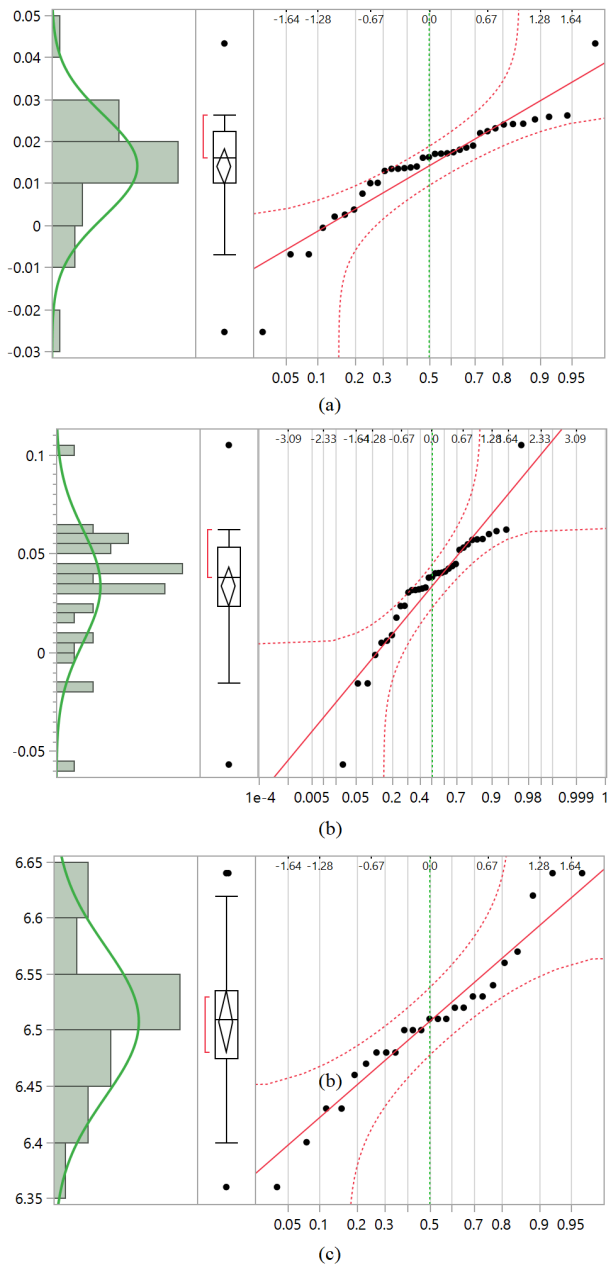

Figure 4.6: Normal quantile plots for (a) ζ factor, (b) demand growth, and (c) solar irradiance using JMP software.

study, there should at least be 7 scenarios (2 $\mathbb{E}$, 2 $\mathbb{V}ar$, 2 sk, plus 1 additional scenario); however, 9 scenarios are chosen to reduce computational burden and guarantee neither under nor over specification [107, 108]. The nodes in the tree represent the states in the planning horizon for the demand growth rate with respect to year 1 and solar irradiance annual average with their respective probabilities. These scenarios are used for both the TSSP and SSLP problems.

Table 4.3: Observed daily solar irradiance per year

Expected Value	Variance	Skewness
6.5076	0.0045107	0.132724

Table 4.4: Demand statistical properties

$\zeta = \log(P^d_{y+1}/P^d_y)$			$\Delta P^d_y = P^d_{y+1} - P^d_y$		
Mean	Variance	Skw.	Mean	Variance	Skw.
0.014148	0.00015	0.0036	0.0335	0.0008112	0.1327

Table 4.5: GBM Statistical properties

Expected Value	Variance	Skewness
$\mathbb{E}(P^d_{y+1}) = 1.014324P^d_y$	$\mathbb{V}ar(P^d_{y+1}) = 0.000151P^d_y$	sk=0.036

4.2.2 Assumptions and Simulation Criteria

The NLP problem needed for the generation of the scenario tree and introduced in Section 4.2.1 was solved in GAMS [143], using the SNOPT solver. The MILP models, described in Sections 4.1.3 and 4.1.4, were solved using GAMS, with the CPLEX solver. All the models were solved in a server with an Intel Xeon CPU at 1.87 GHz. The following are the assumed values for the remaining model parameters:

- The discount rate is $d = 0.08$ pu (8%), which is a typical private investment rate.

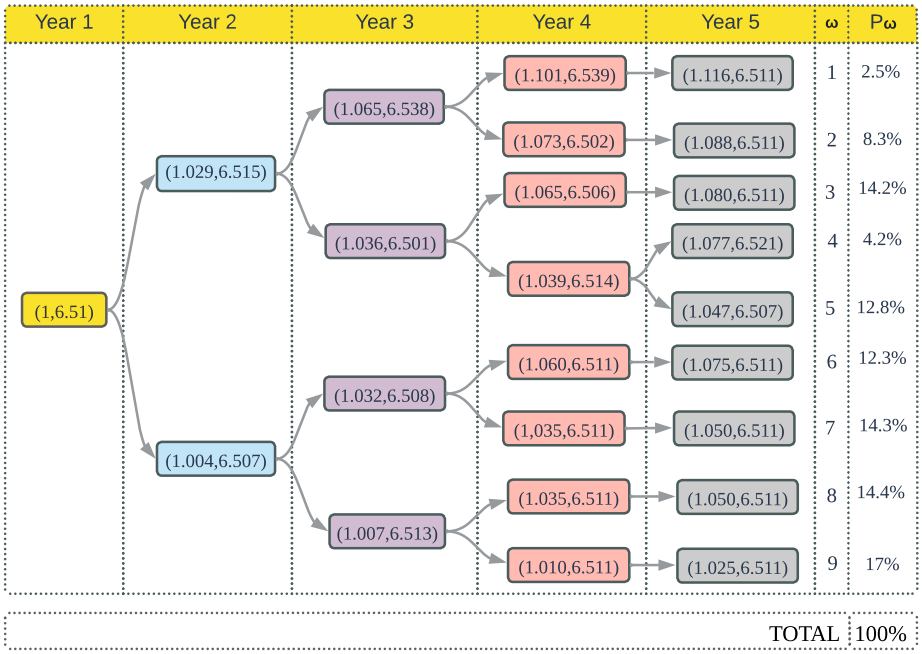

Figure 4.7: Scenario tree for the planning of the MMG system, with a growth factor for variable demand with respect to year 1 and average solar irradiance.

- The planning horizon chosen for this study is 5 years, as per [144–146], which is a typical horizon used in distribution system planning studies in Brazil.
- $\theta_1 = 2$ for the expected value $\mathbb{E}$, $\theta_2 = 2$ for the variance $\mathbb{V}ar$, to prioritize these measures over the skewness sk with $\theta_3 = 1$, as per [108, 110].
- Conservative operation reserves for system adequacy in the deterministic model: 25% for solar ($\gamma = 0.25$), and 10% for load ($\beta = 0.1$), as per [132].
- The base daily prices for a 24-hour operation are, as per [142]: 0.11 \$/kWh for $h = 17$ (intermediate), 0.17 \$/kWh for $18 < h \leq 20$ (peak), and 0.08 \$/kWh otherwise (off-peak). These prices are the same for all participants, and therefore $e_a = e_s = e_m$.
- Electricity price growth 4.81%/year, as per [142].
- The cost of solar panels and batteries decreases every year, by 9% for solar panels and 21.1% for batteries, respectively, as per [147].

- The O&M costs increase by 3% every year, as per the current average inflation in Brazil [148].
- 800 iterations are needed for MCS since the moving average of the objective function converges at around this value.
- The limit for the power transfer at the MG PCCs is 1200 kW, as per the capacity of the existent distribution feeders.
- At least 10% of the maximum available capacity of solar generation should be included for each MG; otherwise, the model does not include them due to the cost minimization approach and low grid electricity costs.

4.2.3 Numerical Results

The results of the simulations are presented and discussed in this section. In Table 4.6, the capacities of solar panels and batteries needed for the MMG system and the total cost associated with each planning model are presented. The following observations can be made from the obtained results:

- The deterministic model is the most expensive and most conservative model, due to the arbitrary and conservative reserve requirements. Thus, the total cost is 15.6% higher than the SSLP model, 14.1% higher than the TSSP model, and 12.7% higher than the MCS model, which is considered the benchmark for the planning results.
- The total cost of TSSP is 16.4% lower than the deterministic model, 1.6% lower than the MCS model, and 1.8% higher than the SSLP model. This seems acceptable since, in this problem, the decisions on the amount of new equipment are made in the first stage, without any realization of the uncertainties. Thus, the mathematical model would attempt to satisfy all the operative conditions associated with the operative scenarios in the second stage. Moreover, the closeness of this model's performance to the MCS model's performance suggests that the number and statistical properties of the scenarios are neither under- nor over-specified.
- The SSLP model is the cheapest, where the total cost is 18.5% lower than the deterministic model, 1.8% lower than the TSSP model, and 3.4 % lower than MCS. This model offers the least conservative results as the decision on the amount of batteries and solar panels that should be installed inside each MG is made considering that the realization of the uncertainties happens beforehand.

In Figure 4.8, the capacity additions for the MMG system are shown, and Figure 4.9 presents the operation of the MMG system for year 5. As observed in Figure 4.8, the majority of the capacity is installed at the beginning of the planning horizon and smaller quantities are added later. This is of special interest to Brazilian distribution companies, as they seek to invest during the first years of the project when government incentives for sustainable technologies are available. Moreover, as observed in Figure 4.9, for each MG the model decides on the energy that needs to be purchased, the energy that can be sold, and guarantees demand-supply considering the internal generation and storage resources for every hour during the planning horizon. In addition, it can be observed how the internal generation is used to trade energy with other MGs, as expected, given the collaboration among the participants. For example, at 10 am, when there is high solar power generation, MG_2 is buying 200 kW from MG_3 and 70 kW from MG_4; similarly, MG_4 is buying 171 kW from MG_1. This decreases the amount of power that needs to be imported from the ADN, which reduces congestion and increases reliability.

As observed in Table 4.6, the total solar capacities for the MMG system are very similar among the planning models, since this RES has to be forced, as previously explained. Nevertheless, there is a difference in the capacities of batteries planned for each independent MG. As explained in Section 2.3.3, TSSP models make an important differentiation of the variables according to whether they are enforced before or after the realization of the uncertain values, which is closer to an actual planning process. As depicted in Table 4.6, the total cost of the TSSP model is closer to the MCS benchmark value than the SSLP model. In addition, the standard deviation of the difference in the battery capacity additions for each independent MG with respect to MCS benchmark is 11.6 kWh for the TSSP model and 19.6 kWh for the SSLP model, which indicates that there is less variability or spread in the TSSP results. Thus, the TSSP model guarantees the optimal distribution of the required RESs and ESSs resources among the participant MGs, making it superior to the SSLP model, at reasonable computational costs. Thus, the solution of the TSSP model is 81.03% faster than the MCS benchmark, and at least 2.43% faster than the SSLP model, which is important considering that the larger the problem the more relevant the computational costs become.

4.2.4 Sensitivity Analysis

The impact of RES and EV penetration levels in the planning problem is examined here by considering different RES targets and EV demand levels. Thus, the RES requirements are varied from 5% to 50%, which is the maximum RES penetration for which a solution can be obtained, in 5% increments of the maximum available capacity of solar generation.

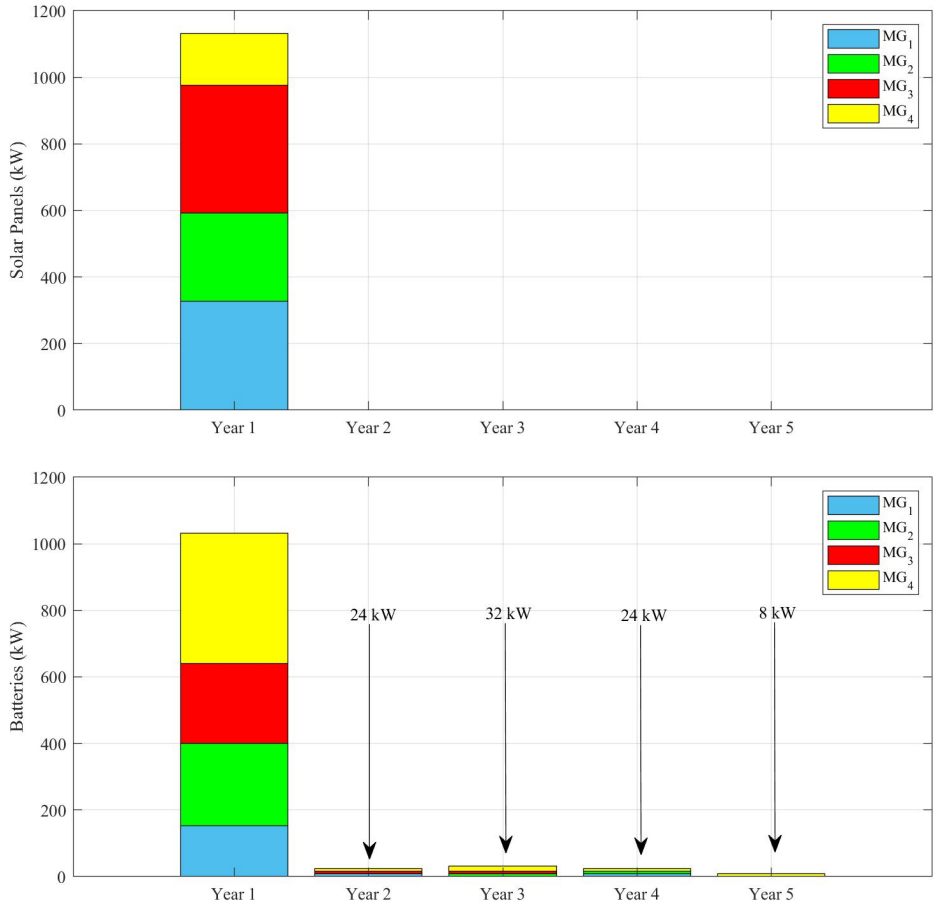

Figure 4.8: Yearly capacity additions for TSSP model.

On the other hand, given the low adoption rate of EVs in the region being studied, their demand is assumed to double in increments of 10%, corresponding to 10 to 50% of the MGs peak loads, which is not very likely in practice; nevertheless, to analyze a more significant EV penetration, an additional increase of 100% in EV demand is also simulated. For these studies, RES minimum penetration requirements are kept at 5% of the maximum available capacity of solar generation, so that proper comparisons with respect to the base values can be made.

The results of increasing the RES penetration requirements are presented in Figure 4.10, where, for example, it can be observed that the total cost of planning is increased

Table 4.6: Total cost, computational cost, and capacities of solar panels and batteries at the end of year 5

Deterministic model					
MG	Batteries [kWh]	Batteries [kW]	Solar [kW]	Total Cost [M$]	Computational Cost [hh:mm:ss]
1	460	184	327		
2	740	296	266		
3	720	288	383	2.18	00:02:13
4	1200	480	156		
Total	3120	1248	1132		
MCS model - Benchmark					
MG	Batteries [kWh]	Batteries [kW]	Solar [kW]	Total Cost [M$]	Computational Cost [hh:mm:ss]
1	429	172	327		
2	689	275	267		
3	661	265	384	1.90	22:07:23
4	1121	449	164		
Total	2901	1160	1142		
TSSP model					
MG	Batteries [kWh]	Batteries [kW]	Solar [kW]	Total Cost [M$]	Computational Cost [hh:mm:ss]
1	420	168	327		
2	660	264	266		
3	640	256	383	1.87	04:11:51
4	1080	432	156		
Total	2800	1120	1132		
SSLP model					
MG	Batteries [kWh]	Batteries [kW]	Solar [kW]	Total Cost [M$]	Computational Cost [hh:mm:ss]
1	405	162	327		
2	642	257	266		
3	628	251	383	1.84	04:17:58
4	1128	451	156		
Total	2802	1121	1132		

by 3.85% with respect to the costs with 5% penetration, if RES are 10% of the maximum

available capacity of solar generation by the end of the planning horizon. Note that there is a sudden cost increase at 45% RES penetration, where the total cost increases by 11.5%, and after 50% RES penetration, the problem becomes infeasible.

Figure 4.11 illustrates the impact of EV penetration increases. Observe that a 10% increment in the EV demand results in a total cost increase of 1.79% on average, which is directly associated with an average 1.78% increase in ESS capacity. Also, observe that there is a slight increase in RES penetration for all MGs, which is also observed when the EV demand is increased to 200%, resulting in a 40.77% increment in total costs due mainly to a 40.71% increase in ESS capacity with respect to the Base case. From all these results, it can be concluded that the increase in RES penetration has a significant impact on the total costs and solution feasibility, while the increase in EV demand affects the total cost in proportion to the additional ESS capacity required to supply the EVs charging in the MMG system.

4.3 Summary

In this chapter, a TSSP model for the planning of MMGs in ADNs was presented. The model aims to minimize the total costs while benefiting from interconnections of MGs, considering uncertainties associated with electricity demand and RES using GBM and associated pdfs. Moreover, the model includes long-term purchase decisions and short-term operational constraints, using GIS to realistically estimate rooftop solar limits. The planning model was used to study the feasibility of implementing an MMG system consisting of 4 individual MGs at an ADN in a municipality in the state of São Paulo, Brazil. The results showed that the TSSP model tends to be less conservative than the deterministic planning model, while performing faster than a SSLP algorithm, with higher accuracy.

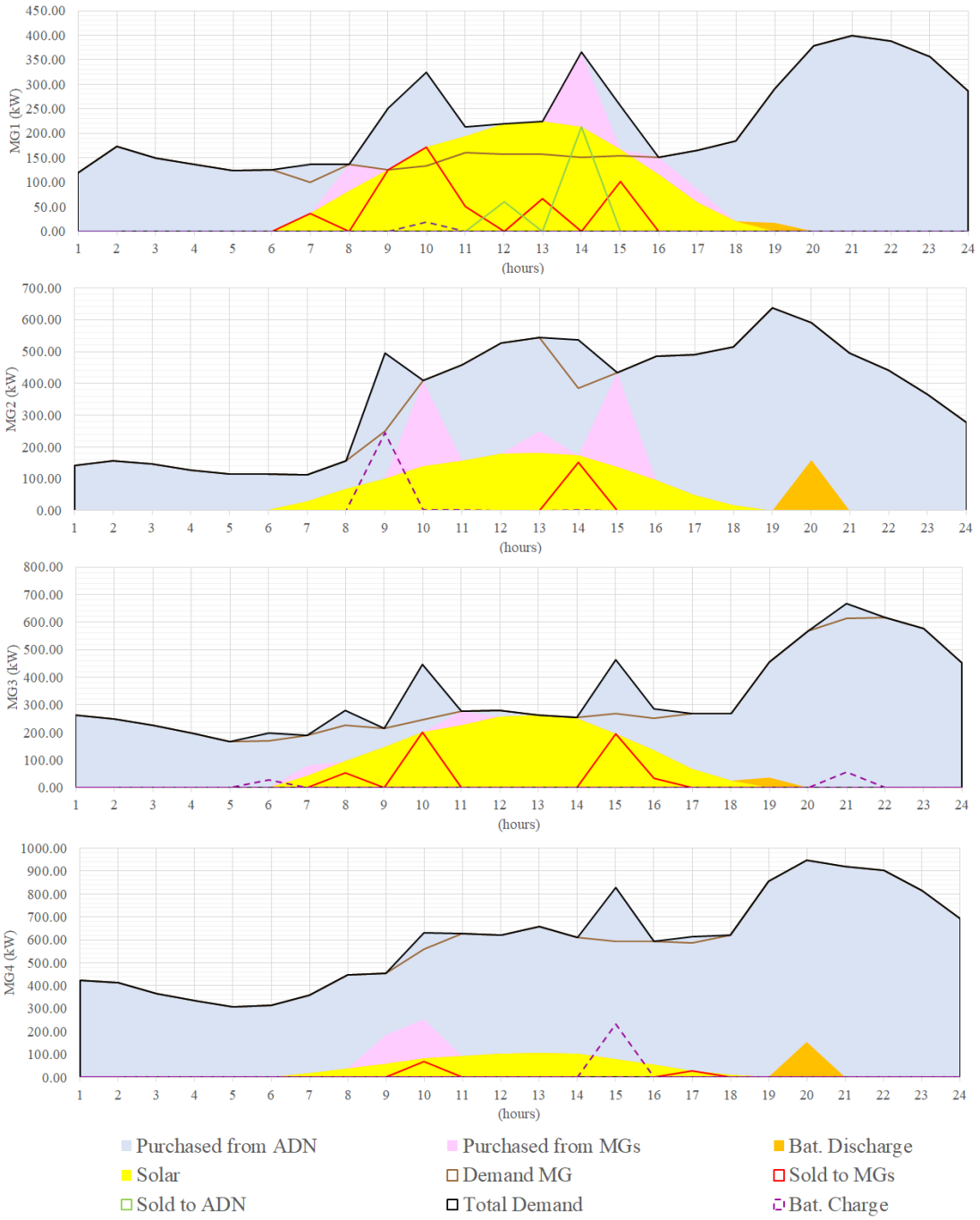

Figure 4.9: Dispatch for each MG for the representative day of January at year 5.

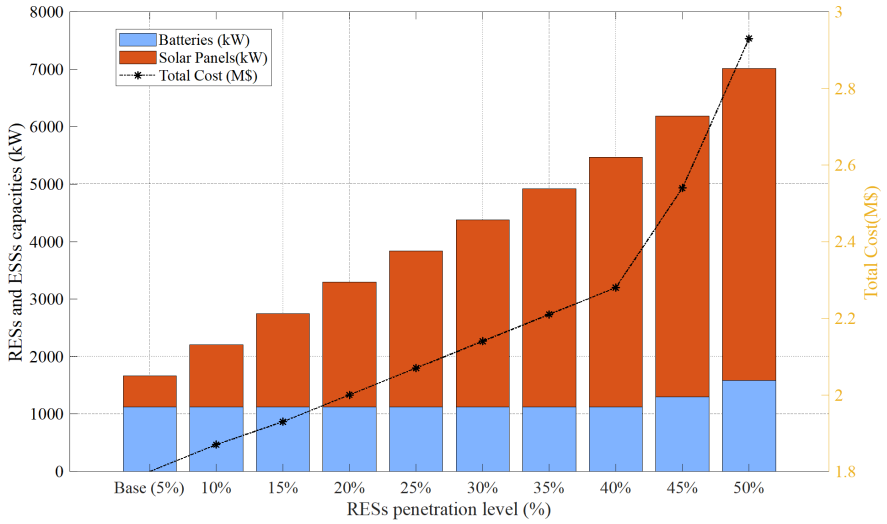

Figure 4.10: Sensitivity analysis with respect to varying levels of RES penetration for the Base case EV demand.

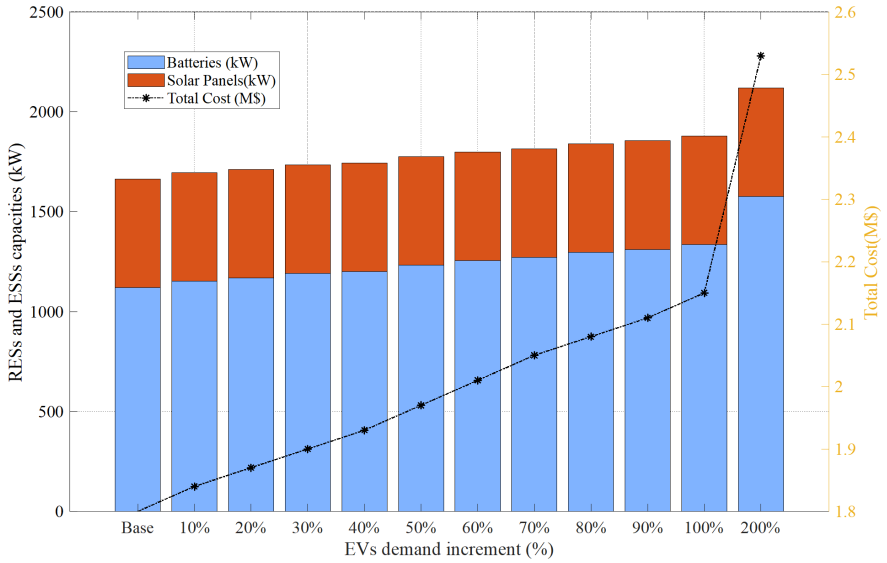

Figure 4.11: Sensitivity analysis with respect to varying levels of EV demand for the Base case minimum required RES penetration.

Chapter 5

GI-based Stochastic Optimization Model for Multi-Microgrid Planning

In this chapter, the TSSP model presented in Chapter 4 is extended by incorporating the ADN LV grid. Here, GIS tools along with DL techniques are used to accurately model the MV/LV ADN, and high-resolution satellite imagery is used to define the actual RES availability, in order to more realistically plan an MMG system within the ADN.

5.1 Medium and Low Voltage Grid Planning Model

The model presented in this chapter is an extension of the one presented in Chapter 4 by incorporating the MV/LV grid, as depicted in Figure 5.1. The objective of the model is to define the minimum required capacity for the transformers to supply demand, while focusing on the investment in DERs within ADNs. Therefore, the sub-index t, which represents the distribution transformers, is introduced in the operational and investment variables and parameters, except for the variables indicating the energy transactions among MGs and the ADN, as they take place at MV levels. Hence, the model decides the location of RES and ESS capacities at the MV/LV transformers for each MG. The output of the model is the planned capacities of RESs and ESSs, and the size of MV/LV distribution transformers required to satisfy the hourly demand of an MMG system over the planning horizon.

Similar to the model presented in Chapter 4, the MV grid is modeled by considering the maximum power transfer capacity at the PCC, whereas the LV grid is modeled by

including the capacity of the MV/LV transformers as well as the number of the served users, without considering the feeders. Furthermore, in this extended model, for every year, the investment in battery capacities is included using integer variables, and solar capacities are included using continuous variables. Binary variables are used to represent the hourly charging and discharging status of batteries, and power transactions between the participant MGs and the ADN, whereas the size of the MV/LV transformers, RESs, and ESSs is specified using integer variables. The variables representing the power generation, battery charge, discharge, and hourly SOC, and the power transactions are continuous. Therefore, this model can also be characterized as an MILP problem. The capital cost of the MV/LV transformers is not considered here so the results of applying the model can be directly compared to those obtained with the model from Chapter 4.

5.1.1 Objective Function

The objective function (4.1) as well as the cost functions (4.5) and (4.6) described in Section 4.1.1 hold for the MMG planning problem presented in this chapter. However, in order to consider the aggregation of DERs at each transformer, functions (4.2) to (4.4) are redefined as follows:

$$C(\mathcal{A}_{i,y,m,t}) = \sum_{i,y,m,t} K_{i,y,m}\mathcal{A}_{i,y,m,t} \tag{5.1}$$

$$O^S_\omega(P_{s,y,h,m,t,\omega}) = \lambda \sum_{s,y,h,m,t} \left(c_{s,y,m}P_{s,y,h,m,t,\omega}\right) \quad \forall\omega \tag{5.2}$$

$$O^B_\omega(P^{ch}_{b,y,h,m,t,\omega}, P^{dch}_{b,y,h,m,t,\omega}) = \lambda \sum_{b,y,h,m,t} c_{b,y,m}\left(P^{ch}_{b,y,h,m,t,\omega} + P^{dch}_{b,y,h,m,t,\omega}\right) \quad \forall\omega \tag{5.3}$$

5.1.2 Constraints

Installed DER Capacity

As observed in Figure 5.1, the solar panels and the RES and ESS capacities within each MG are considered to be distributed among the MV/LV transformers. Thus, for each MG m, (3.2) and (3.2) are used to define the corresponding DERs installed capacities seen at each transformer t as follows:

$$\mathcal{I}_{i,y,m,t} = \mathcal{A}_{i,y,m,t} + \mathcal{I}_{i,y-1,m,t} \qquad \forall i, y, m, t \tag{5.4}$$

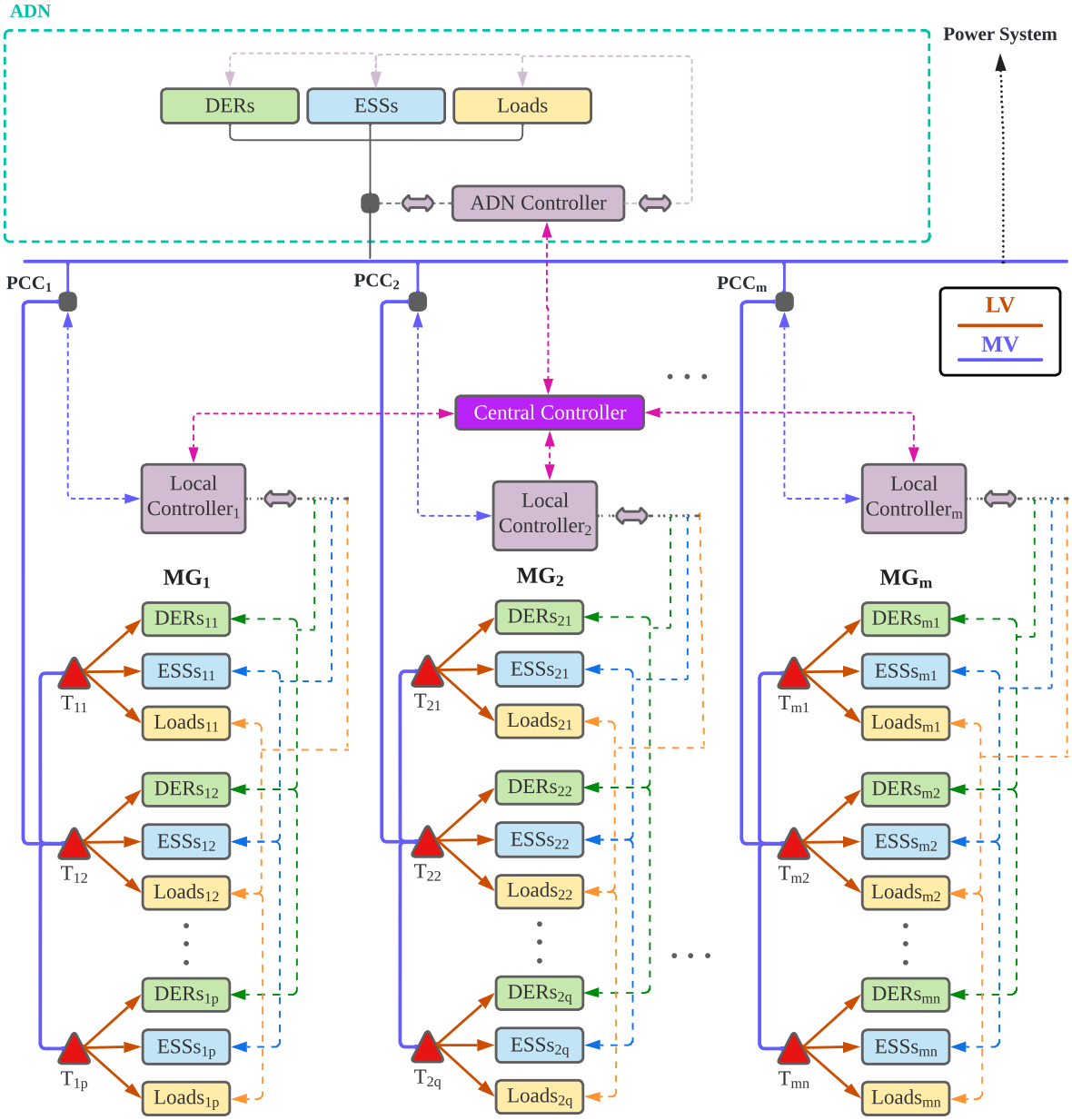

Figure 5.1: General overview of an MMG system with consideration of the LV grid.

where:

$$\mathcal{A}_{i,y,m,t} = \mathcal{N}_{i,y,m,t}\mathcal{R}_i \qquad \forall i, y, m, t \tag{5.5}$$

Furthermore, the capacity of solar panels is limited by the real rooftop area of the houses inside each MG as follows:

$$\sum_{y,t} \mathcal{A}_{s,y,m,t} \leq \sum_{t} \overline{\mathcal{I}}_{m,t} \qquad \forall s, m \tag{5.6}$$

Supply-Demand Balance

The total demand in the MMG system is equal to the summation of the MG consumer's demand, the batteries storage charge, the power sold to other MGs, and the power sold to the ADN. This demand should be satisfied by the summation of the power generated by RESs, batteries storage discharge, the power received from other MGs, and the power received from the ADN, as follows:

$$\begin{aligned} &\sum_{S,t} P_{s,y,h,m,t,\omega} + \sum_{B,t} P^{dch}_{b,y,h,m,t,\omega} + P^{r}_{y,h,m,\omega} + P'^{r}_{y,h,m,\omega} = \\ &\sum_{t} P^{d}_{y,h,m,t,\omega} + \sum_{B,t} P^{ch}_{b,y,h,m,t,\omega} + P^{s}_{y,h,m,\omega} + P'^{s}_{y,h,m,\omega} \\ &\qquad\qquad\qquad\qquad\qquad\qquad\qquad\qquad \forall y, h, m, \omega \end{aligned} \tag{5.7}$$

where the power received/sold from/to other MGs are defined by (4.11) and (4.12) with $P^{r}_{y,h,m,l,\omega} = P^{s}_{y,h,m,l,\omega}$ for any specific hour of the planning horizon. In addition, (4.13) and (4.14) prevent any independent MG from selling/receiving power to/from the ADN at the same time.

Operating Reserves

To guarantee each MG can withstand a failure that may cause their disconnection from the ADN at the PCC, the following constraint, which is based on (4.15), is used to keep an adequate amount of energy in the batteries at all times:

$$\sum_{B,t} SOC_{b,y,h,m,t,\omega} \geq \sum_{t} P^{d}_{y,h,m,t,\omega} - \sum_{S,t} P_{s,y,h,m,t,\omega} \qquad \forall h, y, m, \omega \tag{5.8}$$

Operating Limits

The power that each individual MG can sell to other MGs and the ADN is limited by the available RES power and battery storage discharge seen at each MV/LV transformer, and is enforced by the following constraint, which is based on (4.16):

$$P^{s}_{y,h,m,\omega} + P'^{s}_{y,h,m,\omega} \leq \sum_{t} (P_{s,y,h,m,t,\omega} + P^{dch}_{b,y,h,m,t,\omega}) \qquad \forall b, s, y, h, m, \omega \tag{5.9}$$

In addition, the limit in the power flow at the PCC is represented by (4.29) and (4.30) as a function of the power transacted at that point. Similarly, the capacity of each transformer is limited by its power flow, as follows:

$$|P_{s,y,h,m,t,\omega} + P^{dch}_{b,y,h,m,t,\omega} - P^{d}_{y,h,m,t,\omega} - P^{ch}_{b,y,h,m,t,\omega}| \leq T_{m,t} \qquad \forall b, s, y, h, m, t, \omega \tag{5.10}$$

which is nonlinear and thus absolute value properties are applied for its linearization as follows:

$$(P_{s,y,h,m,t,\omega} + P^{dch}_{b,y,h,m,t,\omega}) - (P^{d}_{y,h,m,t,\omega} + P^{ch}_{b,y,h,m,t,\omega}) \leq T_{m,t} \qquad \forall b, s, y, h, m, t, \omega \tag{5.11}$$

$$-(P_{s,y,h,m,t,\omega} + P^{dch}_{b,y,h,m,t,\omega}) + (P^{d}_{y,h,m,t,\omega} + P^{ch}_{b,y,h,m,t,\omega}) \leq T_{m,t} \qquad \forall b, s, y, h, m, t, \omega \tag{5.12}$$

RES Output

For every MG m, transformer t, and stochastic scenario ω, the power output of solar panels is computed based on (3.18) as a direct function of the hourly incident irradiance, hourly cell temperature, and derating factor, as follows:

$$P_{s,y,h,m,t,\omega} = \varphi \mathcal{I}_{s,y,m,t} \left(\frac{G_{y,h,\omega}}{G_{stc}} \right) [1 + \iota(\tau_h - \tau_{stc})] \qquad \forall s, y, h, m, t, \omega \tag{5.13}$$

Note that RES power from wind is not considered in the model, as wind turbine deployment in urban areas is unlikely as of now. However, such RES can be easily included in the model, based on (3.19), as previously mentioned.

Battery SOC and Limits

For every MG m, transformer t, and stochastic scenario ω, (3.20) to (3.28) and (3.32) can be used to define the battery SOC, its boundaries, and the associated charging and discharging power limits. Hence, the battery SOC and its upper and lower limits are defined, respectively, as follows:

$$SOC_{b,y,h+1,m,t,\omega} - SOC_{b,y,h,m,t,\omega} = \eta^{ch} P^{ch}_{b,y,h,m,t,\omega} - \frac{P^{dch}_{b,y,h,m,t,\omega}}{\eta^{dch}} \qquad \forall b, y, h, m, t, \omega \tag{5.14}$$

$$SOC_{b,y+1,1,m,t,\omega} - SOC_{b,y,\mathcal{H},m,t,\omega} = \eta^{ch} P^{ch}_{b,y,\mathcal{H},m,t,\omega} - \frac{P^{dch}_{b,y,\mathcal{H},m,t,\omega}}{\eta^{dch}} \qquad \forall b, y, h, m, t, \omega \tag{5.15}$$

$$SOC_{b,y,h,m,t,\omega} \leq \mathcal{I}_{b,y,m,t} \qquad \forall b, y, h, m, t, \omega \tag{5.16}$$

$$SOC_{b,y,h,m,t,\omega} \geq \delta \mathcal{I}_{b,y,m,t} \qquad \forall b, y, h, m, t, \omega \tag{5.17}$$

The charge and discharge power upper limits, and minimum charging and discharging power are defined, respectively, by the following constraints:

$$P^{ch}_{b,y,h,m,t,\omega} \leq \left(\frac{1-\delta}{t^{ch}}\right) \mathcal{I}_{b,y,m,t} \quad \forall b, y, h, m, t, \omega \tag{5.18}$$

$$P^{dch}_{b,y,h,m,t,\omega} \leq \left(\frac{1-\delta}{t^{dch}}\right) \mathcal{I}_{b,y,m,t} \quad \forall b, y, h, m, t, \omega \tag{5.19}$$

$$P^{dch}_{b,y,h,m,t,\omega} \geq u^{dch}_{b,y,h,m,t,\omega} \qquad \forall b, y, h, m, t, \omega \tag{5.20}$$

$$P^{ch}_{b,y,h,m,t,\omega} \geq u^{ch}_{b,y,h,m,t,\omega} \qquad \forall b, y, h, m, t, \omega \tag{5.21}$$

And the following constraint is used to guarantee that battery charging and discharging do not take place at the same time:

$$P^{dch}_{b,y,h,m,t,\omega} P^{ch}_{b,y,h,m,t,\omega} = 0 \qquad \forall b, y, h, m, t, \omega \tag{5.22}$$

which is nonlinear and is linearized using the big $\mathcal{M}$ technique, as in (3.28). Finally, the following constraint defines the life span of each battery for $\mathcal{C}$ cycles of charge and discharge:

$$\sum_{h,y} (P^{ch}_{b,y,h,m,t,\omega} + P^{dch}_{b,y,h,m,t,\omega}) \leq \mathcal{C} \sum_{y} \mathcal{A}_{b,y,m,t} \quad \forall b, m, t, \omega \tag{5.23}$$

5.1.3 TSSP Model

Using the set of equations listed previously, the TSSP problem can be formulated as an MILP problem where capital and operating costs are minimized, considering cost functions that reflect the transactions among individual MGs and the ADN and the investment in DERs. This model takes into account the hourly operation of batteries and solar generation, and is defined as follows:

$$\begin{aligned}
\min_{\mathcal{A}_i, P^r, P'r, P^s, P's} \quad & \text{Eq. (4.1)} \rightarrow \text{Total capital and operating costs} \\
\text{s.t.} \quad & \text{Eqs. (5.1) to (5.3), (4.5), (4.6)} \rightarrow \text{Costs functions} \\
& \text{Eqs. (5.4), to (5.6)} \rightarrow \text{Installed capacity} \\
& \text{Eq. (5.7)} \rightarrow \text{Supply-demand,} \\
& \text{Eq. (5.8)} \rightarrow \text{Operating reserves} \\
& \text{Eqs. (5.9), (4.29), (4.30), (5.11), (5.12)} \rightarrow \text{Operating limits} \\
& \text{Eqs. (5.13)} \rightarrow \text{Solar power generation} \\
& \text{Eqs. (5.14) to (5.23)} \rightarrow \text{Batteries}
\end{aligned}$$

5.2 DER and LV Network Identification through GIS Tools

5.2.1 Solar PV Potential

As mentioned in Section 2.4.1, building footprints can be detected using DL, which leads to defining available rooftop areas for the installation of solar panels. This workflow is carried out in ArcGIS Pro over high-resolution imagery, following the steps presented in Figure 5.2. This process includes: data *preparation* by creating labels of the elements to be detected; *sample* creation using Mask R-CNN format for training and testing; and *inference* to generate bounding boxes over the studied region on the high-resolution imagery. Thus, the maximum solar generation availability $\overline{\mathcal{I}}$ in kW can be defined as a function of the available rooftop area A in m^2, peak solar irradiance $\overline{G}$ in kW/m^2, and solar panels efficiency η in p.u., as follows:

$$\overline{\mathcal{I}}_{m,t} = A_t \times \overline{G} \times \eta \qquad \forall t, m \tag{5.24}$$

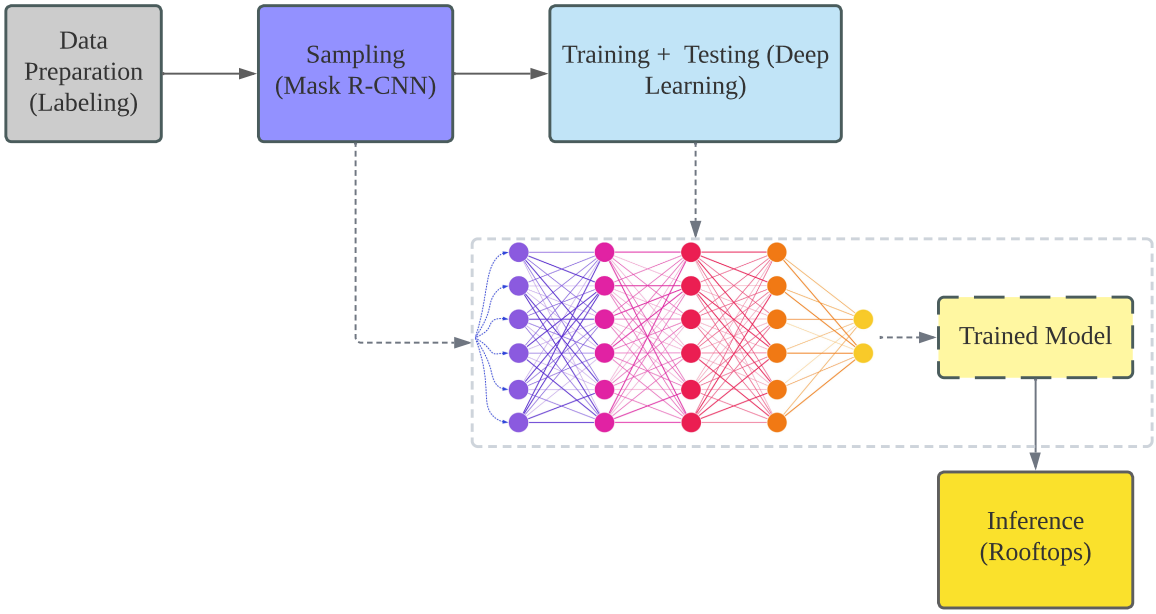

Figure 5.2: DL framework for detecting rooftops.

5.2.2 MV/LV Network Modelling

A methodology is proposed here to obtain an approximate representation of the MV/LV grid in an MMG system. Thus, assuming the LV network is unknown, but the location of the MV/LV transformers is given, the LV network can be outlined by identifying the number of users connected to each transformer. This number can be further utilized to divide each MG's hourly demand proportionally, allowing the representation of the hourly demand at each transformer. This is achieved considering that one or more transformers divide each MG in a series of blocks, as depicted in Figure 5.3. Therefore, metadata regarding the ownership and type of residences (cadastral information) can be used to define the distribution of the users among all the transformers for all the MGs. If this information is not available, 3D imagery or web-based map services can be used as an alternative. For instance, as observed in Figure 5.4, if the element detected in the imagery is an apartment building, the number of users can be estimated based on the number of floors and average use of space per zone.

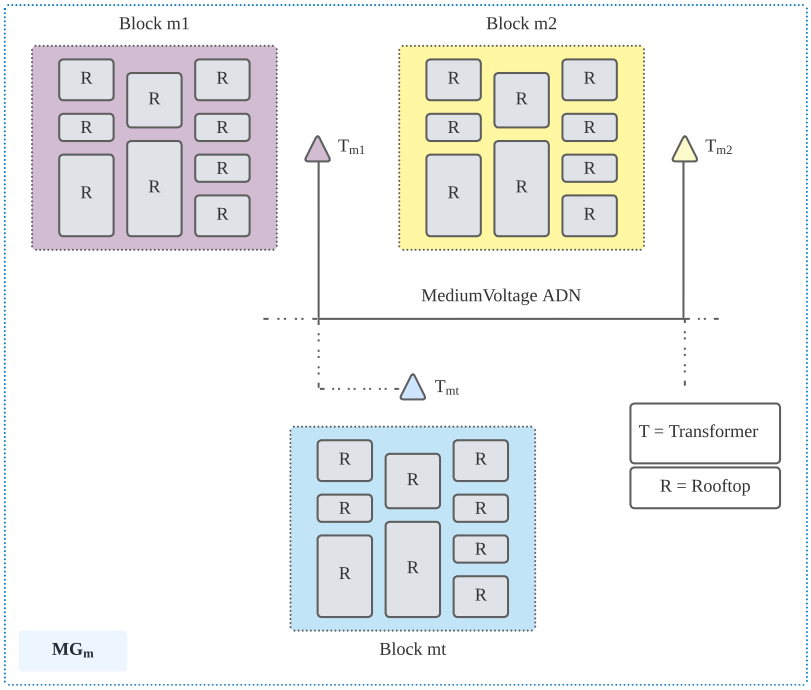

Figure 5.3: Methodology to estimate the number of users for each MV/LV transformer.

5.3 Simulations and Results

5.3.1 Case Study

In this study case, the DL methodologies described in Sections 2.4.1 and 5.2.1 are applied to define the solar generation availability over the studied region, using high-resolution imagery. The methodology presented in Section 5.2.2 is used to define the number of users located at each MV/LV transformers, of which the location is known. These parameters are introduced in the planning model presented in Section 5.1, which is used to study the feasibility of implementing an MMG system consisting of 4 individual MGs at the Brazilian ADN previously studied in Chapter 4. All the input data, including technical, economic, and environmental parameters used for this case study are discussed next.

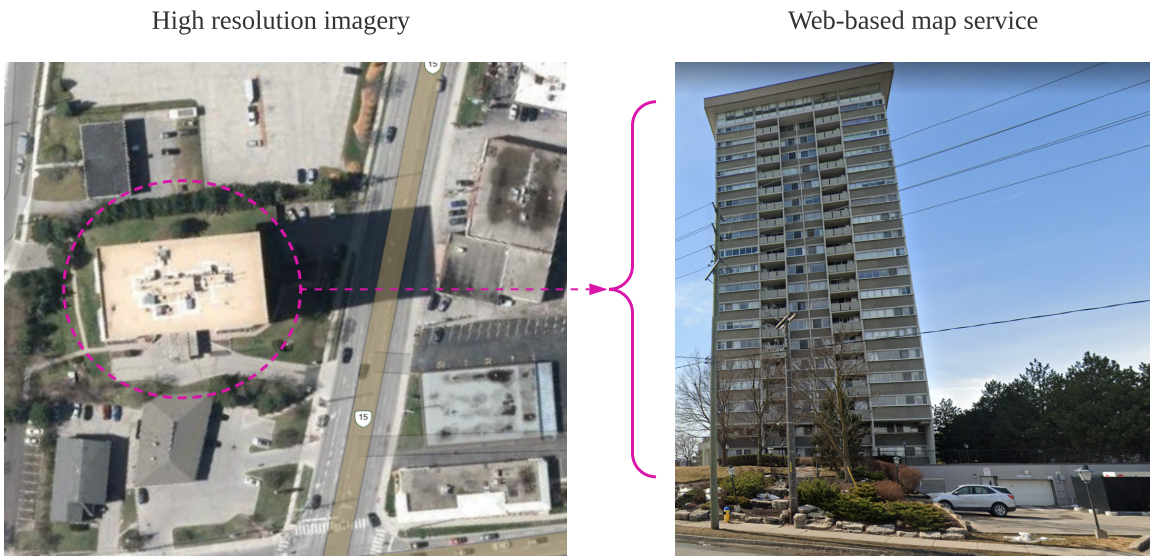

Figure 5.4: Use of high-resolution imagery and web-based map services.

Studied Region

A four-band (RGBN)[1]/multi-spectral high-resolution satellite imagery for the studied municipality is used[2], as recommended in [149].

Electricity Demand

For the 4 MGs identified in 4.2.1, the hourly average demand of a year for the required 288 representative hours is depicted in Figure 4.4.

[1]Four band imagery typically contains red, green, blue, and near-infrared bands. Only three bands can usually be viewed at one time in most software applications, and the imagery's natural color (red, green, and blue bands) is used for this application.

[2]The high-resolution imagery was purchased from Satellite Imaging Corporation, Houston, TX (www.satimagingcorp.com)

Solar Panels

The rooftop solar panels are assumed to be connected through an inverter located at each house. Also, for each MG, all the rooftop solar panels connected downstream from each MV/LV transformer are assumed to be lumped at the corresponding transformer. Average solar irradiance and cell temperature are used to compute the power output using (3.18). The operational parameters and costs associated with the panels are shown in Table 4.1.

Batteries

Lithium iron phosphate battery packs with 20 kWh and 8 kW peak power of charge/discharge, i.e., $t^{ch} = t^{dch} = 2h$ with $\delta = 0.2$, are used for the case study. Additional technical and economic parameters for the batteries are presented in Table 4.2.

Stochastic Scenarios

In this case study, the 9-scenario tree presented in Figure 4.7 is used, in which, at each node, the demand growth rate is shown with respect to year 1 and the solar irradiance annual average, for a 5-year planning horizon, with their respective probabilities.

5.3.2 Assumptions

Solar Generation Capacity

The analysis was performed in ArcGIS Pro in a server with two Intel Xenon Silver 4214 processors at 2.20 GHz, 512 GB ram memory, and NVIDIA RTX A5000 GPUs. For this case study, 10,000 samples have been considered, of which 90% were used for training and 10% were used for validation. The batch size, which is the number of image tiles to be processed for training is 4; the chip size, which sets the image size to train the model is 400 pixels; and the maximum epoch, which indicates the number of times the data set is passed forward and backward through the NN, is set to 20. For the Mask R-CNN approach, RestNet50[3] is used as the backbone/feature extracting NN, which contains 50 layers (48 CNN layers, one Max Pool layer, and one Average Pool layer), and a Regional Proposal Network with 3 layers. In addition, the training process yields an optimal learning rate between $5.24 \times 10^{-}5$ and $5.24 \times 10^{-}6$, which is extracted from the learning curve [122].

[3] RestNet stands for Residual Network [150]

MMG Planning

The MILP model, described in Section 5.1 was solved using GAMS, with the CPLEX solver in a computer with an Intel Xeon CPU at 1.87 GHz. In this case study, in order to promote the integration of RES, at least 10% of the maximum available capacity of solar generation is forced to be included for each transformer, at each MG; otherwise, the model does not include them due to the cost minimization approach and low grid electricity costs. The remaining model parameters are the same as in Chapter 4 and are summarized in Table 5.1.

Table 5.1: Model parameters

Discount rate d	8%
Electricity price growth	4.81%/year
O&M cost increase	3%/year (average inflation)
Solar panels cost decrease	9%/year
Batteries cost decrease	21.1%/year
MCS convergence	700 iterations
PCC power limit $\overline{P}_{PCC}$	1200 kW
Electricity Prices	$(e_a = e_l = e_m)$ \$/kWh 0.11 for $h = 17$ (intermediate) 0.17 for $18 < h \leq 20$ (peak) 0.08 otherwise (off-peak)

5.3.3 Numerical Results

The results of the MMG planning model for the aforementioned ADN using the TSSP approach are first compared with the MCS results, which are considered as a benchmark for the case study. The results of the TSSP model presented in this chapter are also compared with the ones obtained with the simpler TSSP model presented in Chapter 4, based on the same solar PV limits obtained here.

Solar Generation Capacities

The DL methodology described in Section 2.4.1 is used to identify the rooftops of the buildings within the studied region. Hence, the methodology depicted in Figure 5.2 is

applied over the four-band high-resolution imagery that contains the studied region, as per Figure 5.5. In order to train the classifier to assign pixels to the rooftop class, the creation of training samples is needed. In ArcGIS Pro, a classification scheme to define the rooftop class category is created using a geoprocessing tool called "Training Samples Manager", where samples are manually drawn over the imagery. Once all the samples have been placed, these need to be exported in order to feed the DL model. This is achieved by using another geoprocessing tool called "Export Training Data For Deep Learning", in which the imagery's raster and the samples are inputted to create the desired DL training data in Mask R-CNN format, with a chip size of 400 pixels.

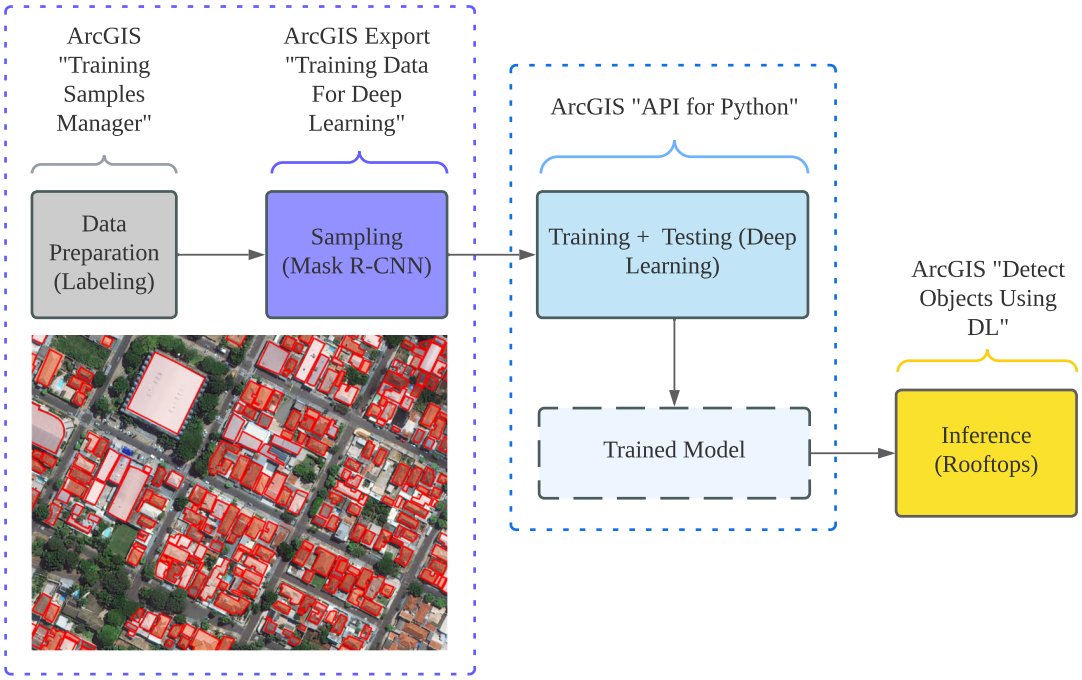

Figure 5.5: DL process applied to the case study.

The training of the DL model is performed using an ArcGIS "API for Python" and was completed in 134 hours and 28 minutes. Figure 5.6 depicts both the training loss and validation error decreasing over time, and thus showing a good fit, with an average precision score of 89.2%. The trained model allows the identification of the rooftop areas for each MG, as depicted in Figures 5.7 to 5.10. Using these areas, the maximum capacity of solar power for each MG is calculated using (5.24), assuming that 75% of the total rooftop area is suitable for solar panels installation, considering the roof characteristics in

the studied region. Also, a maximum solar irradiance of 722 kW/m^2 and a 20% efficiency for solar panels are considered. The results are presented in Tables 5.2 to 5.5.

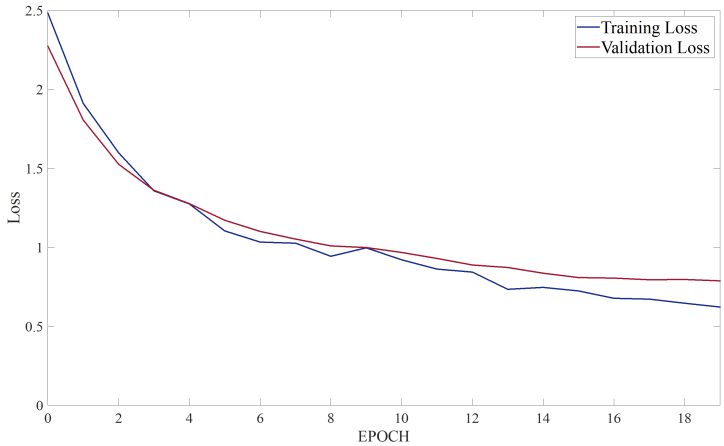

Figure 5.6: Loss graph of training of the DL model.

Figure 5.7: Blocks, rooftops, transformers, and MV grid corresponding to MG1.

Figure 5.8: Blocks, rooftops, transformers, and MV grid corresponding to MG2.

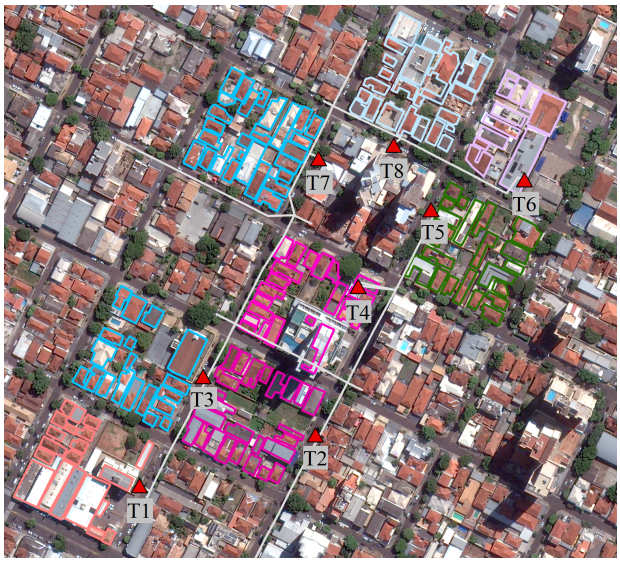

Figure 5.9: Blocks, rooftops, transformers, and MV grid corresponding to MG3.

Number of Users

To estimate the number of users connected to each MV/LV transformer, the methodology presented in Section 5.2.2 is applied, which includes the use of the areas detected in Section

Figure 5.10: Blocks, rooftops, transformers, and MV grid corresponding to MG4.

5.3.3, web-based map services, and some public cadastral information. In addition, it was assumed that a certain number of EVs can be adopted within each MG, based on existing vehicle data. The number of estimated users and EVs are depicted in Tables 5.2 to 5.5.

MMG Planning

The results of the TSSP planning model are presented in Tables 5.6, 5.7, and 5.8. The results in Table 5.6 show that the total cost of the TSSP model is consistently close to the benchmark. In fact, the total cost in the TSSP model is only 3.07% lower than the one obtained with MCS. However, the TSSP model is much faster than the MCS for the large planning problem considered here due to its level of granularity.

The solar generation capacities obtained from the different models are shown in Table 5.7, which shows that all of them yield the same results for the size and location of solar panels since as previously explained, RES requirements have to be forced into the model. The batteries obtained with both TSSP models are very similar, with the standard deviation of the difference in the capacity installed for each independent MG (Table 5.8) with respect to the MCS benchmark being 10.1% or 16.7 kWh in average, which is relatively small, thus validating the TSSP approaches.

In Figure 5.11, the capacity additions for the MMG system obtained with the TSSP are

shown. Note that all the solar panels and 93.5% of the battery capacities are installed at the beginning of the planning horizon, while the remaining battery capacity is added between the second and fourth year. This is particularly beneficial for Brazilian distribution companies, given the limited-time government incentives for initial investments, as previously explained. In addition, unlike the model presented in Chapter 4, the extended model provides more relevant details for decision-making, as the location of solar panels and batteries within the studied region can be obtained. Thus, providing optimal capacities from economic, technical, and geographical points of view, that can be actually implemented within the studied region. Similarly, by enforcing the solar PV capacity at each transformer through (5.6), there is a realistic allocation of RES that cannot be obtained with the model presented in Chapter 4.

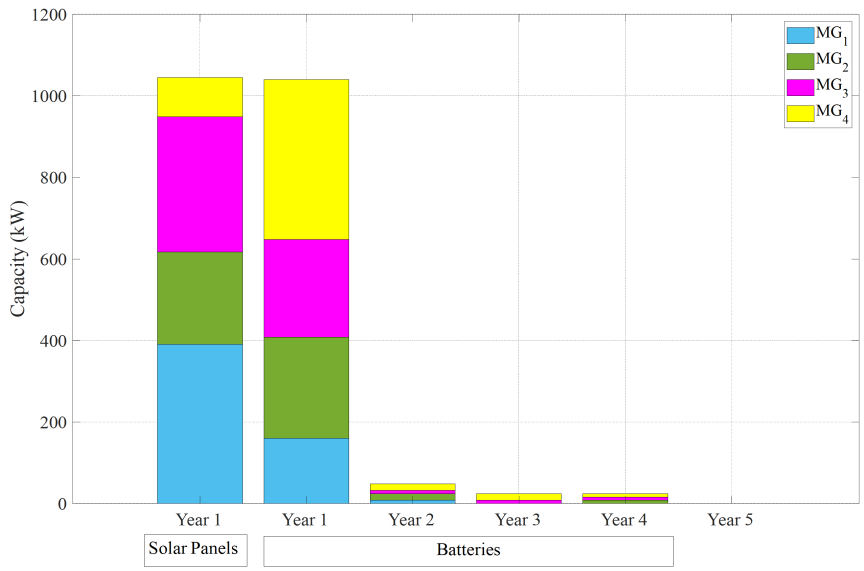

Figure 5.11: Yearly capacity additions from the TSSP MV/LV model.

The minimum capacity of the MV/LV transformers for the TSSP model and MCS are shown in Table 5.9, where the average difference in the total transformer capacity required for the MMG system is only 1.47%. In addition, observe that the relationship between each transformer's capacity and the total transformer capacity inside each MG is not related to the number and location of users exclusively, as (5.11) and (5.12) ensure that the capacity of the transformers accounts for the power of DERs. Note that the location and capacity of these transformers can be used for expansion planning of the complete distribution network.

5.4 Summary

This chapter presented a model for the realistic planning of MMG systems in the context of ADNs with the assistance of GIS. The model considered the distribution system grid as well as the geographic features of the studied region. It also included long-term purchase decisions and short-term operational constraints, and considered uncertainties associated with electricity demand and RESs using a TSSP approach. GIS along with DL were used to estimate the areas of rooftops within the studied region. The proposed planning model was used to study the feasibility of implementing the 4-MG system from Brazil, previously studied in Chapter 4. The results of the model presented in this chapter were compared with the results obtained using MCS and the less detailed TSSP model presented in Chapter 4, showing that the stochastic solutions were close to those obtained with MCS at a lower computational cost, and that the use of GI-data allowed to determine both the capacity and location of the PV panels, batteries, and distribution transformers on the MGs grid, thus providing more precise and useful planning results.

Table 5.2: Number of users and EVs, rooftop area associated with each transformer, and RES limits for MG_1

$T_{1,t}$	EVs	Users	Area (m^2)	RES max. capacity (kW)
1	-	12	1955	212
2	-	28	4970	539
3	2	29	3423	371
4	5	31	4659	505
5	-	22	4230	458
6	1	21	3962	429
7	7	28	3829	415
8	3	27	4262	462
9	-	23	4828	523

Table 5.3: Number of users and EVs, rooftop area associated with each transformer, and RES limits for MG_2

$T_{2,t}$	EVs	Users	Area (m^2)	RES max. capacity (kW)
1	9	43	4477	485
2	-	18	3654	396
3	2	21	2011	218
4	-	21	2011	218
5	-	35	3442	373
6	2	19	3309	359
7	5	32	631	68
8	-	10	1951	211
9	5	14	2091	227
10	-	24	989	107

Table 5.4: Number of users and EVs, rooftop area associated with each transformer, and RES limits for MG_3

$T_{3,t}$	EVs	Users	Area (m^2)	RES max. capacity (kW)
1	-	36	4179	453
2	2	25	3835	416
3	3	18	3512	381
4	17	65	3071	333
5	3	22	3947	428
6	-	35	3128	339
7	3	24	4656	505
8	5	23	4341	470

Table 5.5: Number of users and EVs, rooftop area associated with each transformer, and RES limits for MG_4

$T_{4,t}$	EVs	Users	Area (m^3)	RES max. capacity (kW)
1	2	25	2147	233
2	2	16	1331	144
3	3	20	2033	220
4	4	13	1186	128
5	3	16	2208	239

Table 5.6: Total cost and computational cost

Model	Total Costs (M$)	Computational Costs (hh:mm:ss)
MCS	1.95	632:00:00
TSSP without LV grid	1.87	03:16:44
TSSP with LV grid	1.89	46:25:31

Table 5.7: Total solar installed capacities for the MMG system, for TTSP and MCS

TSSP and MCS with MV/LV				
t	MG_1 (kW)	MG_2 (kW)	MG_3 (kW)	MG_4 (kW)
1	21	49	45	23
2	54	40	42	14
3	37	22	38	22
4	50	22	33	13
5	46	37	43	24
6	43	36	34	-
7	41	7	50	-
8	46	21	47	-
9	52	23	-	-
10	-	11	-	-
Total	391	266	332	96

TSSP without LV grid (kWh/kW)				
Total	391	266	332	96

Table 5.8: Total batteries installed capacities for the MMG system

MCS with MV/LV (kWh/kW)				
t	MG_1	MG_2	MG_3	MG_4
1	71/29	111/44	125/50	667/267
2	47/19	73/29	60/24	13/52
3	45/18	70/28	58/23	113/45
4	46/18	68/27	63/25	112/45
5	46/19	71/28	54/22	116/46
6	48/19	69/28	70/28	-
7	49/19	71/28	93/37	-
8	51/21	69/27	150/60	-
9	56/22	69/28	-	-
10	-	73/28	-	-
Total	459/184	743/297	667/267	1138/455
TSSP without LV grid (kWh/kW)				
Total	420/168	660/254	640/256	1080/432
TSSP with MV/LV (kWh/kW)				
t	MG_1	MG_2	MG_3	MG_4
1	60/24	60/24	80/32	300/120
2	40/16	60/24	40/16	220/88
3	40/16	60/24	80/32	160/64
4	40/16	60/24	120/48	200/80
5	60/24	60/24	100/40	200/80
6	20/8	120/48	60/24	-
7	60/24	60/24	60/24	-
8	60/24	60/24	120/48	-
9	40/16	60/24	-	-
10	-	80/32	-	-
Total	420/168	680/272	660/264	1080/432

Table 5.9: Transformers capacities

MCS (kW)				
t	MG_1	MG_2	MG_3	MG_4
1	41	166	97	455
2	49	54	74	211
3	60	70	67	252
4	81	61	238	187
5	40	88	72	210
6	45	65	82	-
7	92	105	92	-
8	65	41	117	-
9	49	77	-	-
10	-	74	-	-
Total	523	801	839	1316

TSSP (kW)				
t	MG_1	MG_2	MG_3	MG_4
1	40	151	91	362
2	42	51	65	242
3	61	69	80	244
4	74	57	259	211
5	47	83	92	197
6	40	90	79	-
7	104	106	74	-
8	67	38	117	-
9	43	79	-	-
10	-	75	-	-
Total	518	797	855	1256

Chapter 6

Conclusions

6.1 Summary and Conclusions

In this thesis, a framework for the planning of MMG systems in the context of ADNs was proposed. In order to achieve this, an initial model for the planning of individual MGs was presented, which was applied to the planning of RC MGs. This model was then used to consider multiple MGs and the ADN both at MV and LV levels, while including uncertainties associated with RES generation and demand.

In Chapter 3, a comprehensive model for the planning of RC MGs was developed. The goal of this model was the identification of the optimal (most economical) size and mixture of generation and storage resources, and the time of their deployment. It was based on estimated parameters such as electricity demand and RES availability, where historical data was used to reflect their variability. The planning of MGs was thus formulated through an optimization model, consisting of an objective function, a set of parameters, decision variables, and technical and economic constraints. As shown in the simulation results presented in Chapter 3, the inclusion of RESs and ESSs significantly reduced the use of fossil fuels, resulting in lower emissions (between 51.9% and 100%) for the RC MG studied. Its inclusion not only helped lower relevant costs of the energy system, such as fuel storage and its transportation to RCs, but also reduced the uncertainties associated with diesel fuel prices.

The results presented in Chapter 3 clearly showed that wind resources along with solar and storage technologies (batteries and fuel cells) can play a key role in satisfying the electricity demand of RCs, while significantly reducing costs and GHG emissions. Furthermore, using the proposed MILP planning model, the operational and economic feasibility

of RESs and ESSs in Canadian RC MGs was demonstrated. It was observed that these technologies can help enhance electric grid flexibility, while encouraging structural and economical change and supporting Canada's ambitious goal of net-zero emissions by 2050. Therefore, this model could be used by federal, provincial, territorial, municipal, and indigenous governments across Canada to study the integration of clean DERs, including hydrogen systems, in diesel-dependent RC MGs.

The long-term planning of MMG systems from the point of view of the MV grid was studied in Chapter 4 by expanding the planning model presented in Chapter 3, since independent MGs can be interconnected to form MMG systems in the context of ADNs, bringing valuable benefits such as energy use optimization, power quality and stability improvements, network congestion reductions, transmission and distribution system investment deferrals, efficiency, reliability, and flexibility enhancements for both costumers and utilities. This was achieved by incorporating the constraints associated with the transactions among all the participants, i.e, the independent MGs and the ADN, and the uncertainties associated with demand and RES using a TSSP model. Within this approach, decisions can be made in two stages, with the objective function including the first stage function and the expected value of the second stage function. For the MMG problem, the purchase decisions were assumed to happen in the first stage, without any knowledge of the uncertain values, whereas the operation of the MMG system belongs to the second stage of the problem. Therefore, for the computation of the expected value, a set of scenarios (scenario tree) with their respective probabilities, i.e., random variables that are approximated by discrete pdfs, was needed. The uncertainties associated with RES were handled using their inherent statistical properties, whereas the uncertainties related to electricity demand were considered using GBM, since demand evolves with time and there is an annual growth rate relative to previous years.

The planning model presented and discussed in Chapter 4 was used to study the feasibility of implementing an MMG system consisting of 4 individual MGs at an ADN in a municipality in the state of São Paulo, Brazil. The results showed that the TSSP model was less conservative than the deterministic planning model, which was based on simple and pessimistic reserve constraints, while performing faster than a SSLP algorithm, with higher accuracy. In this model, the optimal capacities of RESs and ESSs required to satisfy the demand of each MG were obtained, while offering insight into the operation of the MMG system and its flexibility during the planning horizon. Thus, the proposed model could assist electricity system planners in planning and validating the formation of an MMG system inside an ADN. It is interesting to note that the use of GIS tools allowed having a more accurate estimate of the RES power availability for planning purposes. Therefore, this relevant application of GIS was explored further in Chapter 5.

In order to include the LV grid within the MMG system, the model proposed in Chapter 4 was further expanded in Chapter 5 with the assistance of GIS, since GIS facilitates the inclusion of georeferenced parameters within the optimization formulation, thus allowing the visualization of the results over the real network using maps. This can help enhance the decision-making process while offering tools to better understand and interpret the results, which facilitates its implementation. Hence, a methodology to estimate the details of the MV and LV ADN using GIS tools was proposed, where the number of users connected to each MV/LV transformer inside the MMG system was defined. In addition, using GIS tools and DL techniques over high-resolution satellite imagery, the rooftops of the buildings were identified to determine the actual available solar capacity.

The TSSP approach was used to study the feasibility of implementing an MMG system consisting of 4 individual MGs at the same ADN in São Paulo, Brazil. Therefore, the capacities of RESs and ESSs, and the size of MV/LV distribution transformers required to satisfy the hourly demand of the MMG system over the planning horizon were estimated. The results of the model presented in Chapter 5 were compared with the results obtained using MCS and Chapter 4's model, demonstrating that the use of GIS allows determining both the capacity and location of the PV panels, batteries, and distribution transformers on the MGs grid, thus providing more precise and useful planning results, which can be suitable for their actual deployment. In addition, it was demonstrated that the stochastic solutions are close to those obtained with MCS at a lower computational cost.

The following are the main conclusions from this thesis:

- Despite the feasibility of running RC MGs with fuel cells only, it was concluded that batteries should also be integrated in order to withstand rapid changes that are not captured by the long-term planning, and which should not be taken by fuel cells in real-time operation as this reduces their lifetime. Thus, batteries and fuel cells should always be considered for MG operation in RCs.

- When comparing fuel cells with batteries, it has been demonstrated that the capacity of fuel cells needed for the planning of RC MGs is lower than the capacity of batteries, which is a consequence of the larger energy density of fuel cells.

- It has been shown that a TSSP approach for considering uncertainty in MMG planning provides a solution that is more accurate than the SSLP model, but not overly conservative as the case of a deterministic model. The TSSP model is more precise than the SSLP model because of the hierarchical design of the decision-making process in the TSSP model.

- As the size of the MMG problem increases due to the level of granularity, it has been observed that adequate results can be timely obtained using TSSP models, as opposed to MCS.

- The relevant applicability and assistance of GIS for the formulation and solution of MMG planning problems have been demonstrated, since GIS tools facilitate the modelling of the distribution network by clearly identifying the location of the MV grid and MV/LV distribution transformers. It was also shown that georeferenced parameters can be included within the optimization formulation, which enhances DER quantification and deployment. Finally, GIS allow visualizing the planning results, using optimization tools that provide numerical results.

- In the proposed planning model, it is observed that each independent MG cooperates to satisfy the demand of an MMG system embedded in an ADN. In this context, the generation and storage resources are shared among the participant MGs and the ADN.

6.2 Contributions

The most significant contributions of this thesis can be summarized as follows:

- Development of a long-term multi-year planning model for the integration of RESs and ESSs, including batteries and hydrogen ESSs, in RC MGs for GHG emission reduction. The proposed RC MG model was shown useful for the planning of a real isolated Canadian system using various scenarios and energy mixes.

- Development of a novel long-term multi-year planning model for creating MMG systems considering an ADN at MV level. The model includes long-term purchase decisions and short-term operational constraints, and the formulation of the energy transactions among all participants, i.e., between the independent MGs and between each MG and the ADN. This model timely specifies the RES and ESS capacities required to convert a portion of an ADN into an MMG system, guaranteeing both grid and isolated modes of operation.

- Application of a TSSP approach to consider uncertainties related to RES and demand, relying on an optimization-based scenario tree generation approach, which is based on GBM and statistical measures to represent scenarios.

- Development of a MMG long-term multi-year planning model that considers both the MV and LV grids. In addition to long-term purchase decisions for RESs and ESSs, short-term operational constraints, and the formulation of the energy transactions among all participants, this more detailed model includes long-term transformer capacity selection, which is very useful for actual ADN planning. Moreover, this model has successfully integrated GI parameters and has facilitated the planning of DERs with an increased level of granularity for the ADN.

- Development of a new methodology to estimate the location of the MV and LV ADN using GIS tools and DL techniques to identify the rooftops of the buildings in the studied region, facilitating the definition of the available solar capacity. This methodology is based on the use of high-resolution imagery, web-based map services, and ownership-related information. This methodology facilitates the estimation of the number of users connected to each MV/LV transformer, which increases the level of practicality of the planning model, and provides valuable tools for the modelling of the grid.

- Testing and validation of the TSSP planning models at MV and LV levels in a real system based on an ADN at a municipality in the state of São Paulo Brazil. The practical application of these models has been demonstrated beneficial when compared with the performance of deterministic, SSLP, and MCS approaches.

6.3 Future Work

Based on the work presented in this thesis, the following issues may be undertaken in future research:

- Power flow equations may be included in the model to validate the operation of the MMG system in the long-term, considering parameters such as voltage and frequency at the PCC and at the MV/LV transformers.

- Electricity prices may be considered as variables in order to determine the price of the electricity within the MMG system, and the possibility of competition among the participant MGs in the context of community MG and MMG systems.

- Analyze the possibility of allowing MGs to offer services such as EV charging to neighboring MGs to determine the corresponding electricity prices.

- Expand the model for the planning RC MG to include thermal loads and analyze the technical and economic implications of fuel cells providing both electricity and heating.

References

[1] "Roadmap to 2050. A Manual for Nations to Decarbonize by Mid-Century," The Sustainable Development Solutions Network (SDSN) and Fondazione Eni Enrico Mattei (FEEM), Technical Report, 2019.

[2] "Paris Agreement," United Nations, Technical Report, 2015.

[3] United States Environmental Protection Agency. Global emissions by economic sector. [Online]. Available: www.c2es.org

[4] M. Hafner and M. Noussan, *Technologies for the Global Energy Transition*. Springer International Publishing, 2020, pp. 177–202.

[5] H. Farhangi and G. Joos, *Microgrid Planning and Design: A Concise Guide*, 1st ed. Wiley-IEEE Press, 2019.

[6] Z. Rajab, A. Alfergani, A. Asheibi, A. Khalil, and F. Mohamed, "Optimum microgrid planning and operation for improving reliability and power quality: Review," in *2020 11th International Renewable Energy Congress (IREC)*, 2020, pp. 1–6.

[7] M. Farrokhabadi, C. Canizares, J. W. Simpson-Porco, and et al., "Microgrid stability definitions, analysis, and examples," *IEEE Transactions on Power Systems*, vol. 35, no. 1, pp. 13–29, Apr. 2019.

[8] A. Cagnano, E. De Tuglie, and P. Mancarella, "Microgrids: Overview and guidelines for practical implementations and operation," *Applied Energy*, vol. 258, pp. 1–18, 2020.

[9] M. Erol-Kantarci, B. Kantarci, and H. T. Mouftah, "Reliable overlay topology design for the smart microgrid network," *IEEE Network Journal*, vol. 25, no. 5, pp. 38–43, Sep. 2011.

[10] F. Shahnia, S. Bourbour, and A. Ghosh, "Coupling neighboring microgrids for overload management based on dynamic multicriteria decision-making," *IEEE Transactions on Smart Grid*, vol. 8, no. 2, pp. 969–983, Mar. 2017.

[11] X. Lu and J. Wang, "A game changer: Electrifying remote communities by using isolated microgrids," *IEEE Electrification Magazine*, vol. 5, no. 2, pp. 56–63, 2017.

[12] B. Chen, J. Wang, X. Lu, C. Chen, and S. Zhao, "Networked microgrids for grid resilience, robustness, and efficiency: A review," *IEEE Transactions on Smart Grid*, vol. 12, no. 1, pp. 18–32, 2021.

[13] M. S. Saleh, A. Althaibani, Y. Esa, Y. Mhandi, and A. A. Mohamed, "Impact of clustering microgrids on their stability and resilience during blackouts," in *2015 International Conference on Smart Grid and Clean Energy Technologies (ICSGCE)*, Oct. 2015, pp. 195–200.

[14] P. A. Longley, M. F. Goodchild, D. J. Maguire, and D. W. Rhind, *Geographic Information Science and Systems*, 4th ed. Hoboken, N.J.: Wiley, Mar. 2015.

[15] M. Arriaga, C. A. Canizares, and M. Kazerani, "Long-term renewable energy planning model for remote communities," *IEEE Transactions on Sustainable Energy*, vol. 7, no. 1, pp. 221–231, 2016.

[16] A. Maitra, L. Rogers, and R. Handa, "Program on technology innovation: Microgrid implementations: Literature review," Electric Power Research Institute, Palo Alto, California, USA, Technical Report, Jan. 2016.

[17] M. Arriaga, E. Nasr, and H. Rutherford, "Renewable Energy Microgrids in Northern Remote Communities," *IEEE Potentials*, vol. 36, no. 5, pp. 22–29, 2017.

[18] M. R. Quitoras, P. Cabrera, P. E. Campana, P. Rowley, and C. Crawford, "Towards robust investment decisions and policies in integrated energy systems planning: Evaluating trade-offs and risk hedging strategies for remote communities," *Energy Conversion and Management*, vol. 229, pp. 1–16, 2021.

[19] C. Canizares and I. Das, "Feasibility studies of variable speed generators for Canadian Arctic Communities," WISE, Technical Report, 2017.

[20] M. Arriaga, C. A. Canizares, and M. Kazerani, "Renewable Energy Alternatives for Remote Communities in Northern Ontario, Canada," *IEEE Transactions on Sustainable Energy*, vol. 4, no. 3, pp. 661–670, 2013.

[21] M. M. Kama, I. Ashraf, and E. Fernandez, "Optimal planning of renewable integrated rural microgrid for sustainable energy supply," *Energy Storage*, vol. 4, no. 4, p. e332, 2022.

[22] C. Abbey and G. Joos, "A stochastic optimization approach to rating of energy storage systems in wind-diesel isolated grids," *IEEE Transactions on Power Systems*, vol. 24, no. 1, pp. 418–426, 2009.

[23] K. DePippo and B. A. Peppley, "Canadian remote community power generation: How reformer and fuel cell systems compare with diesel generators," *International Journal of Energy Research*, vol. 43, no. 3, pp. 1161–1170, 2019.

[24] W. Zhang, A. Maleki, F. Pourfayaz, and M. S. Shadloo, "An artificial intelligence approach to optimization of an off-grid hybrid wind/hydrogen system," *International Journal of Hydrogen Energy*, vol. 46, no. 24, pp. 12 725–12 738, 2021.

[25] E. Vera, C. Canizares, and M. Pirnia, "Renewable Energy Integration in Canadian Remote Community Microgrids. The feasibility of hydrogen and gas generation," *IEEE Electrification Magazine*, vol. 8, no. 4, pp. 36–45, Dec. 2020.

[26] S. B. Silva, M. A. de Oliveira, and M. M. Severino, "Economic evaluation and optimization of a photovoltaic–fuel cell–batteries hybrid system for use in the Brazilian Amazon," *Energy Policy*, vol. 38, no. 11, pp. 6713–6723, 2010.

[27] D. C. Young, G. A. Mill, and R. Wall, "Feasibility of renewable energy storage using hydrogen in remote communities in Bhutan," *International Journal of Hydrogen Energy*, vol. 32, no. 8, pp. 997–1009, 2007.

[28] B. Cornelusse, I. Savelli, S. Paoletti, A. Giannitrapani, and A. Vicino, "A community microgrid architecture with an internal local market," *Applied Energy Journal*, vol. 242, p. 547–560, 2019.

[29] L. Che, X. Zhang, M. Shahidehpour, A. Alabdulwahab, and A. Abusorrah, "Optimal interconnection planning of community microgrids with renewable energy sources," *IEEE Transactions on Smart Grid*, vol. 8, no. 3, pp. 1054–1063, 2017.

[30] L. Wu, T. Ortmeyer, and J. Li, "The community microgrid distribution system of the future," *The Electricity Journal*, vol. 29, no. 10, pp. 16–21, 2016.

[31] H. Haddadian and R. Noroozian, "Multi-microgrids approach for design and operation of future distribution networks based on novel technical indices," *Applied Energy Journal*, vol. 185, pp. 650–663, Jan. 2017.

[32] E. Bullich-Massague, F. Diaz-Gonzalez, Aragues-Penalba, Girbau-Llistuella, P. Olivella-Rosell, and A. Sumper, "Microgrid clustering architectures," *Applied Energy Journal*, vol. 212, pp. 340–361, 2018.

[33] E. J. Ng and R.El-Shatshat, "Multi-microgrid control systems (mmcs)," *IEEE PES General Meeting*, pp. 1–6, Jul. 2010.

[34] S. N. Backhaus, L. Dobriansky, S. Glover, C.-C. Liu, , and et al., "Networked Microgrids Scoping Study," Los Alamos National Laboratory - U.S. Department of Energy, Technical Report, 2016.

[35] S. Arefifar, M. Ordonez, and Y. Mohamed, "Energy management in multi-microgrid systems-development and assessment," *IEEE Transactions on Power Systems*, vol. 32, no. 2, pp. 910–922, 2017.

[36] J. Vasiljevska, J. Peças Lopes, and M. Matos, "Evaluating the impacts of the multi-microgrid concept using multi-criteria decision aid," *Electric Power Systems Research Journal*, vol. 91, pp. 44–51, 2012.

[37] S. Al-ttiyah, "Nested Microgrids: Operation and control requirements," *Master Thesis. KTH Royal Institute of Technology, School of Electrical Engineering*, 2016.

[38] X. Zhou, L. Zhou, Y. Chen, J. M. Guerrero, A. Luo, W. Wu, and L. Yang, "A microgrid cluster structure and its autonomous coordination control strategy," *International Journal of Electrical Power & Energy Systems*, vol. 100, pp. 69–80, 2018.

[39] M. Goyal and A. Ghosh, "Microgrids interconnection to support mutually during any contingency," *Sustainable Energy, Grids and Networks*, vol. 6, pp. 100–108, 2016.

[40] M. Zolfaghari, G. B. Gharehpetian, M. Shafie-khah, and J. P. Catalão, "Comprehensive review on the strategies for controlling the interconnection of ac and dc microgrids," *International Journal of Electrical Power & Energy Systems*, vol. 136, pp. 1–18, 2022.

[41] N. Shafaghatian, A. Heidary, H. Radmanesh, and K. Rouzbehi, "Microgrids interconnection to upstream ac grid using a dual-function fault current limiter and power flow controller: principle and test results," *IET Energy Systems Integration*, vol. 1, no. 4, pp. 269–275.

[42] H. A. Gabbar, T. Egan, A. M. Othman, and R. Milman, "Hierarchical control architecture for resilient interconnected microgrids for mass transit systems," *IET Electrical Systems in Transportation*, vol. 10, no. 3, pp. 320–327.

[43] S. Adhikari, "Control and operation of dc microgrids," Ph.D. dissertation, Nanyang Technological University, 2018.

[44] S. Bourbour and F. Shahnia, "A suitable mechanism for the interconnection phase of temporary coupling of adjacent microgrids," in *2016 IEEE Innovative Smart Grid Technologies - Asia (ISGT-Asia)*, 2016, pp. 624–629.

[45] M. Kumar, S. S. Chandra, S. N. Singh, and M. Ramamoorty, "Development of a control strategy for interconnection of islanded direct current microgrids," *IET Renewable Power Generation*, vol. 9, no. 3, pp. 284–296, 2015.

[46] P. Wu, W. Huang, N. Tai, and S. Liang, "A novel design of architecture and control for multiple microgrids with hybrid ac/dc connection," *Applied Energy*, vol. 210, pp. 1002–1016, 2018.

[47] M. N. Alam, S. Chakrabarti, and A. Ghosh, "Networked microgrids: State-of-the-art and future perspectives," *IEEE Transactions on Industrial Informatics*, vol. 15, no. 3, pp. 1238–1250, 2019.

[48] P. Wu, W. Huang, N. Tai, J. Xie, and B. Lv, "An advanced architecture of multiple microgrids interfacing with ucc," in *2017 IEEE Power & Energy Society General Meeting*, 2017, pp. 1–5.

[49] "IEEE guide for design, operation, and integration of distributed resource island systems with electric power systems," *IEEE Std 1547.4-2011*, pp. 1–54, 2011.

[50] L. He, Z. Wei, H. Yan, K.-Y. Xv, M.-y. Zhao, and S. Cheng, "A day-ahead scheduling optimization model of multi-microgrid considering interactive power control," in *2019 4th International Conference on Intelligent Green Building and Smart Grid (IGBSG)*, 2019, pp. 666–669.

[51] W. Jiang, K. Yang, J. Yang, R. Mao, N. Xue, and Z. Zhuo, "A multiagent-based hierarchical energy management strategy for maximization of renewable energy consumption in interconnected multi-microgrids," *IEEE Access*, vol. 7, pp. 325–329, 2019.

[52] B. Alghamdi and C. A. Cañizares, "Frequency regulation in isolated microgrids through optimal droop gain and voltage control," *IEEE Transactions on Smart Grid*, vol. 12, no. 2, pp. 988–998, 2021.

[53] I. P. Nikolakakos, H. H. Zeineldin, M. S. El-Moursi, and N. D. Hatziargyriou, "Stability evaluation of interconnected multi-inverter microgrids through critical clusters," *IEEE Transactions on Power Systems*, vol. 31, no. 4, pp. 3060–3072, 2016.

[54] K. Veerashekar, S. Eichner, and M. Luther, "Modelling and transient stability analysis of interconnected autonomous hybrid microgrids," in *2019 IEEE Milan PowerTech*, 2019, pp. 1–6.

[55] H. Ali, G. Magdy, and D. Xu, "A new optimal robust controller for frequency stability of interconnected hybrid microgrids considering non-inertia sources and uncertainties," *International Journal of Electrical Power & Energy Systems*, vol. 128, pp. 1–20, 2021.

[56] S. Rehimi, R. Mirzaei, and H. Bevrani, "Interconnected microgrids frequency response model: An inertia-based approach," *Energy Reports: 6th International Conference on Power and Energy Systems Engineering*, vol. 6, pp. 179–186, 2020.

[57] G. Wang, X. Zhang, S. Mei, and S. Wu, "Input-to-output stability analysis of interconnecting microgrids," in *2011 4th International Conference on Electric Utility Deregulation and Restructuring and Power Technologies (DRPT)*, 2011, pp. 1097–1103.

[58] M. Naderi, Y. Khayat, Q. Shafiee, T. Dragičević, H. Bevrani, and F. Blaabjerg, "Interconnected autonomous ac microgrids via back-to-back converters—part ii: Stability analysis," *IEEE Transactions on Power Electronics*, vol. 35, no. 11, pp. 11 801–11 812, 2020.

[59] C. Bordons, F. Garcia-Torres, and M. A. Ridao, "Interconnection of microgrids," in *Model Predictive Control of Microgrids*. Springer International Publishing, 2020, pp. 191–225.

[60] N. Bhusal, M. Abdelmalak, M. Kamruzzaman, and M. Benidris, "Power system resilience: Current practices, challenges, and future directions," *IEEE Access*, vol. 8, pp. 18 064–18 086, 2020.

[61] D. Baghbanzadeh, J. Salehi, F. S. Gazijahani, M. Shafie-khah, and J. P. Catalão, "Resilience improvement of multi-microgrid distribution networks using distributed generation," *Sustainable Energy, Grids and Networks*, vol. 27, pp. 1–19, 2021.

[62] G. Wang, Q. Wang, Z. Qiao, J. Wang, and S. Anderson, "Optimal planning of multi-micro grids based-on networks reliability," *Energy Reports*, vol. 6, pp. 1233–1249, 2020.

[63] A. Khodaei and M. Shahidehpour, "Microgrid-based co-optimization of generation and transmission planning in power systems," *IEEE Transactions on Power Systems*, vol. 28, no. 2, pp. 1582–1590, 2013.

[64] A. Arif and Z. Wang, "Networked microgrids for service restoration in resilient distribution systems," *IET Generation, Transmission & Distribution*, vol. 11, no. 14, pp. 3612–3619, 2017.

[65] A. Y. Ali, A. Hussain, J.-W. Baek, and H.-M. Kim, "Optimal operation of networked microgrids for enhancing resilience using mobile electric vehicles," *Energies*, vol. 14, no. 1, 2021.

[66] R. A. Osama, A. F. Zobaa, and A. Y. Abdelaziz, "A planning framework for optimal partitioning of distribution networks into microgrids," *IEEE Systems Journal*, vol. 14, no. 1, pp. 916–926, 2020.

[67] J. López, M. J. Rider, and J. Contreras, "Electric distribution network planning under uncertainty," *Handbook of Optimization in Electric Power Distribution Systems, Springer*, pp. 293–322, 2020.

[68] A. Khodaei, S. Bahramirad, and M. Shahidehpour, "Microgrid planning under uncertainty," *IEEE Transactions on Power Systems*, vol. 30, no. 5, pp. 2417–2425, 2015.

[69] X. Cao, J. Wang, and B. Zeng, "Networked microgrids planning through chance constrained stochastic conic programming," *IEEE Transactions on Smart Grid*, vol. 10, no. 6, pp. 6619–6628, 2019.

[70] R. S. Pinto, C. Unsihuay-Vila, and F. H. Tabarro, "Coordinated operation and expansion planning for multiple microgrids and active distribution networks under uncertainties," *Applied Energy*, vol. 297, pp. 1–15, 2021.

[71] H. Wang and J. Huang, "Cooperative planning of renewable generations for interconnected microgrids," *IEEE Transactions on Smart Grid*, vol. 7, no. 5, pp. 2486–2496, 2016.

[72] C. Stevanoni, Z. De Grève, F. Vallée, and O. Deblecker, "Long-term planning of connected industrial microgrids: A game theoretical approach including daily peer-to-microgrid exchanges," *IEEE Transactions on Smart Grid*, vol. 10, no. 2, pp. 2245–2256, 2019.

[73] L. Ali, S. Muyeen, H. Bizhani, and A. Ghosh, "Optimal planning of clustered microgrid using a technique of cooperative game theory," *Electric Power Systems Research*, vol. 183, pp. 1–9, 2020.

[74] P. Machado, R. S. Netto, L. E. de Souza, and J.-C. Maun, "Probabilistic and multi-objective approach for planning of microgrids under uncertainty: a distributed architecture proposal," *IET Generation, Transmission & Distribution*, vol. 13, no. 7, pp. 1025–1035, 2019.

[75] F. Samadi Gazijahani and J. Salehi, "Stochastic multi-objective framework for optimal dynamic planning of interconnected microgrids," *IET Renewable Power Generation*, vol. 11, no. 14, pp. 1749–1759, 2017.

[76] A. Khayatian, M. Barati, and G. J. Lim, "Integrated microgrid expansion planning in electricity market with uncertainty," *IEEE Transactions on Power Systems*, vol. 33, no. 4, pp. 3634–3643, 2018.

[77] Q. Chen, M. Xia, Y. Zhou, H. Cai, J. Wu, and H. Zhang, "Optimal planning for partially self-sufficient microgrid with limited annual electricity exchange with distribution grid," *IEEE Access*, vol. 7, pp. 123 505–123 520, 2019.

[78] N. E. Koltsaklis, A. S. Dagoumas, G. M. Kopanos, E. N. Pistikopoulos, and M. C. Georgiadis, "A spatial multi-period long-term energy planning model: A case study of the greek power system," *Applied Energy Journal*, vol. 115, pp. 456–482, Feb. 2014.

[79] J. Schallenberg-Rodriguez and N. Garcia-Montesdeoca, "Spatial planning to estimate the offshore wind energy potential in coastal regions and islands. practical case: The canary islands," *Energy Journal*, vol. 143, pp. 91–103, Jan. 2018.

[80] S. Rhythm and B. Rangan, "Estimation of rooftop solar photovoltaic potential of a city," *Solar Energy*, vol. 115, pp. 589–602, 2015.

[81] Z. A. Latif, N. A. M. Zaki, and S. A. Salleh, "GIS-based estimation of rooftop solar photovoltaic potential using lidar," in *2012 IEEE 8th International Colloquium on Signal Processing and its Applications*, 2012, pp. 388–392.

[82] G. Pieter, M. Robert, M. Jennifer, C. Phillips, and E. Ryan, "Rooftop photovoltaic technical potential in the United States," NREL, Technical Report, 2019.

[83] V. M. Phap, N. T. Thu Huong, P. T. Hanh, P. Van Duy, and D. Van Binh, "Assessment of rooftop solar power technical potential in Hanoi city, Vietnam," *Journal of Building Engineering*, vol. 32, pp. 1–11, 2020.

[84] T. Ramachandra and B. Shruthi, "Spatial mapping of renewable energy potential," *Renewable and Sustainable Energy Reviews*, vol. 11, no. 7, pp. 1460–1480, 2007.

[85] M. Mwanza and K. Ulgen, *GIS-Based Assessment of Solar Energy Harvesting Sites and Electricity Generation Potential in Zambia*. Springer International Publishing, 2021, pp. 899–946.

[86] J. Shu, L. Wu, Z. Li, M. Shahidehpour, L. Zhang, and B. Han, "A new method for spatial power network planning in complicated environments," *IEEE Transactions on Power Systems*, vol. 27, no. 1, pp. 381–389, Feb. 2012.

[87] E. Garcia-Garrido, L. A. Fernandez-Jimenez, M. Mendoza-Villena, P. M. Lara-Santillan, P. J. Zorzano-Santamaria, E. Zorzano-Alba, and A. Falces, "Electric power distribution planning tool based on geographic information systems and evolutionary algorithms," in *2017 European Conference on Electrical Engineering and Computer Science (EECS)*, 2017, pp. 396–401.

[88] A. Phayomhom, N. Rugthaicharoencheep, and S. Chaitusaney, "GIS application to distribution substation planning in Bangkok's metropolitan electricity authority power system," *2015 12th International Conference on Electrical Engineering/Electronics, Computer, Telecommunications and Information Technology (ECTI-CON)*, pp. 1–6, Jun. 2015.

[89] M. Mehrtash, A. Kargarian, and A. J. Conejo, "Graph-based second-order cone programming model for resilient feeder routing using GIS data," *IEEE Transactions on Power Delivery*, vol. 35, no. 4, pp. 1999–2010, 2020.

[90] S. Vahedi, M. Banejad, and M. Assili, "GIS-based substation expansion planning," *IEEE Systems Journal*, vol. 15, no. 1, pp. 959–970, 2021.

[91] L. Yu, D. Shi, X. Guo, Z. Jiang, G. Xu, G. Jian, J. Lei, and C. Jing, "An efficient substation placement and sizing strategy based on GIS using semi-supervised learning," *CSEE Journal of Power and Energy Systems*, vol. 4, no. 3, pp. 371–379, 2018.

[92] E. J. Molina Bacca, "Optimal Sizing and Geographic Placement of the Components of a Microgrid," *Master Thesis. University of Calgary, Schulich School of Engineering*, Aug. 2018.

[93] M. Lugo-Alvarez, R. Broderick, and E. I. Ortiz-Rivera, "Strategic placement and design of microgrids using nighttime imagery," in *2020 47th IEEE Photovoltaic Specialists Conference (PVSC)*, 2020, pp. 1730–1734.

[94] S. Xie, H. Wang, S. Wang, H. Lu, Y. Hong, D. Jin, and Q. Liu, "Discovering communities for microgrids with spatial-temporal net energy," *Journal of Modern Power Systems and Clean Energy*, vol. 7, no. 6, pp. 1536–1546, Nov. 2019.

[95] S. Mojtahedzadeh, S. N. Ravadanegh, and M.-R. Haghifam, "Optimal multiple microgrids based forming of greenfield distribution network under uncertainty," *IET Renewable Power Generation*, vol. 11, no. 7, pp. 1059–1068, 2017.

[96] Natural Resources Canada. Satellite imagery and air photos. [Online]. Available: www.nrcan.gc.ca

[97] A. Dane and L. Doris, "Alaska strategic energy plan and planning handbook," U.S. Department of Energy, Office of Indian Energy, Technical Report, 2013.

[98] J. Royer, "Status of remote/off-grid communities in Canada," Natural Resources Canada, Technical Report, Jun. 2013.

[99] N. Hatziargyriou, *Microgrids: Architectures and Control*. WILEY, 2014, ch. 1: The Concept of Microgrids, pp. 1–24.

[100] J. Schlabbach and K.-H. Rofalski, *Planning Principles and Planning Criteria*. John Wiley & Sons, Ltd, 2008, ch. 3, pp. 23–35.

[101] C. Gamarra and J. M. Guerrero, "Computational optimization techniques applied to microgrids planning: A review," *Renewable and Sustainable Energy Reviews*, vol. 48, pp. 413–424, 2015.

[102] J. Sobieszczanski-Sobieski, A. Morris, M. van Tooren, G. La Rocca, and W. Yao, *Uncertainty-Based Multidisciplinary Design Optimization*. John Wiley & Sons, Ltd, 2015, ch. 10, pp. 258–286.

[103] Y. Li, J. Chen, and L. Feng, "Dealing with uncertainty: A survey of theories and practices," *IEEE Transactions on Knowledge and Data Engineering*, vol. 25, no. 11, pp. 2463–2482, 2013.

[104] A. Prekopa, *Mathematics and its Applications. Two-Stage Stochastic Problems.* Springer, 1994, ch. 12, pp. 373–421.

[105] G. Pantuso and T. K. Boomsma, "On the number of stages in multistage stochastic programs," *Annals of Operations Research*, vol. 292, no. 2, p. 581–603, 2020.

[106] J. Dupacová, G. Consigli, and S. W. Wallace, "Scenarios for multistage stochastic programs," *Annals of Operations Research*, vol. 100, pp. 25–53, 2000.

[107] K. Høyland and S. W. Wallace, "Generating scenario trees for multistage decision problems," *Management Science*, vol. 47, no. 2, pp. 295–307, 2001.

[108] S. Jin, S. M. Ryan, J.-P. Watson, and D. L. Woodruff, "Modeling and solving a large-scale generation expansion planning problem under uncertainty," *Energy Systems*, no. 2, p. 209–242, 2011.

[109] H. Heitsch and W. Römisch, "Scenario tree reduction for multistage stochastic programs," *Computational Management Science*, vol. 6, no. 2, p. 117–133, 2008.

[110] B. Calfa, A. Agarwal, I. Grossmann, and J. Wassick, "Data-driven multi-stage scenario tree generation via statistical property and distribution matching," *Computers Chemical Engineering*, vol. 68, pp. 7–23, 2014.

[111] IBM. (2020, Sep.) Geospatial data definition. [Online]. Available: www.ibm.com

[112] W. Bishop and T. H. Grubesic, *Geographic Information, Maps, and GIS.* Springer International Publishing, 2016, pp. 11–25.

[113] M. Neteler and H. Mitasova, *Open source GIS a grass approach*, 3rd ed. Springer, 2009.

[114] ESRI. (2019, Oct.) Getting stated with GIS: GIS fundamentals. [Online]. Available: www.esri.com/training

[115] Y. Li, "Research and application of deep learning in image recognition," in *2022 IEEE 2nd International Conference on Power, Electronics and Computer Applications (ICPECA)*, 2022, pp. 994–999.

[116] L. Deng and D. Yu, "Deep learning: Methods and applications," *Found. Trends Signal Process.*, vol. 7, no. 3–4, p. 197–387, jun 2014.

[117] Mathworks. (2022, Nov.) What is a convolutional neural network? [Online]. Available: www.mathworks.com

[118] Mathworks. (2022, Jul.) What is deep learning? [Online]. Available: www.mathworks.com

[119] IBM. (2022, Jul.) Convolutional neural networks. [Online]. Available: www.ibm.com

[120] S. Shilina, D. Kavazi, V. Smirnov, V. Smirnov, MOZGIII, Mingdong Li, R. Contreras, Hardik Gajera, and D. Lavrenov, "Humanode. whitepaper v. 0.9.6 "you are [not] a bot"," 2021.

[121] K. He, G. Gkioxari, P. Dollár, and R. B. Girshick, "Mask R-CNN," *2017 IEEE International Conference on Computer Vision (ICCV)*, pp. 2980–2988, 2017.

[122] K. H. Rami Alouta. Deep learning with arcgis pro tips & tricks. [Online]. Available: www.esri.com

[123] I. Goodfellow, Y. Bengio, and A. Courville, *Deep Learning*. MIT Press, 2016, www.deeplearningbook.org.

[124] S. Lee, S. Kwak, and M. Cho, "Universal bounding box regression and its applications," in *Computer Vision - ACCV 2018*, C. Jawahar, H. Li, G. Mori, and K. Schindler, Eds. Springer International Publishing, 2019, pp. 373–387.

[125] J. Bisschop, *AIMMS Optimization Modeling: Integer Linear Programming Tricks*. AIMMS B.V., Aug. 2021.

[126] I. Das and C. A. Cañizares, "Renewable Energy Integration in Diesel-Based Microgrids at the Canadian Arctic," *Proceedings of the IEEE*, vol. 107, no. 9, pp. 1838–1856, 2019.

[127] Olivares, Daniel, "An Energy Management System for Isolated Microgrids Considering Uncertainty," Ph.D. dissertation, University of Waterloo, Waterloo, Canada, 2014.

[128] Municipality of Sanikiluaq. (2022, Jan.). [Online]. Available: www.sanikiluaq.ca

[129] E. Vera, C. Canizares, and M. Pirnia, "Electrification of Canadian Northern Communities, using Low Emission Microgrids." Energy Modelling Initiative, Technical Report, 2021.

[130] Energy Efficiency Markets, LLC, "Fuel cell microgrids: The path to lower cost, higher reliability, and cleaner energy," Technical Report, 2017.

[131] GAMS Development Corp. Gams documentation center. [Online]. Available: www.gams.com

[132] Hafez, Omar, "Some aspects of microgrid planning and optimal distribution operation in the presence of electric vehicles," Master's thesis, University of Waterloo, Canada, 2012.

[133] "Canada's Energy Future," Canada Energy Regulator, Technical Report, 2020.

[134] T. B. da Silva, "Electric vehicle charging: what to expect when the fuel of our cars is electricity?" *, FGV ENERGIA Opinion*, Dec. 2017.

[135] A. G. Villela and V. A. de Carvalho, "Calculation of network demand for the addition of new loads to the low voltage distribution network of Eletropaulo," *National Seminar on Electricity Distribution*, Oct. 2008.

[136] Emanuel Cella Simon, "Some aspects of microgrid planning and optimal distribution operation in the presence of electric vehicles," Master's thesis, Federal University of Rio de Janeiro, Brazil, 2013.

[137] PVsyst, "Meteo databases, synthetic data generation," 2022.

[138] NASA. (2021, Jun.) Prediction of worldwide resources. [Online]. Available: power.larc.nasa.gov

[139] J. Duffie and W. Beckman, "Available solar radiation," in *Solar Engineering of Thermal Processes*. John Wiley & Sons, Ltd, 2013, ch. 2, pp. 43–137.

[140] Portal Solar. Photovoltaic solar energy kit: Everything you need to know. [Online]. Available: www.portalsolar.com.br

[141] "Strategic study: Photovoltaic market for distributed generation in Brazil," Greener, Technical Report T2, Jul. 2019.

[142] Brazilian Ministry of Mines and Energy, "Electricity demand," in *Statistical Yearbook of Electric Energy*, 2021, ch. 3, pp. 87–182.

[143] M. H. S. Boloukat and A. A. Foroud, "Multiperiod planning of distribution networks under competitive electricity market with penetration of several microgrids, part i: Modeling and solution methodology," *IEEE Transactions on Industrial Informatics*, vol. 14, no. 11, pp. 4884–4894, 2018.

[144] S. R. Khuntia, B. W. Tuinema, J. L. Rueda, and M. A. van der Meijden, "Time-horizons in the planning and operation of transmission networks: an overview," *IET Generation, Transmission & Distribution*, vol. 10, no. 4, pp. 841–848, 2016.

[145] F. H. Pereyra, A. P. Cunha, J. C. Guaraldo, H. Kagan, M. R. Gouvêa, and E. Vicentini, "Planning the expansion of distribution systems with distributed generation," *SBSE 2012 – IV Brazilian Symposium on Electrical Systems*, pp. 1–6, 2012.

[146] "Electricity Distribution Procedures in the National Electric System: Distribution System Expansion Planning," National Electric Energy Agency - ANEEL, Technical Report 7, 2017.

[147] "U.S. solar photovoltaic system and energy storage cost benchmark: Q1 2020," NREL, Technical Report, 2020.

[148] Marcotrends. Brazil Inflation Rate 1981-2022. [Online]. Available: www.macrotrends.net

[149] ESRI. Automate building footprint extraction using deep learning. [Online]. Available: www.esri.com

[150] K. He, X. Zhang, S. Ren, and J. Sun, "Deep residual learning for image recognition," in *2016 IEEE Conference on Computer Vision and Pattern Recognition (CVPR)*, 2016, pp. 770–778.